MESENCHYMAL STEM CELL MECHANICS ON OSTEOINDUCTIVE PEPTIDE NANOFIBERS

A DISSERTATION SUBMITTED TO
THE GRADUATE SCHOOL OF ENGINEERING AND SCIENCE
OF BILKENT UNIVERSITY
IN PARTIAL FULFILLMENT OF THE REQUIREMENTS FOR
THE DEGREE OF
DOCTOR OF PHILOSOPHY
IN
MATERIALS SCIENCE AND NANOTECHNOLOGY

By
Ahmet Emin Topal
July 2017

MESENCHYMAL STEM CELL MECHANICS ON OSTEOINDUCTIVE PEPTIDE NANOFIBERS

By Ahmet Emin Topal

July 2017

We certify that we have read this dissertation and that in our opinion it is fully adequate, in scope and in quality, as a dissertation for the degree of Doctor of Philosophy.

Aykutlu Dâna (Advisor)

Ayşe Begüm Tekinay (Co-advisor)

Mustafa Özgür Güler (Co-advisor)

Çağlar Elbüken

Hamdi Torun

Melih Önder Babaoğlu

Bilge Baytekin

Approved for the Graduate School of Engineering and Science:

Ezhan Karaşan
Director of the Graduate School

ABSTRACT

MESENCHYMAL STEM CELL MECHANICS ON OSTEOINDUCTIVE PEPTIDE NANOFIBERS

Ahmet Emin Topal
Ph.D. in Materials Science and Nanotechnology
Advisor: Aykutlu Dâna
July 2017

In this thesis, changes in Young's modulus of mesenchymal stem cells (MSCs) were investigated during their osteogenic differentiation on bioactive peptide nanofibers that bear triple glutamic acid sequence (EEE), a non-collagenous protein sequence of some extracellular matrix (ECM) proteins (e.g. bone sialoprotein) found in bone tissue. MSCs formed spherical cell aggregates on the osteoinductive peptide nanofibers, here also called osteospheroids, of which their cells made intensive cell-cell contacts and showed osteoblast-like cell morphology. Mechanical characterization of the osteospheroids on the peptide nanofiber hydrogel was performed using atomic force microscope (AFM) where AFM probes modified with a thin film coating of octafluorocyclobutane (C_4F_8) were used to measure force maps of the cells at days 3, 7 and 14 of osteogenic differentiation. Hertz Cone model, same as Sneddon, was applied to approach curves of 12 force curves per cell to calculate the Young's modulus values. As a result, an increasing pattern was observed in the average Young's modulus of rMSCs on the peptide nanofibers throughout the osteogenic differentiation. Mineral deposition by the cells on the peptide nanofibers was checked by Alizarin red staining and a large amount of mineral deposition by the osteospheroids was observed, proving that an efficient osteogenic differentiation of the rMSCs happens on the osteoinductive peptide nanofibers. In the literature, a gradual decrease is shown in AFM measured average Young's modulus values of adhered MSCs throughout their osteogenic differentiation. When gelatin-coated glass was used as substrate instead of the peptide nanofibers, rMSCs showed a decreasing pattern in their Young's moduli, similarly to the literature, due to osteogenic differentiation. However, there was no significant calcium mineral deposition on the gelatin group, even until day 14 of osteogenic differentiation, indicating that a limited or a slower progression of osteogenic differentiation of rMSCs is present on the gelatin compared to rMSCs on the osteoinductive peptide nanofibers. A correlation between the observed increase in average Young's moduli of osteospheroid rMSCs and

their mineral production on the peptide nanofibers may suggest a predominant role of biomineralization on the cell mechanics.

Keywords: Atomic force microscopy, mesenchymal stem cells, osteogenic differentiation, peptide amphiphiles, self-assembly, nanofibers.

ÖZET

OSTEOİNDÜKTİF PEPTİT NANOFİBERLER ÜZERİNDE MEZENKİMAL KÖK HÜCRE MEKANİĞİ

Ahmet Emin Topal
Malzeme Bilimi ve Nanoteknoloji, Doktora
Tez Danışmanı: Aykutlu Dâna
Temmuz 2017

Mezenkimal kök hücrelerin (MSC'lerin) osteojenik farklılaşması sırasında Young katsayısı değişimleri, bone sialoprotein gibi kemik dokusunda bulunan ve kollajen olmayan bazı hücreler arası matris (ECM) proteinlerinin yapısında bulunan üçlü glutamik asit (EEE) dizisi taşıyan biyoaktif peptit nanofiberler üzerinde araştırılmıştır. Osteoindüktif peptit nanofiberler üzerindeki MSC'ler burada osteoküremsi olarak da bahsedilen, birbirleriyle yoğun etkileşim içerisinde bulunan ve osteoblast gibi hücre morfolojisine sahip olan hücre kümeleri oluşturur. Atomik kuvvet mikroskobu (AFM) ve oktaflorosiklobütan (C_4F_8) ince filmi kaplanmış AFM ölçüm uçları kullanılarak peptit nanofiber hidrojel üzerinde osteojenik yönde farklılaşmakta olan sıçan MSC'lerin (rMSC'lerin) kuvvet haritalaması ölçümleri yapılmıştır. Hücre başına 12 adet kuvvet-uzaklık eğrisi ölçümünün yaklaşma eğrileri, Hertz Cone (Sneddon ile aynı) modeline göre fit edilerek hücrelerin Young katsayısı değerleri hesaplanmıştır. Peptit nanofiberler üzerindeki osteoküremsi hücrelerin ortalama Young katsayısının osteojenik farklılaşma sırasında arttığı gözlemlenmiştir. İkinci olarak, peptit nanofiberler üzerindeki hücreler tarafından çok miktarda mineral biriktirildiği Alizarin red boyaması sonucunda gözlemlenmiştir ve bu sonuç rMSC'lerin peptit nanofiberler üzerinde etkili bir osteojenik farkılaşma yaşadığını kanıtlamaktadır. Literatürde, osteojenik farklılaşan MSC'lerin AFM ile ölçülmüş Young katsayısı çalışmalarında, hücrelerin ortalama Young katsayısında yavaş yavaş bir düşüş trendi gözlenmektedir. Peptit nanofiberler yerine jelatin kaplı cam yüzey kullanıldığında Young katsayısında düşüş gözlenmektedir; ve bu düşüş osteojenik farklılaşmadan dolayıdır. Ancak, kalsiyum minerallerinin jelatin üzerindeki hücrelerde yeterli miktarda birikmemesi jelatin üzerindeki hücrelerde sınırlı veya daha yavaş bir osteojenik farklılaşmanın gerçekleştiğini gösteriyor olabilir. Osteoindüktif peptit nanofiberler üzerinde osteojenik farklılaşan hücrelerin geniş kapsamlı kalsiyum minerali ürettiğinin gözlenmesi ile hücrelerin ortalama Young

katsayısındaki artışı arasındaki korelasyon biyomineralizayonun hücre mekaniği üzerinde baskın bir rolü olduğunu destekleyebilir.

Anahtar sözcükler: Atomik kuvvet mikroskopisi, mezenkimal kök hücreler, osteojenik farklılaşma, peptit amfifiller, kendiliğinden bir araya gelme, Young katsayısı, nanofiberler.

Acknowledgement

Dedicated to my family and friends. . . . . .

I would like to thank my thesis supervisors Prof. Aykutlu Dâna, Prof. Ayşe Begüm Tekinay and Prof. Mustafa Özgur Güler for allowing me to participate into their scientific research groups that provided the research and experiences during my PhD for writing this thesis, and for their remarkable supervisions.

I would like to thank Alper Devrim Özkan for being a close and sincere friend of mine during my PhD, for helping me writing a project related to nanomechanical characterization of osteogenic differentiation using AFM that I struggled for a long time. I acknowledge Alper Devrim for his contributions, kind proofreadings of the manuscripts and presentations, and fruitful discussions during my undergraduate and PhD years.

I would like to thank Merve Şen and İdil Uyan for sharing their vital, supportive, and cheerful friendships with me. Thanks for joining me at walkings, runnings, and swimmings, all have been important reinforcements to me; I appreciate their friendship and support very much. Not only I felt so good and relaxing as we swam together, but also the swimming enhanced my strength and physical capability for measuring force maps of cells more easily when I needed to stay for long at the lab for AFM measurements like 9-10 hours in a day. I should thank you for inviting me very kindly to countless breakfasts and for being my best friends at the second half of my PhD.

I would also like to give my thanks to Fatma Begüm Dikeçoğlu for being a sincere friend and sharing many things with me including her countless breakfasts, meals, fruits and coffee. Begüm's kind supports without expecting anything in return have been remarkable and important to me for the last few years of my PhD.

I would like to acknowledge Dr. Gülistan Tansık for her valuable contributions

to my research, for maintenance of the cells, and doing most of the molecular biology characterization experiments. I would like to also thank Aygül Zengin for her technical help at synthesis and characterization of peptide amphiphiles, and Fatma Begüm Dikeçoğlu for her kind technical help at rheology characterization of the resulting hydrogel, respectively. I would like to thank Canelif Yılmaz and Nurcan Haştar for preparing cell samples of rMSCs and HUVECs, respectively, for some of the AFM experiments.

I would like to acknowledge the PhD scholarships from TÜBİTAK (The Scientific and Research Council of Turkey) BİDEB 2211-C and BİDEB-2211-E.

I would like to thank Nanoscale Devices and Imaging (NDI) research group alumni members Sencer Ayas, Hasan Güner, Okan Öner Ekiz, Ayşegül Abdelal, and current members Mustafa Ürel and Dr. Gökhan Bakan. I acknowledge Sencer Ayas for being a leading researcher in our group in the plasmonics field. I thank Mustafa Ürel for sharing his expertise at AFM.

I would like to express my thanks to current and past members and of Nanobiotechnology (NBT) and Biomimetic Materials (BML) research groups for providing me scientific, professional, enthusiastic, nice and joyful working environment. I thank Dr. Göksu Çınar Çiftçi, Dr. Berna Şentürk, Dr. Hakan Ceylan, Dr. Rashad Mammadov, Dr. Samet Kocabey, Elif Arslan, Hilal Ünal Gülsüner, Dr. Melike Sever, Canelif Yılmaz, Şehmus Tohumeken, Dr. Ruslan Garifullin, Dr. Handan Acar, Dr. Aref Khalily, Hepi Hari Susapto, Dr. Özlem Erol, Dr. Melis Şardan Ekiz, İbrahim Çelik, Çağla Eren, Egemen Deniz Eren, Gökhan Günay, Seren Hamsici, Merve Şen, İdil Uyan, Nurcan Haştar, Zeynep Orhan, Fatih Yergöz, Hatice Kübra Kara, Dr. Gülistan Tansık, Oya İlke Şentürk, Dr. Gülcihan Gülseren, Seher Üstün Yaylacı, Meryem Hatip, Aygül Zengin, Dr. Bhavna Rajasekaran, Alper Devrim Özkan, Jorge Montanari, Özge Uysal, İslam Oğuz Tuncay, Burak Demircan, Mustafa Beter, Özüm Şehnaz Günel, Mevhibe Geçer, Nuray Gündüz, Yasin Tümtaş, Dr. Büşra Mammadov, Dr. Gözde Uzunallı, İmmihan Ceren Yaşa, Öncay Yaşa, Zahide Diğdem Mumcuoğlu, Ayşegül Tombuloğlu, Yavuz Selim Dağdaş, Selma Bulut, Murat Kılınç, Melis Göktaş,

Fatma Begüm Dikeçoğlu and Dr. Ashif Shaikh.

I would like to thank my ex-office friends Dr. Ömer Faruk Sarıoğlu, Tolga Tarkan Ölmez, Ebuzer Kalyoncu, Türkan Gamze Ulusoy, Alper Devrim Özkan, Amir Ghobadi, Yıldız Gözde Sağlam, Sami Bolat, Türkan Bayrak and Mehmet Can Yağcı, for being good and sincere officemates.

I would like to thank Seylan Ayan and Begüm Dikeçoğlu for encouraging me to go running in the soccer field in main campus.

I would like to thank all my friends at UNAM who participated to shared purchases of coffee.

I would like to thank Prof. Salim Çıracı for offering me choices and paths to follow at UNAM at the mid-phase of my PhD after my former advisor suddenly left at my second year. Here, I would like to again thank Prof. Aykutlu Dana for kindly accepting me to join his group.

In addition to my three brilliant supervisors, I would like to thank my PhD committee members Prof. Çağlar Elbüken for kindly helping me at improving my experiences in research, providing useful advices and evaluating my progress, Prof. Hamdi Torun for his kind participation and analytical evaluations, also Prof. Ali Osmay Güre, member of my earlier committe and also my undergrad advisor for helping me not to give up and lose my hopes for doing science.

Finally, I would like to thank my family (i.e. my mom, dad and sister) for their invaluable supports that they provided throughout my PhD. I am very lucky to have them.

Contents

1 Introduction **1**

1.1 Osteoinduction . . . 2

1.1.1 Mesenchymal stem cells (MSCs) . . . 2

1.1.2 Osteogenic differentiation of MSCs . . . 5

1.1.3 Biomineralization . . . 7

1.1.4 Mechanical properties of mineralized tissues . . . 12

1.1.5 Stem cell aggregates . . . 13

1.2 Mechanical analysis techniques for single cells . . . 15

1.2.1 Micropipette aspiration . . . 15

1.2.2 Microrheology . . . 17

1.2.3 Optical trapping, optical tweezers and the optical stretcher (OS) . . . 18

1.2.4 Traction force microscopy (TFM) . . . 18

1.2.5 Atomic force microscopy (AFM) . . . 19

1.2.6 Brillouin microscopy . . . 20

1.3 Mechanical models for cell mechanics . . . 20

1.3.1 Continuum mechanics models . . . 21

1.3.2 Micro/nanoscale approach . . . 28

1.4 Behind the AFM . . . 29

1.4.1 History . . . 29

1.4.2 Working principles . . . 30

1.4.3 Elastic modulus characterization studies of osteogenic differentiating MSCs in the literature . . . 33

1.5 Bioactive peptide nanofibers as osteoinductive biomaterials . . . 36

1.5.1 What is a peptide amphiphile? . . . 36

1.5.2 Osteoinductive peptide nanofibers 37
1.6 What are the attributes of cells that influence their mechanical properties? 43

2 Design of custom atomic force microscope (AFM) probes for imaging and force mapping of live cells 45
2.1 Study background and hypothesis 45
2.2 Materials and methods 46
2.2.1 Fabrication of AFM probes with Teflon-like coating 46
2.2.2 SEM imaging 46
2.2.3 Contact angle measurement 46
2.2.4 AFM imaging 47
2.3 Results and discussion 47
2.3.1 Characterization of Teflon-like coated AFM probes 47
2.3.2 AFM imaging and force mapping of live cells via AFM probes with Teflon-like coating 47
2.3.3 Optimization of Teflon-like thin film coating recipe at ICP 50
2.4 Conclusion 51

3 Force mapping and Alizarin red staining reveal that Young's moduli of differentiating mesenchymal stem cells increase with biomineralization on osteoinductive peptide nanofibers 56
3.1 Study background and hypothesis 57
3.2 Materials and methods 58
3.2.1 Design and synthesis of peptide amphiphile (PA) molecules 58
3.2.2 Characterizations of PA molecules and the peptide nanofibers 60
3.2.3 Force mapping and data analysis 60
3.3 Results and discussion 61
3.3.1 Characterization of the PAs and peptide nanofibers 61
3.3.2 Commitment of rat mesenchymal stem cells (rMSCs) to osteogenic differentiation on the peptide nanofibers 66
3.3.3 Force mapping reveals stiffening of rMSCs differentiating on the osteoinductive self-assembled peptide nanofibers . . 68

3.3.4 Mineralization profile of the differentiating cells on the peptide nanofibers 74
3.4 Conclusion and future perspectives 75

4 Force Mapping the Osteospheroids with Colloidal Microbead AFM Probes 76
4.1 Study background and hypothesis 76
4.2 Materials and methods 76
4.3 Results and discussion 77
4.4 Conclusion and future perspectives 81

5 Conclusions and Future Perspectives 85
5.1 General conclusions 85
5.2 Future perspectives 86
5.3 Challenges encountered during AFM measurements for mechanical characterization of spheroids on the peptide nanofiber hydrogels . 87

A Protocol for cantilever spring constant calibration for mechanical analysis of living cells by an Asylum Research MFP-3D model AFM 112
A.1 Materials 112
A.2 Methods 113
A.2.1 Calibration of the AFM probe 113
A.2.2 Sample preparation 116
A.2.3 Measuring force curves on live cells 116

B Supplementary information 118

List of Figures

1.1 Bone remodeling cycle with osteogenic lineages from mesenchymal stem cell (MSC) and hematopoietic stem cell (HSC). 6
1.2 Bone structure and organizations of compact (cortical) bone at macro, micro and nanoscales 8
1.3 Regions of biomineralization in the bone. Osteoblast-osteocyte interaction is present. 10
1.4 Chromosomal location and size, and protein structure of bone sialoprotein (BSP). 11
1.5 Spheroids or stem cell aggregates are promising for tissue engineering because of their regenerative potential 15
1.6 Mechanical models for mechanical property characterization of cells and other biological materials 21
1.7 Sphero-conical probe and a related fitting with a proposed contact mechanical model 24
1.8 AFM components and setup, force mapping and a force-distance curve explained 31
1.9 Young's modulus scale of various materials 32
1.10 Chemical structure of a peptide amphiphile (PA) molecule with its chemical formula and space-filling model, hypothetical assembly into nanofiber structure, and bundles formed from the nanofibers. 36
1.11 Osteoinductive effect of noncollagenous protein mimetic PA (E_3-PA) bearing peptide nanofibers on hMSCs. 38
1.12 Glycosaminoglycan (GAG) mimetic PA (SO_3-PA) promotes mineralization 39

1.13 Glycosaminoglycan (GAG) mimetic PA promotes osteogenic differentiation of rMSCs 40
1.14 Tenascin-C mimetic PA promotes osteogenic differentiation of rat MSCs 41
1.15 Chemical structures of E_3-PA molecule and K_3-PA, zeta potential measurement result, hydrogel appearance in an upside down tube, SEM image, TEM images of E_3/K_3-PA 43

2.1 Characterization of Teflon-like coated silicon nitride AFM probe. . 48
2.2 AFM images of confluent rMSCs using Teflon-like thin film coated AFM probes. 49
2.3 64 x 64 force map measurement trial using Teflon-like coated AFM probes. 50
2.4 Tapping mode AFM images of less confluent rMSCs measured using Teflon-like coated SiNi AFM probes. 52
2.5 Bending problem of Teflon-like probes fabricated with a power of 400 W at ICP 53
2.6 Appearance of AFM probe coated at 150 W in aqueous environment; the bending problem was solved. 54
2.7 SEM images of 150 W coated probe and AFM images of live HUVECs using the same probe. 55

3.1 Chemical representations of PA molecules Lauryl-VVAGEEE (E_3-PA) and Lauryl-VVAGKKK-Am (K_3-PA), and their self-assembly into proposed E_3/K_3-PA nanofiber structure. 59
3.2 LC-MS of E_3-PA 63
3.3 LC-MS of K_3-PA 64
3.4 SEM image of the PA hydrogel network 65
3.5 Tapping mode AFM images of E_3/K_3-PA dried on a cleaned glass coverslip. 66
3.6 Contact-mode AFM images of self-assembly process of E_3/K_3-PA nanofibers formed on mica surface in solution. 67
3.7 Time sweep rheology analysis of E_3/K_3-PA 68
3.8 Live/dead assay of rMSCs on E_3/K_3-PA nanofiber gel 69

3.9 Optical microscope images of rMSCs on glass, E_3/K_3-PA, and gelatin, force maps and force curves of rMSCs on glass and E_3/K_3-PA nanofiber gel 70
3.10 Young's modulus histograms of rMSCs on days 3, 7 and 14 of osteogenic differentiation on E_3/K_3-coated glass, bare glass and gelatin-coated glass 71
3.11 Nanomechanical characterization results graphed as frequency distribution histograms with Gaussian curves. 72
3.12 Young's moduli derived from AFM force mapping of E_3/K_3 only control samples incubated in osteogenic medium 73
3.13 Calcium deposition profiles of cells on the bioactive peptide nanofibers and on the TCP 75

4.1 SEM images of gold colloidal microsphere AFM probes 77
4.2 Live/dead assay repeat experiment result of rMSCs cultured on E_3/K_3-PA nanofibers 79
4.3 Optical microscope images of rMSCs on osteoinductive peptide nanofiber-coated glass coverslip in osteogenic medium versus rMSCs on bare glass coverslip in maintenance medium are shown . . 80
4.4 Representative force map results of rMSCs cultured on bare glass and rMSC on E_3/K_3-PA-coated glass. 81
4.5 AFM Young's modulus results of differentiating rMSCs cultured on E_3/K_3-PA peptide nanofibers shown via columns with scatter plot. 83
4.6 AFM Young's modulus results of differentiating rMSCs cultured on bare glass coverslip 84

A.1 Thermal noise versus frequency spectrum of Teflon-like coated silicon nitride AFM probes 115
A.2 Appearances of the sample on the AFM stage to make it ready for the measurements. 117

B.1 Time sweep frequency sweep and amplitude sweep tests of E_3/K_3-PA gel, three replicates are explicitly shown. 119

List of Tables

1.1 AFM studies of single cells of osteogenic differentiating MSCs, undifferentiated MSCs and osteoblasts 35

Chapter 1

Introduction

Using mesenchymal stem cells (MSCs) in cell therapies for bone diseases like osteoporosis, osteoarthritis, and for other osteochondral injuries and orthopedic defects is promising for regenerative medicine due to their abilities of multilineage differentiation and tissue regeneration [1, 2, 3, 4]. Understanding identity and properties of MSCs and the cells differentiated from MSCs is important to better exploit their therapeutic potential for treating such conditions. Stem cells' physical properties have been studied in detail in the recent decades and their mechanical properties seem to have been well-characterized *in vitro*. However, majority of studies characterizing their mechanical properties do not use extracellular matrix (ECM) or ECM mimicking moieties in their microenvironment; rather, they usually measure cells adhered on a flat glass substrate or a Petri dish. It is remarkable to note that a stem cell's niche might be very influential on its character and identity not only biochemically but also physically. Therefore, it is crucial to accurately characterize the mechanical properties of stem cells when they are in an *in vivo*-like state. Here, I focus on the characterization of Young's moduli of MSCs in an environment that mimics the ECM by utilizing bioactive peptide sequences within a nanofibrous mesh network so that when I measure mechanical properties of the cells on the bioactive peptide nanofibers, measurement results might better represent *in vivo* conditions. I used atomic force microscopy (AFM) to measure force maps of MSCs to characterize their

Young's moduli when differentiating into the osteogenic lineage on a bioactive peptide nanofiber hydrogel. AFM probes modified with a Teflon-like thin film coating were used to obtain easier and smoother force curve measurements on the cells and to reduce the adhesion between the cells and the probe.

1.1 Osteoinduction

1.1.1 Mesenchymal stem cells (MSCs)

A stem cell describes any cell that can both self-renew and give rise to cells found in tissues. MSC is a nonhematopoietic adult stem cell type and has multipotency (*i.e.* the potential to give rise into more than one cell type but is more limited than pluripotency) to fully differentiate into lineages of mesenchymal tissues, that are bone, cartilage, fat, muscle, stroma, marrow, connective and tendon/ligament tissues, and controversially the neuronal cells [5, 6, 7, 8]. Founder of MSC biology was Alexander Friedenstein who firstly isolated fibroblastic cells from bone marrow that could differentiate into osteoblasts, osteocytes, chondrocytes, adipocytes and into myoblasts [1, 6]. Friedenstein called them "osteogenic stem cells" and Arnold Caplan first used the term "mesenchymal stem cell" [9]. MSCs are also known to have immunosuppressive abilities [10].

Osteoinduction is the phenomenon of encouraging undifferentiated cells like MSCs to become active osteoblasts and it is also a generally used term for osteogenesis induced by bone grafting materials [11]. Autologous bone grafting is the surgical operation for replacement of a missing bone from another place of the patient's body and it is the current standard of care when natural bone repair mechanisms fail [12]. In addition to bone grafting, development of novel osteogenic tissue engineering methods might be necessary for treatment of diseases such as osteoarthritis (OA) of which there has been no therapy that can neither stop or reverse the disease progression yet [13]. All of the joints contain MSCs and their healthy development depends on MSC activity, and hence

OA might be associated with changes in MSC quantity, phenotype, morphology and/or function [1]. In osteoporosis (OP), effect of MSCs was pointed out to be more prominent as the MSC number and responsiveness to bone morphogenetic protein (BMP) were reported to influence the disease progress [14]. BMP is a protein found in the ECM of bone tissue and it enables morphogenesis of cells differentiating towards the osteogenic lineage. Infusion of wild type MSCs to osteoporosis imperfecta (OI) mouse models ends up with improvement of bone mineralization and collagen synthesis [9]. As such, MSC-based cell therapies are holding their promise for promoting bone and cartilage repair, and there is a continuing need for readily-available source of MSCs and biomaterials like microcarriers and hydrogels to inject the cells with to the patients and to enhance the repair of damaged tissues. Bioreactors with stirred microcarriers have been shown to provide higher potency for osteogenic differentiation when MSCs are cultured in three-dimensional scaffold cultures [15].

There may be great heterogeneity within MSC populations, hence obtaining a homogenous MSC population is a difficult task. Careful identification and characterization of the cells are needed. Cell surface markers that MSCs express are CD105, CD73, CD90, CD146, CD13, CD29, CD44, CD166 and CD10, Nestin, Stro-1, SSEA-4, CD271 and Sca-1, but they lack expressions of CD45, CD34, CD14 or CD11b, CD79a or CD19, and HLA-DR [16, 17]. Heterogeneous expression of such markers by cells from clones might be observed, which might be a cause of heterogeneity in differentiation potential observed within MSC populations [9]. MSCs have been isolated from bone marrow, adipose (fat), dermis (skin), synovial fluid, periosteum, umbilical cord blood, placenta and amniotic fluid [18]. So, another important cause of heterogeneity is the site of derivation because it influences the commitment of MSCs and the lineages by biasing differentiation trajectories, and thus functions of the differentiated cells [19].

MSCs are highly responsive to environmental cues and they have ability to modulate their microenvironment through regulating their secretions of humoral and structural proteins as well as their ECM proteins [20]. It has been suggested that MSC niche in the bone marrow has distinct locations named endosteal niche, stromal niche and perivascular niche [16]. Native ECM of bone marrow as a key

component of the MSC niche has been reported to be very important in preserving the stemness and differentiation potential of bone-marrow derived-MSCs (BM-MSCs) [21]. CD271, MSCA-1/Stro-3/non-specific alkaline phosphatase, Stro-1, CD146, CD49a, CD106, CD51, CD200, CD90, PDGFRα (CD140a), PDGFRβ (CD140b) and Leptin R (CD295) were listed as markers of native BM-MSCs in a recent report [14]. BM-MSCs are isolated via bone marrow aspiration and separated from other cells by density centrifugation followed by seeding to tissue culture polystyrene for their proliferation [22]. Population doubling of BM-MSCs is several times a week; culture medium should be replenished within every 3-4 days, and the cells should be passaged upon near-confluence (*i.e.* 70-80% of confluency). Usually, trypsin passaging is preferred in which the cells are treated with the enzyme trypsin, a serine protease, to remove adhesive peptide bonds between the cells and the tissue culture polystyrene, incubated for 3-5 minutes at cell culture incubator and the cells are then transferred to a new tube in the suspended state and seeded to a new tissue culture polysterene flask. After prolonged *in vitro* culture, in other words, at senescent passages (*i.e.* P8 or later), MSCs start losing their multipotency and some of the cells start differentiating with a tendency towards the osteogenic lineage [16].

To induce differentiation, maintenance medium that contains Dulbecco's modified Eagle's medium (DMEM), 10% fetal bovine serum (FBS) and 1% pencillin/streptomycin) is replaced with a differentiation induction medium. An osteogenic differentiation medium is usually maintenance medium supplemented with ascorbic acid, dexamethasone and β-glycerophosphate because those factors are known to induce/promote osteogenic differentiation of MSCs [23]. As the MSCs start differentiating, their proliferation is repressed (but not stops, it is decreased to a minimal rate). There occurs changes in gene expression and protein production levels that are related to the lineage of differentiation. Multipotency, cell function and morphology are also subject to remarkable changes.

1.1.2 Osteogenic differentiation of MSCs

Bone cells include bone-forming osteoblasts that make up the osteoid matrix and aid the bone mineralization, osteocytes that are found in the bone matrix and have dendritic lamellipodia, and bone-degrading osteoclasts that take role in the bone resorption (Figure 1.1) [24]. Through transitory steps, intermediary cells are formed during osteogenic differentiation where MSCs differentiate first into osteoprogenitor cells and later into pre-osteoblasts. Next immature osteoblasts are formed, and then there is a maturation period of osteoblasts followed by a mineralization stage. Mature osteoblasts either operate as bone lining cells or further differentiate into osteocytes. If not either, they enter apoptosis and die. Osteoblast differentiation has been argued to be positively regulated with increased direct cell-cell contact [25]. On the contrary, osteocyte differentiaton has been suggested to be positively regulated with intercellular separation [26].

Chemistry, topography and stiffness of substrate/matrix used for cultivating MSCs matter for lineage specification. Interestingly, very stiff substrates like graphene were shown to accelerate the osteogenic differentiation of MSCs [28]. Discher group argues that for 2D gels, 20-100 kPa interval is the efficiency range and 30 kPa is the optimum value of matrix stiffness to promote osteogenic differentiation with calcification, because the stiffness of the osteoid matrix is 30-40 kPa [29]. Mooney group's claim for the optimum value of hydrogel elastic modulus for bone formation at osteogenic differentiation of MSCs is 60 kPa, however, they did not test 20 kPa in some of their analyses (instead they used 5 kPa) in their study, thus leaving their investigation not fully answered because they did not rule out 20-60 kPa interval in all of their experiments [30].

There are osteogenic markers found within the cells from MSCs to osteoblasts whose expression levels vary in each of the different cell type. Runt-related transcription factor 2 (Runx2), one of these osteogenic markers, is a transcription factor that binds to promoter sequences of osteogenic genes in the cell nucleus and is expressed at high levels in osteoprogenitor cells and pre-osteoblasts during the early periods of osteogenic differentiation, which are the commitment and

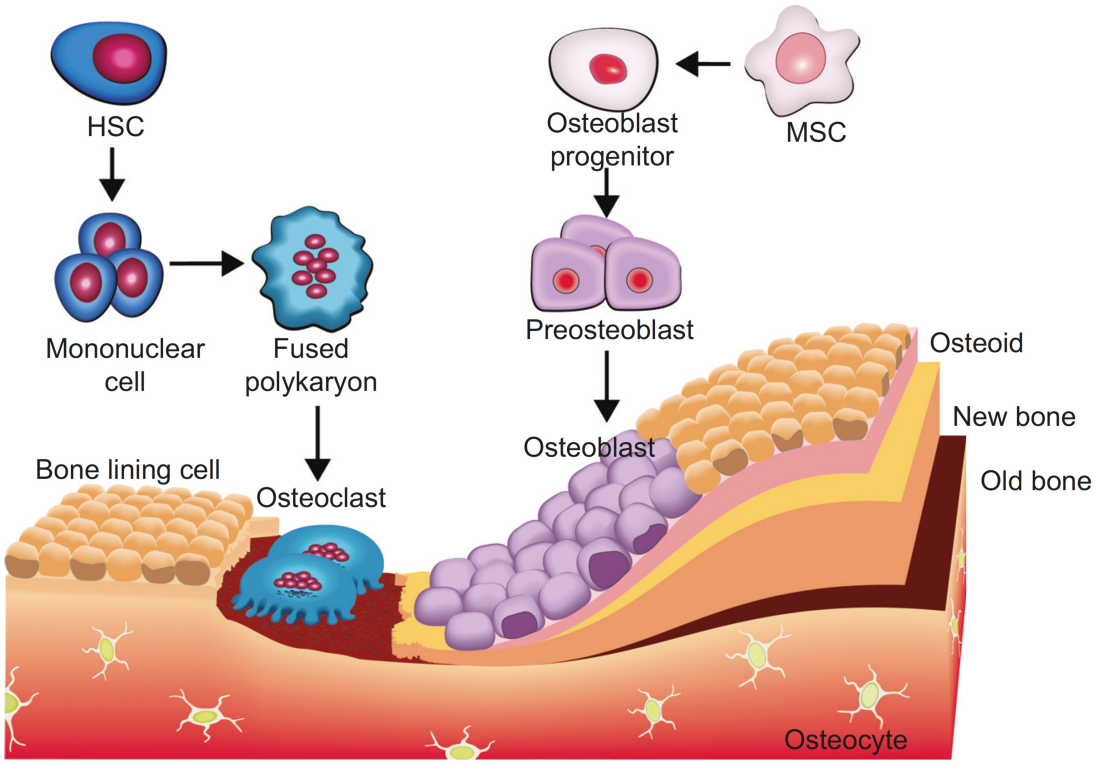


Figure 1.1: Bone remodeling cycle with osteogenic lineages from mesenchymal stem cell (MSC) and hematopoietic stem cell (HSC). Osteoblast progenitor (or osteoprogenitor cell) and pre-osteoblast cells are transitions between MSC to osteoblast. Illustration reprinted with permission from Rahman *et al.* [27].

proliferation stages [24]. Runx2 is the master regulator of transcription and is essential for the osteogenic differentiation process to proceed to the osteoblasts [31]. Osterix (Osx) is another obligatory osteoblast-specific transcription factor which takes a transcriptional regulatory role in the proliferation stage of which it favors osteoblast differentiation and may inhibit the proliferation of cells [32, 33]. Transforming growth factor-beta (TGF-β)/bone morphogenetic protein (BMP) signaling plays an important role in osteoblast differentiation through the activation of receptor serine/threonine kinases [27]. BMP is a cytokine and a ligand of BMP receptor (BMPR) which is a serine/threonine kinase receptor and belongs to the TGF-β superfamily group of proteins [27]. There are more than 20 recognized BMPs and some of them like BMP2, BMP4 and BMP7 are potent osteoinductive factors and inducers of osteogenesis [27]. Wnt signaling pathway also promotes the commitment of MSCs to osteoblast differentiation and inhibit

chondrogenic differentiation at the same time [34].

At the matrix maturation step, a mid-stage of osteogenic differentiation between pre-osteoblasts and early osteoblasts, alkaline phosphatase (ALP) enzyme activity, and collagen I and bone sialoprotein (BSP) protein expressions increase while Runx2 expression decreases [24]. High level expression of ALP enzyme prevents effects of biomineralization inhibitors like pyrophosphates by degrading pyrophosphate groups and releasing phosphate ions [35]. BSP promotes biomineralization through functioning in mineral nucleation [35]. Detailed information about BSP protein structure and function is present at the next subsection (1.1.3). Osteocalcin (OC) and osteopontin (OPN) are late stage markers of osteoblast differentiation and they both bind calcium, and their expression levels are increased during the mineralization stage [36, 37]. Because BSP and OPN bind to integrin proteins, they are also classified as small integrin-binding ligand, N-linked glycoproteins (SIBLINGs) [35]. Tenascin-C (TN-C), another matricellular protein like BSP and OPN, causes cell rounding during morphogenesis, thus osteoblasts fail to spread because of tenascin-C expression according to some studies [38, 39]. However, there is some controversy on the role of tenascin-C as some studies that claim a TN-C-mediated cell spreading are also present [40].

Parathyroid hormone (PTH) is a peptide hormone that has regulatory roles in calcium and phosphate homeostasis, and in bone formation and resorption by being a ligand of PTH/PTH-related peptide (PTHrP) type I receptor [41], a G-protein-coupled receptor (GPCR) that is expressed in pre-osteoblasts, osteoblasts, MSCs and bone lining cells in bone, and downregulates sclerostin expressed by osteocytes to rescue the inhibition of the canonical Wnt/β-catenin signaling, therefore favoring the osteoanabolic actions to proceed [42].

1.1.3 Biomineralization

Biomineralization is a dynamic and lifegoing process in which living organisms produce and deposit minerals. In healthy people, biomineralization occurs in bone, cartilage and teeth. Bone is a natural composite material and 90% of its

organic components are type I collagen and the remaining part contains noncollagenous proteins [43]. Inorganic components of bone are mainly composed of hydroxyapatite, $Ca_{10}(PO_4)_6(OH)_2$ [43]. Deposition of hydroxyapatite crystals occurs in an organized manner to provide a hierarchical organization to the bone (Figure 1.2). Mineral deposition is regulated by bone cells and the ECM they produce, where promoters of mineralization activate mineral nucleation and inhibitors of mineralization protect the ECM by preventing the nucleation at the times when mineralization is not desired [44].

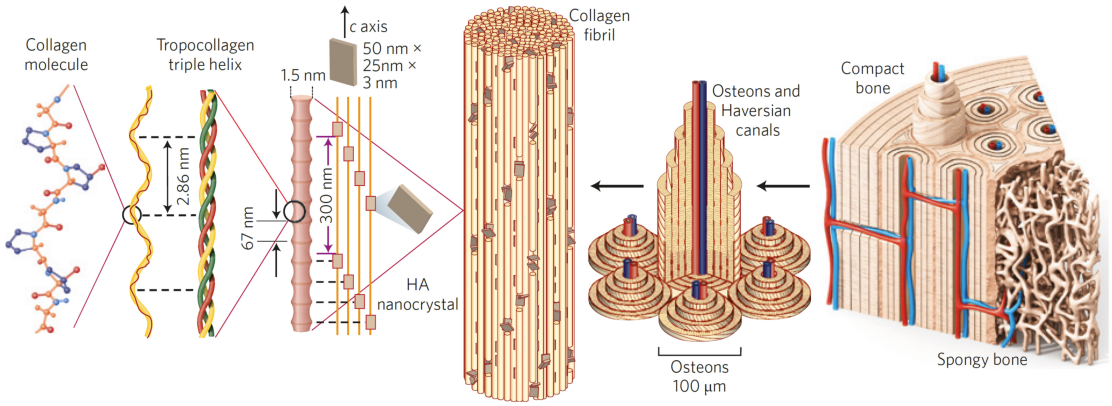


Figure 1.2: Bone structure and organizations of compact (cortical) bone at macro-, micro- and nanoscales. Compact bone is diagrammatically shown with osteon structures at the microscale that contain collagen fibrils and hydroxyapatite nanocrystals at the nanoscale. Illustration reprinted with permission from a review by Wegst *et al.* [45].

Osteoblasts function in the initiation of mineral deposition [46]. Osteoblasts first secrete a non-mineralized osteoid matrix that contains type I collagen fibrils and noncollagenous ECM proteins [47, 48]. There occurs a progressive stiffening of the collagen fibrils due to nucleation of minerals during the maturation stage of osteoblast differentiation. This stiffening is known to be physiologically important but its mechanism still remains to be elaborated [49]. Osteoblasts secrete the calcium and phosphate ions into bone ECM [50, 51]. Osteoblasts and osteocytes are known to interact with each other which might also be an aiding/contributing factor to the biomineralization (Figure 1.3). Participation of osteocytes to the mineralization process and, specifically, what roles they actually take on remain to be investigated further [35], even though there have been investigations on the subject and osteocytes were argued to play a regulatory role

in mineral homeostasis and osteoblast behavior [52].

Secretion of some non-collagenous ECM proteins regulates hydroxyapatite nucleation on the collagen fibrils. BSP, a SIBLING protein found mostly in the bone ECM, has important roles in skeletal mineralization and has a binding segment to collagen (Figure 1.4). Functions of BSP include initiation of hydroxyapatite crystal formation, attracting phosphates and concentrating calcium ions via electrostatic interactions [53]. Moreover, its expression was claimed to help formation of the osteoblastic cell morphology [54]. In the protein structure of BSP, there are repeats of glutamic acid (Glu) amino acids (polyglutamate stretches) at the Ca^{2+} binding site (Figure 1.4). On the role of amino acids in biomineralization, one group reported that Glu has an inhibiting effect on hydroxyapatite nucleation [55]. However, BSP protein having polyglutamate sequences at the Ca^{2+} binding site favors mineral nucleation [56, 57]. In a comparison study of variable-length polyglutamate addition to a collagen-mimetic peptide (DGEA), binding of the peptide to β-tricalcium phosphate significantly increased as the number of glutamate amino acids added was increased from 0 to 2, 4 and 7 glutamates [58].

OPN, another SIBLING, is a key regulator that can inhibit the hydroxyapatite nucleation upon its phosphorylation [36]. Absence of BSP causes an upregulation of OPN expression [59] and OPN is the only SIBLING protein expressed in a BSP knockout (BSP-/-) mice, whose expression level is higher than that of wild type mice (BSP+/+) [60]. Absence of BSP causes impairment of terminal osteoblast differentiation, however, does not prevent commitment of MSCs into the ostogenic lineage, recruitment of MSCs, and their initial differentiation into osteoprogenitors [53]. Overexpressing BSP leads to an enhancenment of osteoblast differentiation via increases in expresions of osteogenic markers including Runx2, osterix and osteocalcin [53].

Osteonectin, also known as SPARC, is a bone tissue specific protein that selectively binds to both hydroxyapatite and collagen, primarily found in the ECM and is responsible for linking minerals to collagen fibrils [41]. Osteonectin activity leads to increased fibril assembly, cross-linking and accumulation of collagen in the ECM [12].

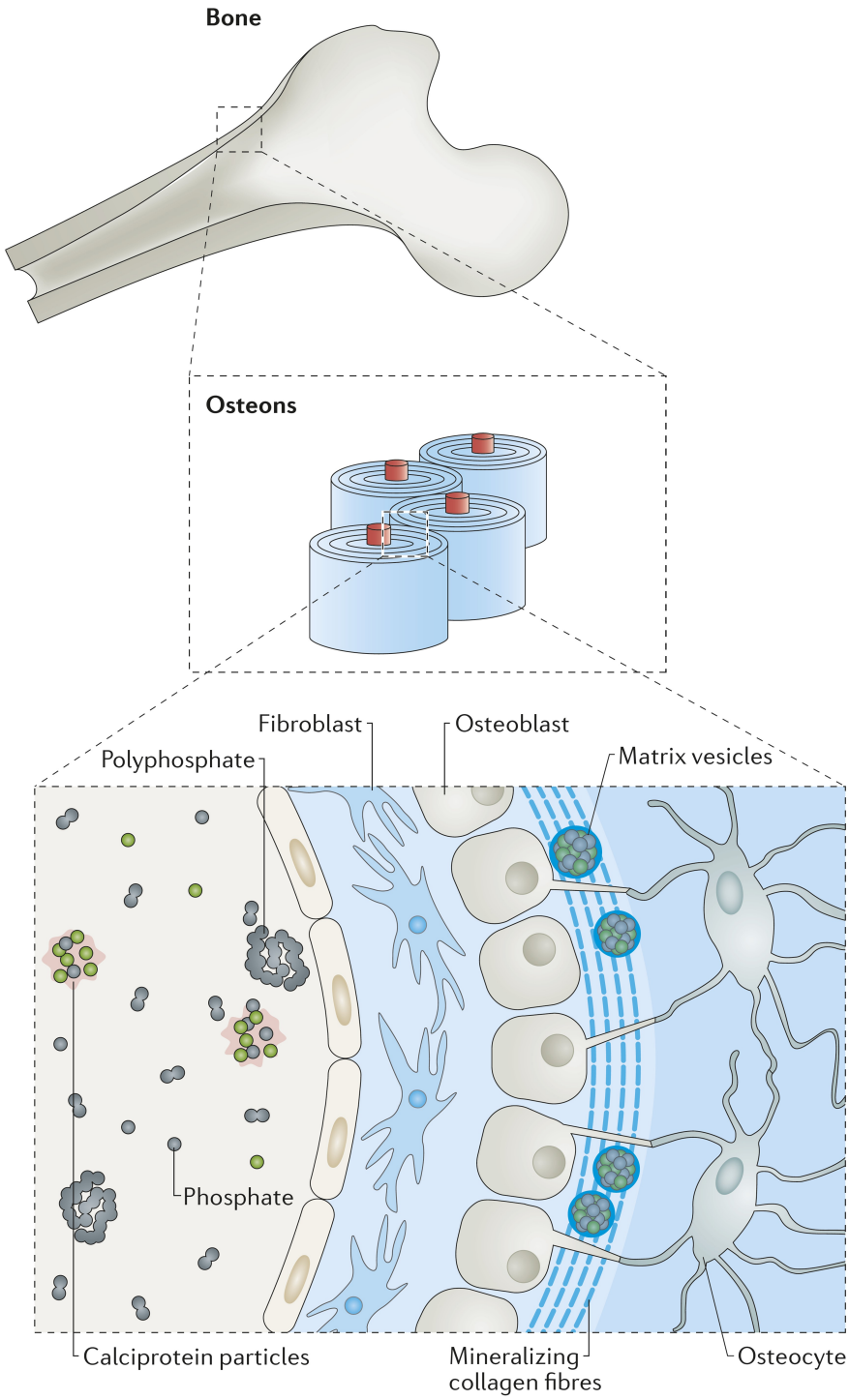


Figure 1.3: Regions of biomineralization in the bone. Osteoblast-osteocyte interaction is shown. Osteons contain osteoblasts and osteocytes communicating with each other. Role of osteocytes on biomineralization is to be investigated further. Figure is a reprint from a review by Reznikov *et al.* [35] with permission from Nature Publishing Group.

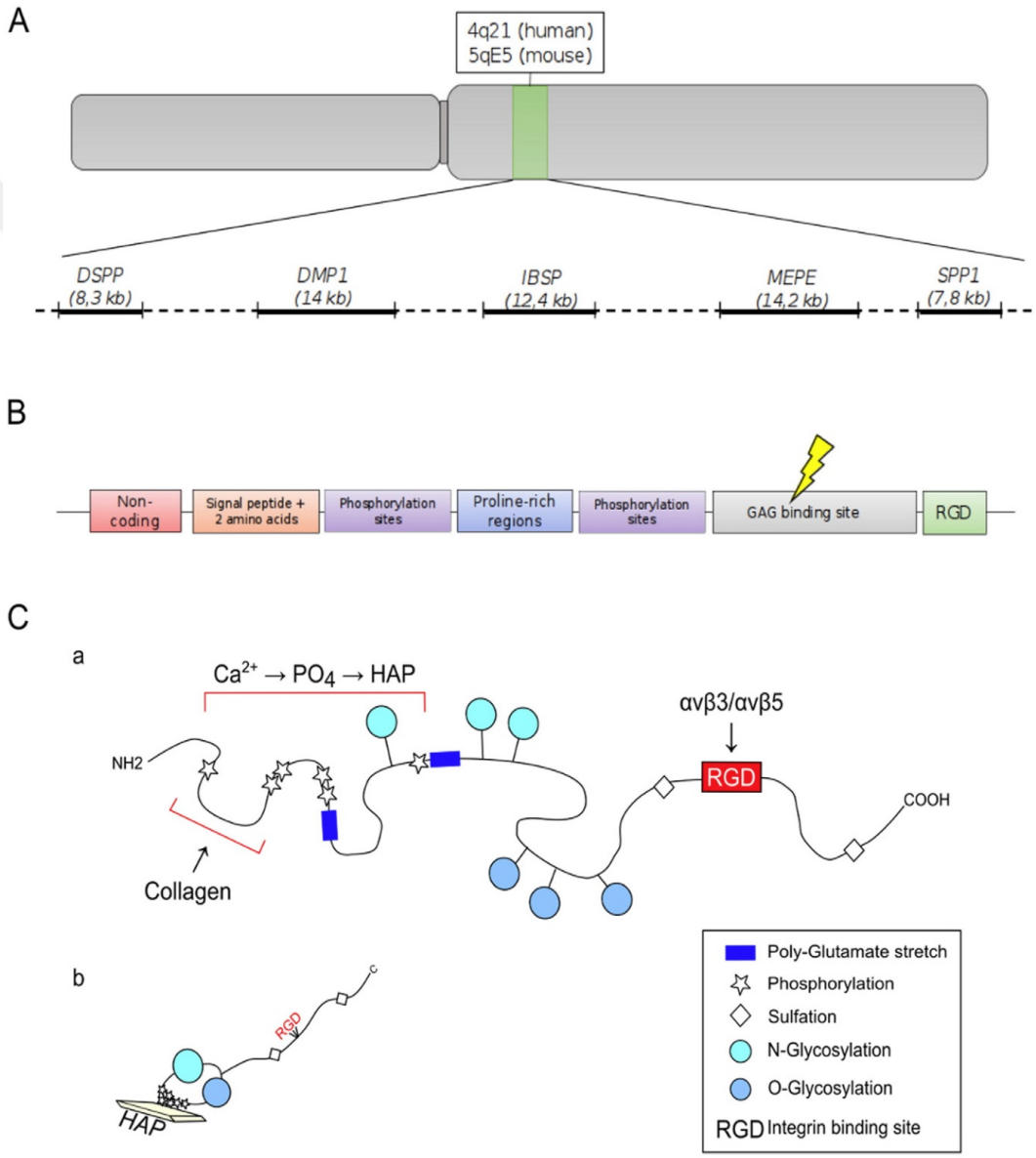


Figure 1.4: Chromosomal location and size, and protein structure of bone sialoprotein (BSP). This figure is a reprint obtained with permission [53].

Contribution of matrix metalloproteases (MMPs) to osteogenic differentiation has also been reported. For instance, metalloproteinase MT1-MMP is important in formation of bone nodules and mineral nucleation [61, 62].

Structural disorder of proteins favors growth phase of mineralization [63, 64]. Peptide nanofibers might be good candidates to provide disordered nano- and microstructures (*e.g.* fibers and bundles, respectively) to the cells. Peptide nanofibers are discussed in Section 1.4. Most noncollagenous proteins of bone ECM including BSP and OPN are intrinsically disordered proteins (IDPs), which allows them to have different interactions because of having flexibility (*e.g.* random coil) in their shape [44] and being multifunctional as they usually have different binding sites like calcium binding site, collagen binding segment and RGD sequence (Figure 1.4).

An example to novel approaches of biomineralization-inspired studies could be a noncovalent vaccine engineering study where viruses were engineered to secrete peptides with abilities of inducing biomineralization via calcium phosphate [65]. Although the goal of the study was immunization, novel methods like this can be tried for promoting bone regeneration.

1.1.4 Mechanical properties of mineralized tissues

Calcium content is correlated to high Young's modulus and hardness values in mammalian mineralized tissues like long bones and dental tissues [66]. Because having high elastic moduli is proportional to the mineral content, clinical conditions that involve deficiency in calcium-phosphorus product end up with a decrease in stiffness values of the tissues [35].

Young's modulus of dentin tissue is usually found within 10-30 GPa value range according to measurements with compression, nanoindenter, atomic force microscopy and 4-point bending methods [67]. Ultrasound and microtensile measurements gives an average trabecular (cancellous) bone Young's modulus of 14.8 GPa $\pm$ 1.4 and 10.4 GPa $\pm$ 3.5, and an average Young's modulus of cortical

bone Young's modulus of 20.7 GPa ± 1.9 and 18.6 GPa ± 3.5 [68]. In a recent nanoindentation based study performed with Berkovich tip, Young's modulus values of human periosteal cortical bone, endoosteal cortical bone and trabecular bone were found to be 7.63 ± 1.31 GPa, 7.48 ± 3.09 GPa and 5.11 ± 2.82 GPa, respectively [69].

Mineralizing collagen fibers take role in the regulation of physiological mineralization of bone where the calcium rich matrix vesicles are located on according to a recent review [35]. Hence, mechanical properties of the bone are influenced remarkably by collagen matrix. There has been reports on the predominant role of fibrillar collagen on the bone biomineralization based on control of the size, three-dimensional distribution, and nucleation of apatite crystals at larger scales [70].

Human MSCs-seeded into calcium phosphate mineral deposited scaffolds were investigated for analyzing their mechanical properties via compression system and it was found that mineralized scaffolds had dramatically higher and increasing elastic modulus values than non-mineralized scaffolds which were very low and steady according to measurements performed at days 14, 28 and 56 of osteogenic differentiation [71].

Spherical cellular aggregates, also known as spheroids, have been mentioned as good candidates in the literature for studying tissue mechanics *in vitro* [72, 73] and they are introduced and discussed in the following subsection.

1.1.5 Stem cell aggregates

MSC aggregation mechanism was proposed before as assembly, reorganization and compaction of cells via involvement of integrin and cadherin proteins, and the contribution of tension forces, cortical tension and actin stress fibers [74]. Similarly, E-cadherin was also pointed out to play important roles for embryonic tissue compaction and three-dimensional organization of stem cells into spheroids [75, 76]. Some of the integrin alpha subunits (*i.e.* α1, α2, α4, α9, α10, α11) have

collagen binding specificity [77], which might be helpful to suggest that some osteogenic cells within differentiating MSC aggregates, such as mature osteoblasts, increase deposition of extracellular minerals via mechanosensing their microenvironment consisting of mostly type I collagen fibrils. Recently, osteogenic differentiating MSC spheroids in collagen gels were shown to deposit higher amounts of calcium than a monolayer of adherent MSCs on the collagen gels [78]. Spheroids are known to be promising for tissue engineering and regenerative medicine (Figure 1.5). I am referring the cell aggregates and spheroids here because I observed similar compact aggregates of differentiating MSCs on the peptide nanofibers that I utilize for promoting osteogenic differentiation, as discussed in Section 1.4. Spheroid organization of mouse embryonic stem cells was argued to be regulated by physical confinement signals [75]. Similarly, peptide nanofibers might be causing MSCs to be in a physically confined microenvironment and thus forcing the MSCs to aggregate as spheroids. I intended to measure Young's modulus of the cells of the aggregates which may have more realistic values, or in other words, might better represent the native cellular organization of osteoblast-like cells *in vivo* because they resemble bone nodules in cell morphology and mineral deposition ability.

Cell aggregates were suggested in the literature to migrate in a collective manner where cells can be thought to be linked to each other with springs [79]. About the spreading dynamics, it was pointed out that cells of the aggregate/spheroid act like a liquid drop whereas cells escaping from the spheroid were claimed to act in a 2D gas state [80].

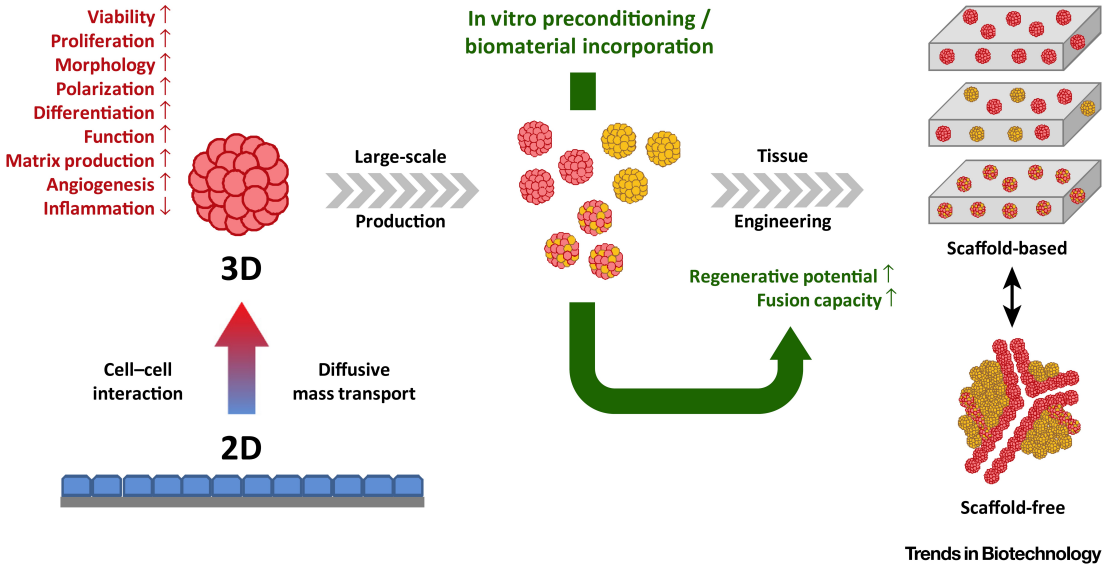


Figure 1.5: Spheroids or stem cell aggregates are promising for tissue engineering because of their regenerative potential. In this diagram both scaffold-based and scaffold-free approaches for using spheroids are presented. This figure is reprinted with permission of Laschke *et al.* [81].

1.2 Mechanical analysis techniques for single cells

1.2.1 Micropipette aspiration

The mechanical properties of cells can be studied by using a micropipette, a rigid tube, at which a cell is drawn into, which leads to the formation of a cell protrusion. Then the surface tension can be calculated based on the length of the cell protrusion and the pressure difference between inside and outside of the micropipette [82]. Typically, cells in suspension are analyzed, but substrate-adhered cells can also be studied by using the micropipette aspiration technique [83].

Sea urchin embryos were measured in 1954 with "cell elastimeter" that Mitchison and Swann described, of which the results provided a better understanding

of cytokinesis, the cytoplasmic cell divison [72]. Since then, micropipette aspirations were used for cell mechanics studies, especially with the suspended cells to measure their surface tension and viscosity and thereby also to determine their elastic modulus. Cytoskeletal surface tension (cortical tension) is tensile (stretching) force per unit area within the cell membrane, and can be measured using this technique assuming that the cell behaves like a liquid drop. There are various liquid drop mechanical models like Newtonian model and Maxwell model which can be applied to calculate the surface tension from the micropipette aspiration measurements [84], which I will not discuss here.

Micropipette aspiration measurements of chondrogenic differentiating human MSCs showed that the differentiated cells increased their stiffness [85]. According to a micropipette aspiration based cell mechanics study, while human MSCs also increase their elastic modulus during osteogenic differentiation, they decrease their elastic modulus during adipogenic differentiation [86].

Plasticity of cell nucleus was also studied using the micropipette aspiration and nuclei of embryonic stem cells were found to stiffen 6-folds through terminal differentiation [87].

It is also possible to analyze cellular aggregates (or spheroids) by using the micropipette aspiration technique at the suspended state because of collective mechanical behavior of cellular aggregates as intercellular junctions (*i.e.* cadherins) allow the cells to have strong chemo-mechanical interactions with each other. Micropipette aspiration of cellular aggregates was first reported in 2010, where the study estimated a 700 Pa elastic modulus and 5-7 mN/m surface tension of spherical cellular aggregates of sarcoma (S180) cell lines expressing various levels of E-cadherin molecules at their cell surface [88]. It might be beneficial to study cellular aggregate mechanics to better understand tissue mechanics because spheroids are closer to tissues than monolayers of cells in that they express ECM material and that there are intercellular junctions between the cells that are in close contact with each other in three-dimensions unlike the monolayers of cells which express ECM material and connect with intercellular junctions. Furthermore, micropipette aspiration technique can be applied *in vivo* as well.

Disadvantages of micropipette aspiration technique are that the curvature drawn into the micropipette might cause damage to the cell(s) and that the friction between wall of glass micropipette and the cell(s) is usually neglected in the measurements, assuming that the glass wall is non-adhesive to the cell(s) [89]. Other than those, it is a simple and inexpensive technique, is possible to apply to both suspended and adherent cells, and can even be used for *in vivo* tissue mechanics, which make it a really interesting and advantageous technique.

1.2.2 Microrheology

Rheology is the study of deformation and flow of matter in response to an applied stress. It is conventionally performed with a rheometer equipment which performs parallel plate compression on several millimeters of a material. A new way of doing rheology is microrheology where a micron scale probe embedded in the material is used to deform locally. This might be more advantageous for the case of cellular measurements because traditional rheometer measures bulk samples at macroscopic scale whereas microrheology has a measurement capability at the cellular scale and single cells can be studied more easily. Microrheology is classified as active and passive. Approach of active microrheology techniques is very similar to traditional rheology because there is stress applied to the material in both, however, differently in active microrheology, a micrometer-sized bead is used and the elastic and viscous properties of the cell determine how the bead moves on or inside the cell [90]. Magnetic twisting cytometry (MTC) is one of the active microrheology methods and a magnetic micrometer-sized bead is rotated on top of a cell via magnetic forces exerted from twisting and magnetizing coil [90]. The bead position is tracked to determine the mechanical response, thus MTC is good for measuring the mechanical properties of adherent-cells [90]. Notably, Francis Crick tried to measure physical properties of cytoplasm using MTC technique [91]. Magnetic pulling is another active microrheology method where magnetic tweezers are used to pull the magnetic microbead [90].

Passive microrheology is different from active microrheology and simpler in

terms of laboratory equipment need because there is no applied stress on the material (*i.e.* picoNewton or nanoNewton forces are needed in active microrheology which requires advanced laboratory equipment) and rather the approach is based on thermal excitation of bead particle without application of an external force [90]. Laser particle tracking microrheology is an example to passive microrheology in which the viscoelastic modulus can be measured with wide bandwidth inside the cells after inferring from the Brownian motion of particles embedded in the cytoskeletal network [92].

1.2.3 Optical trapping, optical tweezers and the optical stretcher (OS)

Arthur Ashkin realized in 1969 that manipulation of dielectric particles might be possible by using intense laser based on its radiation pressure [93]. In 1980s, he demonstrated a single focused beam trapping in a three-dimensional optical trap for dielectric particles [93, 94]. Optical stretching (OS) in the time domain introduced by Guck and Käs surpasses optical tweezers or optical traps for use in cell mechanics studies because it is not limited in force since focusing is not required and hence OS can deform the cells unlike the optical tweezers, which are not sufficient in force range for deforming the cells [95]. Notably, OS can be used to measure the deformability of adherent cells and non-adherent cells in suspension high-throughputly, about 100 cells per hour [22, 96].

1.2.4 Traction force microscopy (TFM)

Cell traction force microscopy, a relatively newer technique than those aforementioned, is used to determine tractions for quantitation of cell mechanics of adherent cells first through the computation of displacement fields from embedded fluorescent marker beads and then by reconstruction of the cellular traction [97]. Three-dimensional reconstruction and distribution of cellular tractions were recently studied with hydrogel substrate and matrices [98, 99]. Traction forces

exerted by cells are lateral to the substrate/matrix and inward to the cell center [100]. Deformation of substrate/matrix induced by these traction forces is measured in TFM [82]. Therefore, an understanding of the mechanical properties of the matrix utilized is also required for TFM measurements [101]. Another important requirement is to have an ability for tracking the motion of beads such as cross-correlation which allows precise determination of position hence the displacement fields of particles [82]. Resolution of TFM is 1-3 µm [102] and the force range is between 2 and 120 nN [101]. TFM allows studying inherent contractility of adherent cells by measuring distribution and magnitude of traction stresses generated through their focal adhesions [103].

There is an issue of non-linearity of fibrous structures in substrate materials like in the native ECM, that is, the stiffness of individual nanofibers is relatively much larger than the network of fibers and bundles, which might complicate the characterization of appropriate properties relevant to cells [101]. In other words, stress over strain ratio is not constant through changes unlike the linear elastic materials, but rather is dependent on the magnitude of the strain for the native ECM or ECM-mimicking fibrous networks [101]. Another issue could rise from reliability of determination of displacement fields because there might be possible effects of change of cell mechanical over the displacement fields and furthermore if the level of confluency is high, the displacement fields might overlap [101].

1.2.5 Atomic force microscopy (AFM)

AFM is a powerful technique that allows to measure images of atoms in real space. Not only it has sub-nanometer high-resolution imaging capability for any type of material, but AFM has capabilities like mechanical analysis and electrical characterization measurements. Imaging and force-distance curve measurements in a physiological environment make AFM a very valuable tool for cell mechanics studies of substratum-adhered cells. Preferring AFM for mechanical analysis of cellular aggregates on peptide nanofibers is feasable, although there might be certain challenges like undesired adhesions of the sample to the AFM probe and

limited Z range of AFM (*i.e.* usually 10 µm or 20 µm) for performing force curve measurements on cellular aggregates, which can typically be higher and thus difficult to measure. AFM will be described in more detail in section 1.3.

1.2.6 Brillouin microscopy

Brillouin scattering is inelastic scattering of an incoming light with acoustic waves (phonons) in the sample. Confocal Brillouin microscopy is based on this scattering and the analysis of Brillouin spectrum, that can be used to obtain the Brillouin frequency shift and longitudinal modulus of the sample analyzed. It is a very new technique and is still under development. Living cells and tissues can be analyzed non-contact and thus with a less invasive way compared to the AFM. After spectrometers that contain virtually imaged phased array (VIPA) etalons were first used by Scarcelli and Yun in 2008 to improve spectral contrast up to gigahertz spectral resolution [104], popularity of Brillouin microscopy started to increase towards analysis of biomechanical properties of cells and tissues, and recently noncontact three-dimensional mapping of intracellular hydromechanical properties of living cells was demonstrated [105]. The technique has highlights for use not only in cell mechanics but also in ophthalmology [106], and for imaging developing embryos [107].

1.3 Mechanical models for cell mechanics

Mechanical models directly influence characterization of the mechanical properties of living cells. They are generally grouped under two main categories, which are continuum-based models and micro/nanostructural models [84, 108], as shown in Figure 1.6.

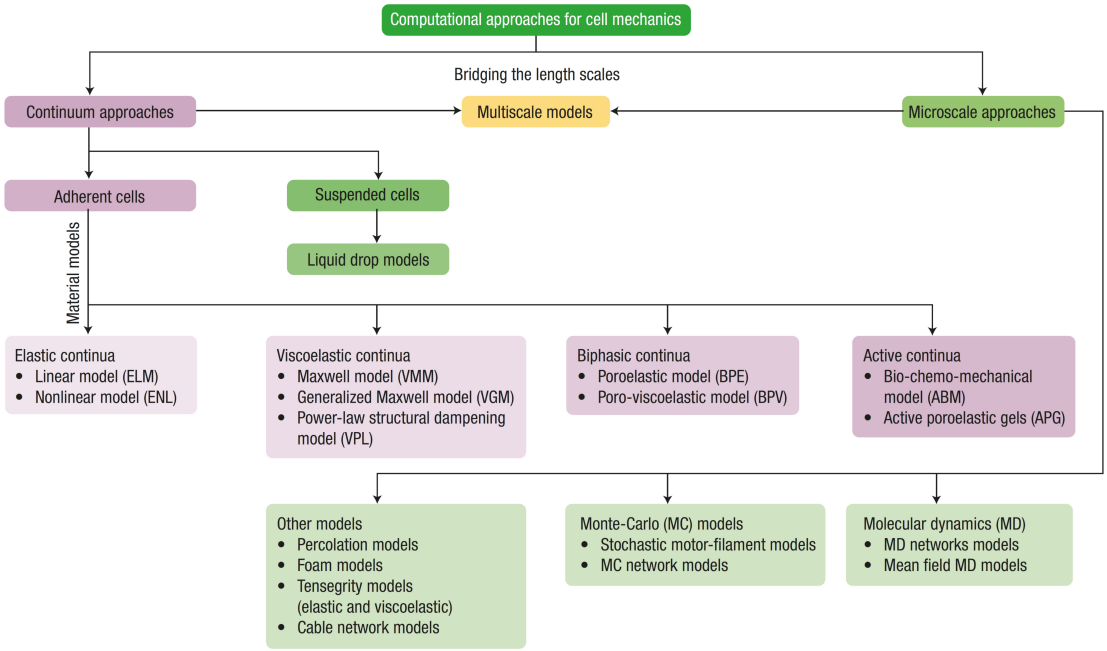


Figure 1.6: Mechanical models or computational approaches for analyzing the mechanical properties of cells, biomolecules and other biological materials can be listed as shown here. The figure is a reprint from [108] with permission from Nature Publishing Group.

1.3.1 Continuum mechanics models

1.3.1.1 Continuum based models for adhered cells

The elastic model is a simplified version of viscoelastic model where viscosity effects and time are not taken into consideration for calculation of elastic properties (*i.e.* elastic modulus) [84]. Elastic solid models can be divided based on linearity into two: linear elastic solid model and non-linear elastic solid model [108].

Viscoelastic modelling can be performed by combining spring elements that represent elastic deformation and dashpot elements that represent the viscosity. They can be used in combination to describe, for example, instantaneous and delayed elastic deformations [109]. Parallel combination of spring (stiffness) and dashpot (viscosity) is known as Kelvin Voigt element of which the elasticity determines the stationary state [109]. Combination of the two in series is known

as Maxwell element where a summation of contributions of elastic deformations and the viscous contributions (that depends on time) is taken into consideration for the Maxwell model, which is the simplest viscoelastic model [110].

There have been significant advances in the recent decades on modelling of adherent cells. Rheological behavior of cytoskeleton was argued to follow soft glassy rheology model, a power law model, based on experimental investigations [108], and then a more recent report carrying experimental work validated a poroelastic model that assumes a biphasic continuum for the behavior of cytoplasm rheology of which the cytosol as an interstitial liquid phase allows water redistribution to be plausible through a porous elastic solid phase consisting of cytoskeleton, organelles and macromolecules [111].

Even three-dimensional cell culture was argued to be only partially mimicking the *in vivo* tissue architecture and it was reported that the *in vivo* tissue follows non-linear rheological behavior [112].

1.3.1.2 Continuum mechanics models for AFM analysis of adherent cells

Transformation of AFM's force curve data to material properties like Young's modulus is accomplished usually by elastic solid models like Hertz contact mechanics model and viscoelastic continuum models like power-law material models [113, 114]. However, none of the aforementioned mechanical models can simulate every aspect of cells due to the complexity present in living matter but the existing models only make approximations to the conditions and parameters. Even if that is the case, present models are somewhat good for obtaining relatively reliable values of elastic modulus values of cells, for example, Hertz contact mechanics model has been used for fitting force curves in the majority of studies that use AFM for mechanical characterization of cells, and Hertzian fitting of approach curves are surprisingly well although it is a very old model originated by Heinrich Hertz, who first produced a solution based on theory of elasticity to the deformation related problem of contact between two smooth bodies in 1881

[115].

Force volume mapping is very suitable for using Hertz model because it is a quasi-static mechanical analysis method, however, when a dynamic model is used where peak force tapping is involved, viscoelastic contributions should be taken into consideration for deriving the Young's modulus values. Moreover, with dynamic AFM modes, it is possible to obtain mechanical properties other than elastic modulus such as power-law exponent, dissipation energy, and separately the storage modulus and loss modulus.

Hertz contact model assumes indenting of a linear elastic solid, an infinite homogeneous half-space, on a rigid substrate surface with small indentation [115, 116]. It was reported that Hertz model failed when applied to thin layers of soft materials like thin (*i.e.* submicrometer thickness) polymer gels [117]. It was pointed out about the conventional Hertz cone and sphere models that they worked well when applied to sectioned tissue samples with an indenting probe with a radius up to 2.5 µm [118]. Regarding errors encountered at AFM data analyses, especially to that are led by Hertz model at force curves of living cells, 20% error can be expected for rounded cells and a 10% error can be expected for well-spread cells of MSCs and osteoblasts according to a report [119].

Lifshitz and Landau studied theory of elasticity and extended the Hertz contact mechanics model by deriving the results of Hertz's again and adding expressions for stress and displacement fields [117]. Love and Sneddon studied Bossinesq's problem for a rigid cone [120, 121]. Bossinesq's problem was the first to address the determination of the state of stress that is normal to an isotropic elastic half-space of which the load is applied [122]. Hertz model (can also be referred as Hertz sphere model) describes the indentation of a spherical tip to the sample and takes the radius in the calculation whereas Hertz cone model, also known as the Sneddon model, assumes that the tip geometry is conical and therefore, the calculation depends on the half-cone angle instead of the tip radius.

When the tip geometry is something between a sphere and a cone, neither Hertz nor Sneddon model can truly describe the indentation measurement, where the

analysis and the result might possibly be wrong. To solve that problem and to rule out such a possibility, some reports like a recent one by Ros group proposed a contact model for a conical indenter with a spherical tip that took a piecewise depth-dependent fitting method (Figure 1.7). However, as can be observed from the Figure 1.7D, the Sneddon model appears to work well for indentations larger than 2 µm, as the Young's modulus result converges to that of the simulation modulus.

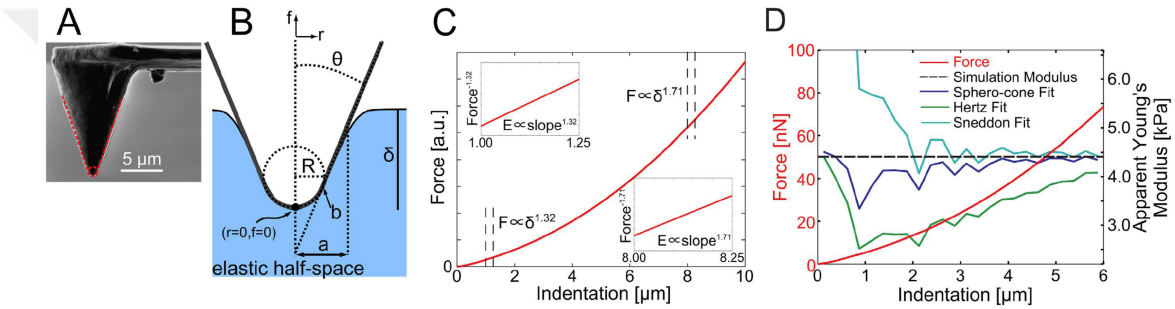


Figure 1.7: Sphero-conical probe A) shown with SEM image and B) diagrammatically drawn to describe indentation. D) Sphero-conical fitting with a contact mechanical model proposed for the sphero-conical indenter, which is shown with comparisons fits of Hertz and Sneddon models, all applied to a theoretical force-indentation curve data generated by finite element analysis. The figure is a reprint from [123].

JKR (Johnson–Kendall–Roberts) model can be used for studying contact between two spheres when strong adhesive forces are desired for consideration in conversion of force curve data to Young's modulus data of cells and gels [124]. Attractive forces are not included in the Hertz model. Applying JKR to retraction curves makes sense for living cell samples because force curves of cells have adhesion force on the retraction curve but not on the approach curve. After a maximum load, there is a transition between Hertz to JKR model due to viscoelasticity of cells [124]. Hydrogels were studied using Hertz model and JKR model fittings to the approach and the retraction curves, respectively [125]. The differences in the results between the two approaches utilized were not too much. High crosslinked gel was measured to be 16.6 ± 0.9 kPa according to Hertz fit to the approach curve and 14.6 ± 0.8 kPa based on JKR fit to the retraction curve [125]. Low croslinked gel had 8.1 ± 0.4 kPa according to Hertz fit to the approach curve and 6.02 ± 0.8 kPa based on JKR fit to the retraction curve [125]. The

study used AFM for the measurement and the authors named the technique as nano-rheology because the AFM measurements were performed at the nanoscale for obtaining both the storage and loss moduli, same as the parameters obtained from a traditional rheology measurement. So, when a microsphere probe is used for the mechanical characterization of the sample, the technique can be so-named as microrheology and microindentation measurements as well.

There is the issue of substrate effects when AFM is used for mechanical characterization and it can be expected that cellular elastic modulus values might be influenced not only by the indenter but also significantly by the substrate as well and indenting cells on stiff substrates may lead to overestimation of Young's modulus values while indenting cells on much softer substrates might end up with significant underestimations. Interestingly, in a recent report, multi-cellular nodule formation of fibroblasts was present on substrates having elastic modulus values less then the elastic moduli of fibroblasts but the fibroblasts did not form multi-cellular nodules on glass coverslip and instead were as single cells, where polyacrylamide hydrogel substrates were used with differing elasticity values of 0.3 kPa, 0.5 kPa, 1.4 kPa in the study [126]. On 1.4 kPa polyacrylamide substrate, there were nodules first and then plaques of the cells in the following days [126], which may imply that there is a tendency within the cell population to form spheroids when the substrate is soft while there are more single cells and monolayers of cells on stiff substrates like glass coverslip. As such, cellular behavior might change on different matrices and hence cellular aggregates like spheroids might need to be treated differently from single cells and monolayers of cells on flat, stiff substrates like bare glass coverslip when AFM based mechanical measurements are preferred and their analysis using contact mechanics models is to be done so that a better approximation to the cellular responses during indentation measurements can be achieved if suitable modifications can be done to existing mechanical models or even new models can be suggested for such special cases. While contact models typically consider only the interaction between the probe and sample, Glaubitz *et al.* developed a bipartite contact model that accounts for sample deformation due to both the indenting probe and the pressure expressed by the substrate underneath the sample [116]. Accordingly, the Hertz model

was employed to describe the probe-sample interaction while the JKR model was used for sample-substrate interactions. This "mixed double contact model" might especially be useful for microindentation analysis of spherical cellular aggregates, as the error it addresses depends on the radius of the indenter, the sample and the substrate [116].

Although AFM studies mostly use linear elastic or linear viscoelastic models for calculation of mechanical properties of cells, non-linear viscoelastic models are also sometimes studied. For example, a recent report targeted viscoelastic identification of breast cancer cells and involved measurement of the shear relaxation modulus and determination of the nonlinear elastic contributions, for which a neo-Hookean model was used in the report, and also came up with a novel inverse analysis of results of AFM indentations [127].

Brush model was proposed by Sokolov group to achieve consistency in quantitative use of AFM for characterization of Young's modulus values of cells to utilize as a marker [128, 129, 130]. Assuming that cell is a spherical object and the cell surface brush is softer than the cell itself, the model separates the elastic deformation of the cell body from the elastic deformation of the brush layer [130]. The same group proposed a double-brush layer model in a recent study with fibroblast cells in which the AFM tip first encounters long, hyaluronan-based pericellular brushes followed by a brush layer of corrugated cell membrane [131]. As such, derivation of elastic modulus has been considered challenging not only due to the presence of non-linearity, that is, the cell is acting like an elastic solid at small deformations and behaving as a viscous liquid-like body, but also due to the complexity of the nanoscale outer layers of cell surface brushes might require some use of advanced mechanical models for quantitative, accurate and reliable determination of the mechanical responses by better exploiting and fitting different regions of the force curves measured on the cells.

Measured Young's modulus values can differ significantly depending on the frequency used during force curve measurements. Higher frequencies, such as those used in peak force tapping mode measurements, have been associated with higher Young's modulus values of single cells, indicating an overestimation of the

values [132]. One reason for that may be because the cells cannot see the tip and properly respond to it at such high frequency measurements.

AFM can be used to determine cortical tension of adherent cells from force curve data. Tension model, developed by Sen *et al.* [133], was used in a study where epithelial cells were used and their mesenchymal-like state was characterized based on the changes of tension due to loss of intercellular junctions, and approach curve was fitted based on the tension model to derive the compressibility modulus and the tension [134].

1.3.1.3 Continuum based models for suspended cells

Micropipette aspiration technique and optical tweezers have commonly been used for both non-adherent cells and adherent cells in suspension. A suitable model for deriving the mechanical properties of cells from such experiments can be liquid drop models, where the cells are considered to behave like spherical liquid drops. For example, cortical shell-liquid models like Newtonian liquid drop model in which the membrane cortex is modelled to have a certain tension and the cell body as a droplet body [84], were developed mainly for studying deformability of neutrophils and determining their cytoplasmic viscosity via micropipette aspiration [135, 136].

In a recent report that used micropipette aspiration of cells of *Dictyostelium*, social amoeba, three models were examined for deformations of different extents, linear viscoelastic model and liquid drop model with a tense cortex for small deformations, and a third model for large deformations which was Newtonian viscous fluid model [137]. In a report that used optical tweezers for mechanical characterization of suspended Jurkat cells, a model based on membrane theory was used [138]. In another report that preferred using a microfluidic platform for probing cell stiffness at high-throughput, a real-time deformability cytometry (RT-DC) was used to study suspended cells where a perturbation approach was used for calculating the elastic deformation via first-order approximation and by assuming that the cells were linear elastic and isotropic solid spheres [139]. This

study compared cell stiffness values of a human promyelocytic HL60 leukemia cell line measured by AFM and RT-DC, where the results were E = 170 ± 85 Pa (N=169) and E = 1:47 ± 0:51 kPa (N=281, mean ± SD), respectively [139].

In studies that investigated the viscoelastic behavior of human MSCs (hMSCs), a linear viscoelastic solid model was preferred for the micropipette measurements, that assumed the pressure applied was uniform and the cell had incompressibility, where the viscosity and Young's modulus of the cells being measured were derived [86, 140]. In a study carried out by Maloney *et al.*, optical stretching was used for analyzing hMSCs in the suspended state whose creep compliance measurements were performed and the authors concluded that hMSCs showed power-law rheology behavior as a result of stretching and recovery measurements where they were both modelled with a single exponent [141].

1.3.2 Micro/nanoscale approach

Tensegrity is a building design principle term coined by Buckminister Fuller [142]. The term is a combination of tension and integrity and describes a network of tensed structural elements that resist shape distortion and stabilize the overall shape by resisting to compression by the use of tensile prestresses [142, 143]. Cellular tensegrity model proposes a prestressed inhomogeneous model where the cells generate prestresses by contractile elements of cytoskeleton such as actins to balance the tensile forces coming from other structural components of the cytoskeleton [144, 145, 146]. In this model, mechanical forces can be transferred fastly over long-distances on the order of miliseconds, quicker than the diffusion based transfer of chemical signals [145].

Two-dimensional cable network model was proposed to study the effects of propagation of intracellular stresses on focal adhesion distributions where the cables (*i.e.* actins) are prestressed due to tension but does not show resistance to compression unlike the cellular tensegrity model [147, 148]. Other than cable network and tensegrity models, there is open cell foam model for modelling of adherent cells using micro/nanoscale approaches. In all these three models, the

elastic modulus can be calculated based on the mechanical properties of cytoskeletal elements [149]. In a study where the cellular elastic moduli were calculated and compared based on these three models, open cell foam model gave higher values (10^3-10^4 Pa) than the elastic moduli value that cable network and tensegrity models resulted (10^1-10^2 Pa) [149].

There are simulation based network models like molecular dynamics simulations that are usually preferred for studying biomolecular mechanics [123]. Monte-Carlo simulations can be used to study elastic modulus and equilibrium conditions of overall tissue constructs that contain cells and ECM [150].

1.4 Behind the AFM

1.4.1 History

Gerd Binnig and Heinrich Rohrer first developed scanning tunneling microscope (STM) in 1981, which earned them jointly half of the Nobel Prize in Physics 1986. The other half was awarded to Ernst Ruska for the electron microscope. In 1986, AFM was invented by Binnig, Christoph Gerber and Calvin Quate [151]. AFM uses cantilever sensors as probes which typically has a sharp tip at its end, typically cone or pyramid shaped and having a nanoscale sized apex, which allows contouring non-conducting materials. In recent years, a tremendous progress on measuring AFM images in real-time has been made by researchers, and also recent developments on high-speed AFM technology have allowed to obtain an AFM image at the video frame rate.

AFM has become a versatile platform for manipulating single-molecules and living cells [152]. Simplicity of AFM tempered researchers not only to establish various imaging modes and append more capability to the AFM such as electrical, magnetic, chemical characterizations but also master existing modes by customizing and improving them, establishing new techniques and methodoloical approaches [153]. Furthermore, various AFM probes have been designed and

fabricated to better image and characterize the samples via AFM [154, 155].

Gerd Binnig, Christoph Gerber and Calvin Quate was awarded 2016 Kavli Prize in Nanoscience "for the invention and realization of atomic force microscopy, a breakthrough in measurement technology and nanosculpting that continues to have a transformative impact on nanoscience and technology" [156].

1.4.2 Working principles

In principle, AFM is STM plus stylus profilometer [151]. STM can only measure conductive samples but AFM can measure any materials including insulators and conductors, and AFM can perform the measurements not only in air but also in liquid environment. Both STM and AFM can operate in ultra-high vacuum environment. AFM allows atomic resolution imaging of any type of material and its mechanical analysis at the micro- and nanoscales.

AFM tip or the sample is raster scanned and a three-dimensional topography map is obtained with a very precise height information of the sample. AFM has two basic working modes: contact-mode (DC mode) and noncontact-mode (AC mode). Tapping mode is a noncontact-mode where AFM tip scans the surface of the sample via intermittent contacts with constant oscillation amplitude or frequency whereas in contact-mode AFM, the tip slides on the surface always in full contact position during scanning. Levering can either be optical or mechanical in an AFM system whereas optical levering and detection is mostly preferred in the commercial microscopes. Laser is aligned on the back of the cantilever and the reflected laser light goes to quadrant photodetector (Figure 1.7).

Deflection of the cantilever is calculated based on the angle of reflection and the position of the laser on the photodetector. All signals are recorded in voltage units including the force, and then they are converted to other units (*i.e.* Newton for force, meter for distance). AFM is a very sensitive sensor with attoNewton (10^{-18} N) sensitivity [151]. There are both sample scanning (*e.g.* Asylum Research MFP-3D AFM, Bruker AFMs) and probe-scanning AFMs (*e.g.* JPK Instruments

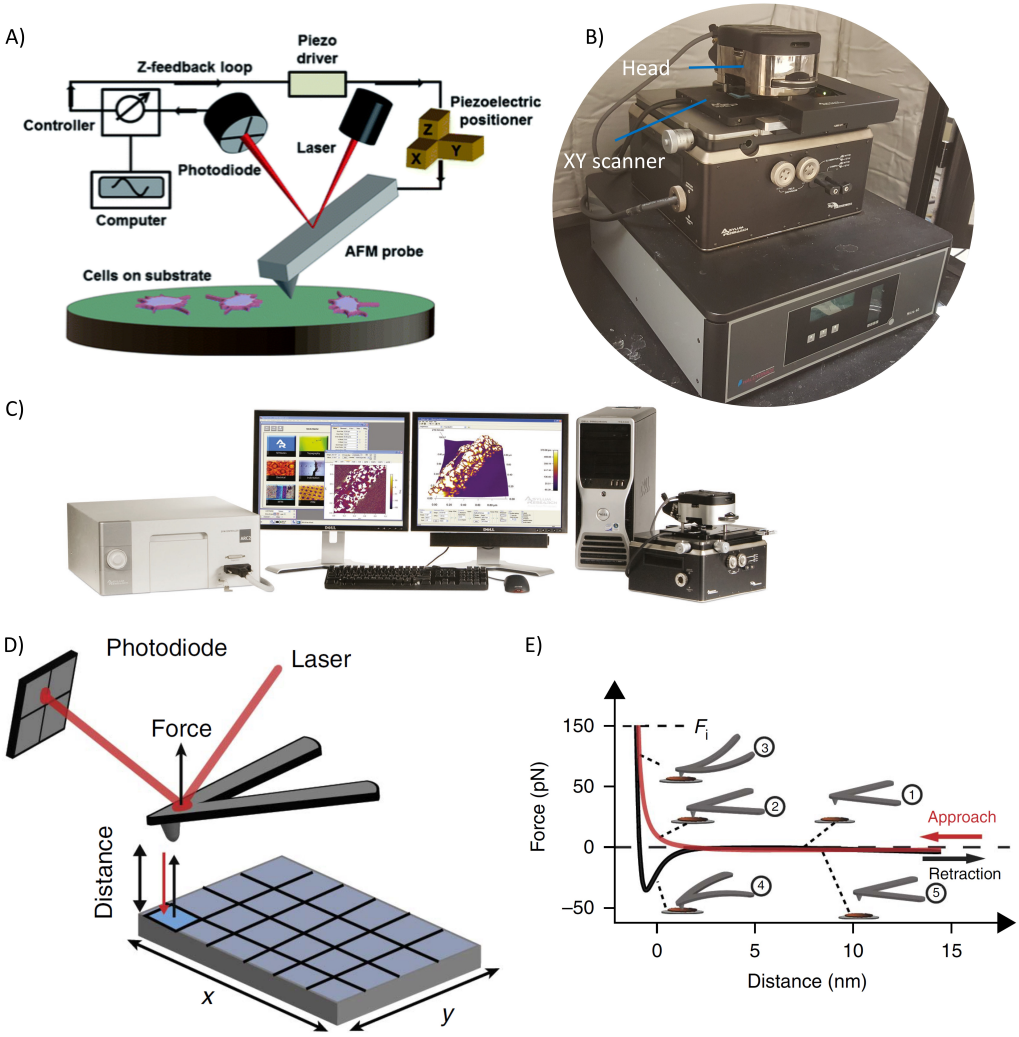


Figure 1.8: A) AFM schematic diagram was reproduced with permission [157]. B) AFM scanner head, XY scanner and base, and C) view of whole setup of Asylum Research brand Molecular Force Probe-3D (MFP-3D) AFM with controller on the very left of the picture. D) Force mapping illustrated and E) a force curve example with respective steps of cantilever movements. D and E reprinted from [158] with permission from Nature Publishing Group.

NanoWizard AFM) that are commercially available.

Young's modulus (or elastic modulus) is the ability of a material to elastically resist to deformation under an applied force or in other words, it is a one-dimensional property defined as the ratio of the stress applied to the material (along an axis) over the strain (at the same axis). Young's modulus is a measure of stiffness and has the same units as the pressure (stress) because the strain is dimensionless as it is the ratio of deformation over an initial reference length. Force-distance curve measurements (Figure 1.7E) allow calculation of Young's modulus upon indentation to various materials from soft biological cells at the kilopascal (kPa) to hard materials like steel at hundreds of gigapascal (GPa) Young's modulus values (Figure 1.8).

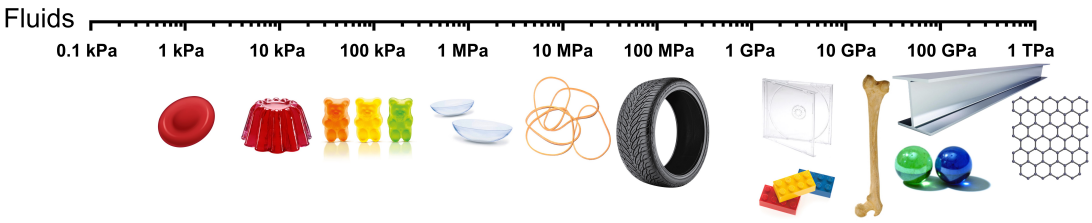


Figure 1.9: Young's modulus scale of various materials, adapted from [159]. Scales are logarithmic.

Force mapping, also called force volume mapping, is recording an array of force curves with a grid pattern in a pixel-by-pixel manner from a specified area of the sample [158, 160] (Figure 1.7D). It is a quasi-static analysis mode of the AFM and allows both obtaining the topography information of the sample and the calculation of elasticity map (or Young's modulus map) when a contact mechanics model like Hertz model is applied for fitting the force curves afterwards (after finishing the measurement). Most of the modern AFMs are capable of simultaneously obtaining the force curves while scanning the sample, named force scanning [161], and this capability allows performing dynamic mechanical analysis and obtaining Young's modulus image of the sample in real-time when using,

for example, the tapping mode. Peak Force Tapping Quantitative Nanomechanical Mapping (QNM) of Bruker and Contact Resonance Mode of Asylum Research and Quantitative Imaging (QI) mode of JPK Nanowizard are some examples to such a capability. Force mapping is quite slow when compared to force scanning when same resolution measurements are desired. For instance, a high-resolution 2056 x 2056 force map would take 1.5 years to finish the measurement while completion of a force scanning measurement with the same resolution would only take an hour [161]. On the other hand, because AFM performs ramping in one dimension, that is Z, during force mapping, it might be more suitable for measurement of force curves for more precise determination of the Young's modulus of the sample than the force scanning because Young's modulus is a one-dimensional term as aforementioned in this subsection whereas force scanning or Peak Force QNM modes require movement of the AFM tip at both X and Z directions at the same time, while taking the force curve measurements.

1.4.3 Elastic modulus characterization studies of osteogenic differentiating MSCs in the literature

The field of cell mechanics and its relation to cell and development biology, physiology, nanophysiology are very important and are still growing as many groups continue to explore more of the nanoworld and the microscopic world. As such, cellular differentiation might be influencing the cellular mechanical properties and since AFM is the most frequently preferred tool for characterization of elastic modulus of substratum-adherent cells, I hereby applied AFM's force mapping capability to osteogenic differentiating MSCs on peptide nanofiber-coated glass substrates and tried to characterize Young's modulus changes throughout the differentiation process. In general, cells, both single cells and multicellular organisms, and tissues have widely been measured by using AFM and some of such studies are listed in a study by our group as well [162]. However, AFM based elastic modulus characterization of cellular aggregates and spheroids is still lacking and Young's modulus of cells on peptide nanofibers also has not been characterized using AFM so far to my knowledge and observation. Hence, here I focused on

AFM measured elastic modulus characterization studies of the MSCs, osteoblasts and osteogenic differentiating cells, and gave an overview about what has been done on the subject.

MSCs were reported to have around 2 kPa (1.9 kPa of spherical cells and 2.4 kPa of spread cells) Young's modulus on poly-L-lysine (PLL) coated polystyrene Petri dishes whereas Young's modulus of osteoblasts vary from 2 to 5 kPa Young's modulus values (2.0 kPa of spherical and 5.8 kPa of spread cells) [163], where the cells were not allowed for differentiation. But when MSCs are allowed to differentiate into the osteogenic lineage for a certain duration, a significant decrease in their Young's modulus values is detected as a result of AFM force measurements [164, 165]. Young's modulus of hMSCs dropped from 3.2 $\pm$ 1.4 kPa to 2.1 $\pm$ 0.9 kPa within a period of 10 days in the study by Titushkin *et al.*, and hMSCs had $\sim$2.8 kPa elastic modulus and differentiated human osteoblasts had $\sim$1.4 kPa, and around 30 cells were measured for each day of osteogenic differentiation analyzed in the study by Bongiorno *et al.*, as also shown in Table 1.1. However, whether these results are representative of *in vivo* is an important point. Growing the cells on ECM or ECM mimetic materials such as peptide nanofibers and performing the measurements *in situ* might be helpful to approximate the actual Young's modulus values of cells *in vivo*.

Osteogenic differentiation of MSCs have been studied by cultivating them in the presence of bioactive peptide nanofibers [167, 168, 169, 170, 171]. However, mechanical characterization of MSCs differentiating on bioactive peptide nanofibers remains to be poorly investigated. An analysis of cells at single cell level is needed, separately from peptide nanofibers. Traditional rheometer is not suitable for measurements at single cell level because it is used for analysis of bulk materials (*i.e.* peptides and cells combined), hence it might be difficult to distinguish individual cell elasticity. For instance, in a very recent study where a micron-scale parallel-plate compression test system was used for measuring embryonic stem cell aggregates incorporated with mineral-coated gelatin microparticles, the authors of the study noted that the compression test they performed only made it possible to measure bulk mechanical properties of entire aggregates that were composed of the stem cells and the gelatin microparticles, and that they

	Matrix/ substrate	**Culture medium**	**Cell type**	***E* (kPa)**	**Ref.**
OD MSCs	Glass	Osteogenic medium	Human MSCs at P3-P9	Drops from 3.2 ± 1.4 to 2.1 ± 0.9 in 10 days	[165]
	Glass	Osteogenic medium	Human BM-MSCs at P4	hMSCs ∼2.8, differentiated osteoblasts ∼1.4	[164]
MSCs	PLL-coated Petri dish	Growth medium	Human BM-MSCs at P4	Spherical cells 1.9, spread cells 2.4	[163]
	TCPS dish	MesenCult^{TM} Proliferation Kit	Human BM-MSCs from P1-2 to P8-9	∼1 kPa at P1-2, increased up to 8 kPa at P8-9	[141]
OBs	PLL-coated Petri dish	Osteogenic medium	OBs from human femoral heads	Spherical cells 2.0, spread cells 5.8	[163]
	Glass	α-MEM	MC3T3-E1	0.9 ± 0.4	[166]

Table 1.1: AFM studies of single cells of osteogenic differentiating MSCs (OD MSCs), undifferentiated MSCs and osteoblasts (OBs) that are not differentiated *in vitro*. BM-MSCs: bone marrow-derived MSCs, P indicates the passage number of the cells, TCPS: tissue culture polystyrene.

were both counted in the results of the measurement [172]. Advantageously, AFM can measure mechanical properties of substratum-adhered individual cells and it has been preferred in most of the experiments for the characterization of Young's modulus of adherent cells where Young's modulus of the cells can be obtained from the force-distance curves. Moreover, AFM can also be used to obtain complex modulus of cells using power-law rheology approach [173, 174]. Peptide amphiphile hydrogels loaded with cells were previously analyzed using traditional bulk rheology [175], however, there is a lack of single-cell level Young's modulus characterization of stem cells on peptide nanofiber hydrogels. Elucidation of stem cell mechanics on the peptide nanofiber hydrogels may help obtaining Young's modulus values nearer to *in vivo* values of cells and lead to a better analysis of mechanical markers and understanding the relationships between mechanical

responses and events during cellular differentiation.

1.5 Bioactive peptide nanofibers as osteoinductive biomaterials

1.5.1 What is a peptide amphiphile?

Peptide amphiphile (PA) molecules are a class of self-assembling peptides that have a hydrophilic alkyl tail attached to the peptide part (Figures 1.9 and 1.13A) and they can be designed to produce well-defined molecular and nanoscale architectures that allow bioactivity in the presence of bioactive sequences or bioactive ligands as epitopes [167].

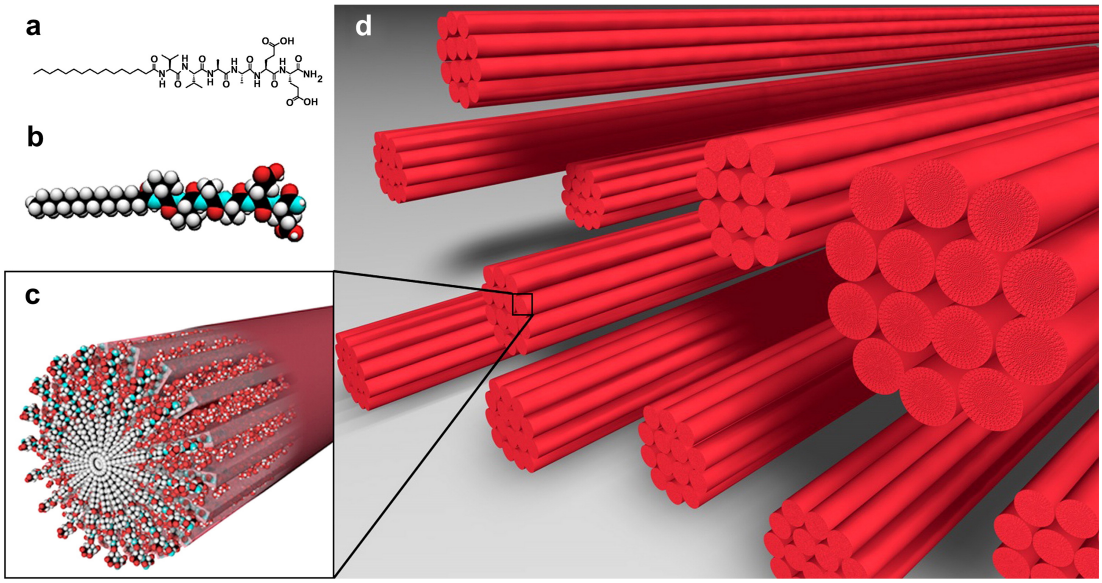


Figure 1.10: Chemical structure of a peptide amphiphile (PA) molecule with its chemical formula (A) and space-filling model (B), a hypothetical self-assembled nanofiber structure (C), nanofiber-containing bundles (D). Illustration is reprinted with permission from [176].

As differentiation of MSCs into a specific lineage can be induced by chemicals, biological factors and mechanical stimuli within the environment of the cells [177,

178, 179], PA molecules can be designed to obtain self-assembled nanostructures (*e.g.* nanofibers, nanospheres) defined via non-covalent interactions [180] and can be used as well for manipulating the differentiation of MSCs by providing bioactive peptide nanostructures to the niche of the MSCs [167, 169, 170, 181, 182, 183, 184, 185]. PA nanofibers are also promising biomaterials for local MSC delivery to patients with traumatic injuries and chronic diseases.

1.5.2 Osteoinductive peptide nanofibers

A bioactive PA molecule that contains Glu-Glu-Glu (EEE) sequence was first studied by Stupp group for manipulation of differentiation of MSCs into osteogenic lineage [184]. The bioactive EEE sequence is found in the structures of BSP protein, that is, an osteogenic marker protein and its expression helps the formation of an osteoblastic cell morphology, which can be an important parameter for characterization of osteogenic differentiation of bone marrow derived MSCs [54]. Osteoinductive peptide nanofibers that contain E_3-PA molecules were shown to induce bone-like mineral nucleation when human MSCs (hMSCs) were cultivated on them [167]. E_3-PA bearing peptide nanofibers promoted calcium mineral deposition of hMSCs better than other PA groups utilized in the study (Figure 1.10). Later, our research group reported that MSCs can commit to osteogenic differentiation on E_3-PA bearing peptide nanofibers better than DGEA peptide [168], which is found in the cell binding domain of collagen I, thus known to have a promoting effect on osteogenic differentiation of MSCs [186].

Glycosaminoglycan mimetic peptide nanofibers were shown to induce migration of Saos-2 cells (human osteosarcoma cell line) and formation of spheroids, and promoted mineralization by the cells (Figure 1.11).

Recently, the same glycosaminoglycan mimetic peptide nanofibers were also shown to promote osteogenic differentiation of rat MSCs (rMSCs) *in vitro* (Figure 1.12), and enhanced bone regeneration and biomineralization process *in vivo* in a rabbit tibial bone defect model [171]. In that study, a tendency of rMSCs to form cell clusters was observed at day 14 in the SEM image and confocal fluorescence

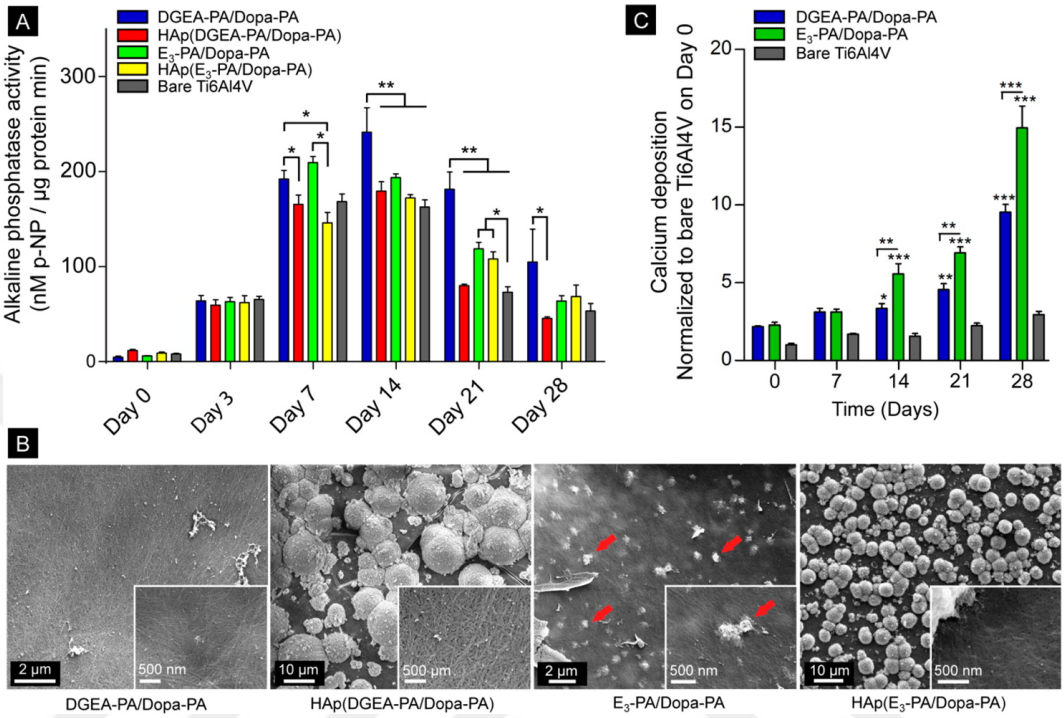


Figure 1.11: Alkaline phosphatase (ALP) activity of hMSCs in the presence of PA groups applied (A) and calcium deposition by the cells on the PA groups indicated, revealing that E_3-PA better enhances the biomineralization abilities of the cells (C), and SEM images of cell-seeded PA nanofiber-coatings bundles formed from the nanofibers are shown below (B). The figure is reprinted with permission from [167].

image of the cells on the glycosaminoglycan mimetic peptide nanofibers (Figure 1.12E). E-PA/K-PA was assumed/considered as a nonbioactive PA in the study.

Another example to the osteoinductive peptide nanofibers are the peptide nanofibers that mimic fibronectin binding domain of tenascin-C protein, which were reported to promote the osteogenic differentiation of rMSCs [170]. In this study, commitment of MSCs on the tenascin-C mimetic peptide nanofibers were confirmed at late stage of osteogenic differentiation via detection of higher level of osteopontin and collagen I gene expressions [170]. At the early stage, osteogenic differentiation of rMSCs was confirmed by ALP assay and for late stage assay Alizarin red staining was also used to show the mineralization profile (Figure 1.13).

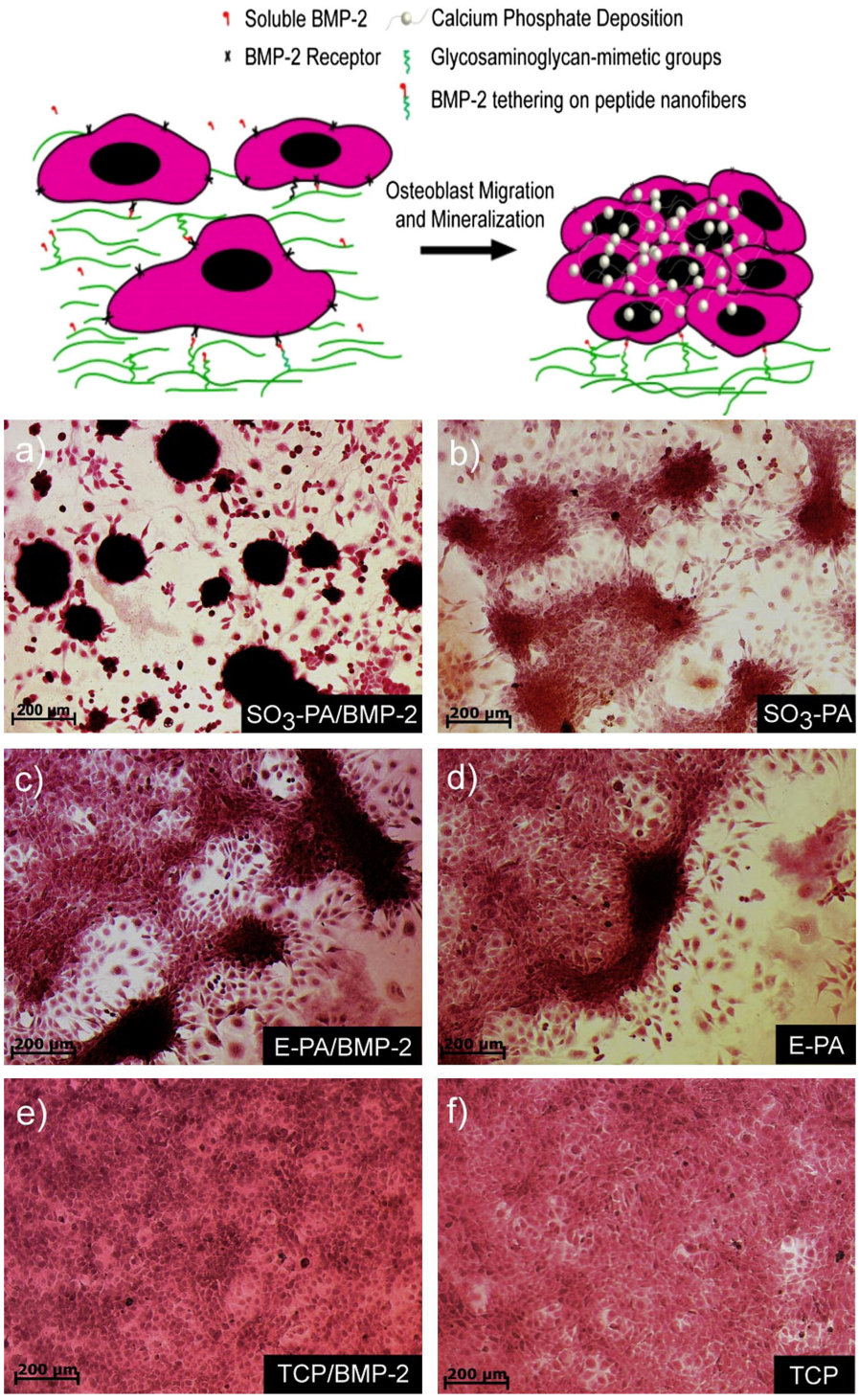


Figure 1.12: Schematic drawing at the top summarizes the effect of the glycosaminoglycan (GAG) mimetic PA (SO_3-PA) on behavior of Saos-2 cells. Microscope images below show Alizarin Red stained Saos-2 cells in the presence of SO_3-PA, BMP-2 and in their absence. All figures are reprinted with permission from [187].

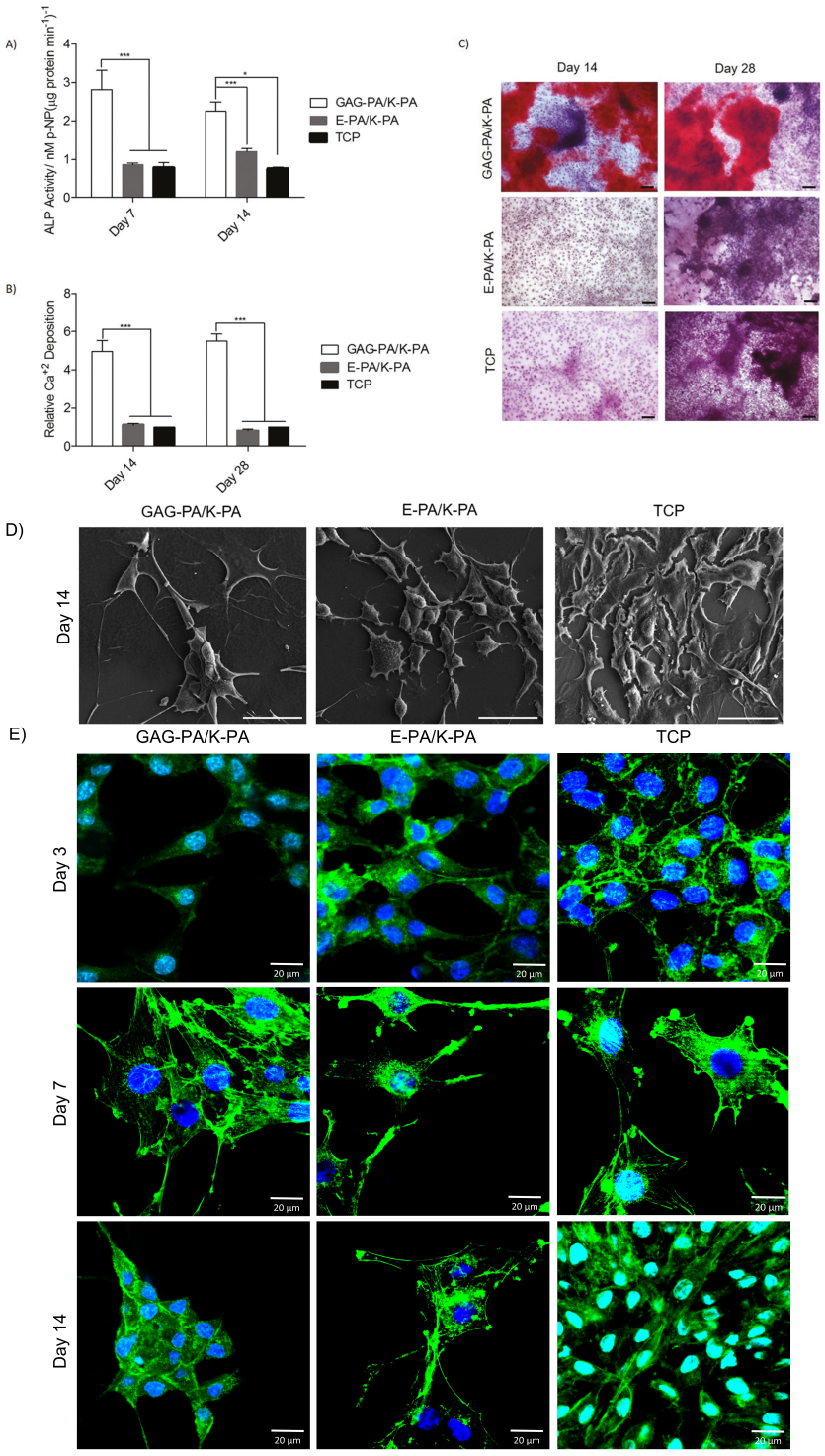


Figure 1.13: ALP activity A) and quantification of calcium deposition by rMSCs B). Microscope images in C) are Alizarin Red stained rMSCs. Scale bars are 100 µm. D) SEM images of rMSCs at day 14 are shown in the middle. Scale bars are 40 µm. E) Confocal fluorescence images of rMSCs on the scaffolds are shown at the bottom. All figures are reprinted with permission from [171].

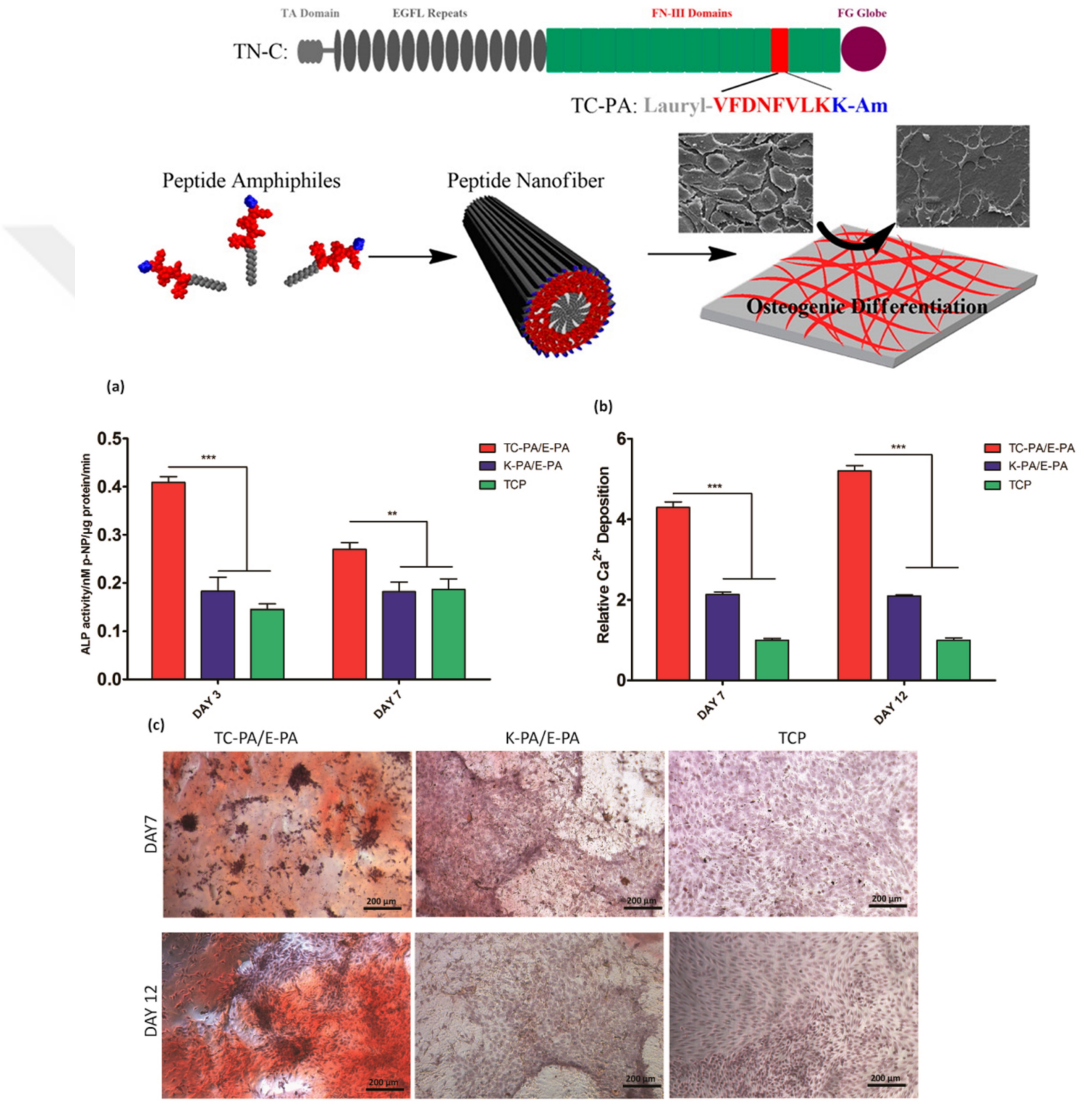


Figure 1.14: Tenascin-C mimetic PA promotes osteogenic differentiation of rat MSCs. Fibronectin binding domain of native tenascin-C protein was imitated. Induced osteogenic differentiation with higher level of ALP activity at early stage (day 3) and higher amount of calcium deposition at later stages were observed on the tenascin-C mimetic peptide nanofibers. All figures are reprinted with permission from [170]. Copyright (2014) American Chemical Society.

In this thesis study, mechanical properties of MSCs were investigated when differentiating on osteoinductive peptide nanofibers containing triple glutamic acid sequence which is expected to aid MSCs to commit to osteogenic differentiation and enhance mineralization at late stages for long-term stability. EEE sequence bearing osteoinductive PA (E_3-PA) molecule was mixed with an oppositely charged PA molecule having the same backbone sequence, Lauryl-VVAG, followed by a triple lysine sequence (KKK) instead to enhance nanofiber self-assembly. Charge neutralization and electrostatic interactions make it easier to form β-sheet secondary structure, thus nanofiber formation, even at low concentrations. Very recently, electron microscopy images of nanofiber structures composed of a mixture of these two individual PAs, also named as E_3/K_3-PA, were reported by our group (Figure 1.14). Here, effectiveness of E_3/K_3-PA for promoting the osteogenic differentiation and biomineralization of rMSCs was investigated *in vitro* and AFM was used for force mapping of rMSCs on the peptide nanofibers at different days of osteogenic differentiation to characterize Young's modulus changes of the cells throughout the differentiation process. Results were intriguing for better understanding the mechanical properties of MSCs at the osteochondral lineage because of approximating to their native state, and ended up with identification of biophysical markers related to osteoprogenitor cells, pre-osteoblasts, osteoblasts and osteocytes.

An appropriate matrix stiffness should be provided to MSCs to have a better control at engineering their fate using biomaterials. Because cells mechanically feel and sense their environment, differentiating cells act with respect to incoming signals from the surroundings by rearranging activities of cell signaling within the cell. For instance, YAP/TAZ proteins were shown to play a significant role in the progress of osteogenic differentiation and they were also shown to be activated in the nucleus of MSCs on a stiff substrate with 40 kPa stiffness [190, 191]. For osteogenic differentiation to occur efficiently, a suitable substrate stiffness (*i.e.* close to osteoid matrix) and presence of cell-cell contact were both demonstrated to be important requirements [25]. According to Discher group, osteoblast calcification on 2D gels would occur better within an elastic modulus range of 20-100 kPa [29].

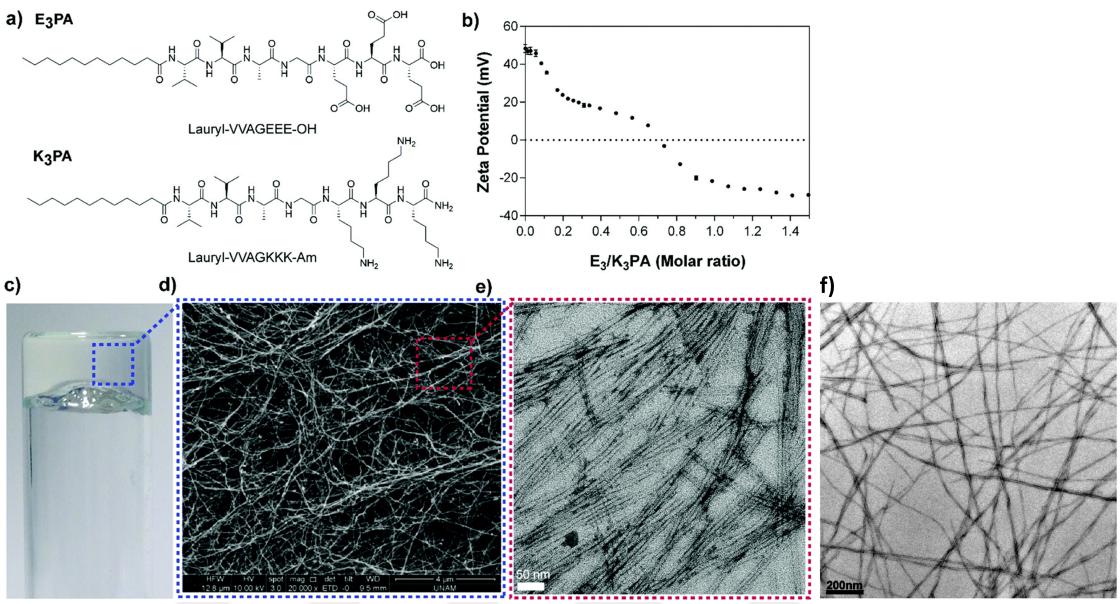


Figure 1.15: Chemical structures of E_3-PA and K_3-PA molecules (a), zeta potential measurement result (b), hydrogel appearance in an upside down tube (c), SEM image of 0.5% (w/v) (d), TEM images (e and f) of 1% (w/v) E_3/K_3-PA. (f) is reprinted from [188] with permission, other parts of the figure are reprint from [189] with permission. I included both TEM images of E_3/K_3-PA because Cinar *et al.*'s TEM image has nanosheet like structures but Zengin *et al.*'s TEM image does not have those nanosheets.

1.6 What are the attributes of cells that influence their mechanical properties?

Cytoskeletal elements are known to be key players that might change the bulk elastic modulus of a cell. John M. Maloney found that MSCs effectively stiffen in response to detachment of substratum-adherent cells from substrate surface within one hour [22]. Regarding to osteogenic differentiation of MSCs, several research groups reported that substrate-adhered MSCs underwent softening throughout osteogenic differentiation [192, 164]. Here I argue that MSCs might increase their Young's moduli on osteoinductive peptide nanofibers when differentiating into the osteogenic lineage. Mineralization might be an important factor to obtain differentiating cells with increased stiffness profiles during osteogenic differentiation. Subbiah *et al.* used gelatin matrix to study cell mechanics during

differentiation of pre-osteoblast MC3T3 cells into osteoblasts and found that cell stiffness increased correlated to increased matrix mineralization [193]. Effect of mineralization on osteoblast stiffening might overcome influences of cytoskeletal elements which are known as main determinants of the mechanical properties of cells.

Actin filaments are one of the most important factors that can modulate cell stiffness as they likely have important influences on cell mechanics via dynamic rearrangements [194]. Amount and length of the fibers may affect the stiffness profile of a cell, however, alignment and thickness of actin and myosin filaments were found to have a less order in contribution or have no direct relation to the cell stiffness [195]. Myosin motor proteins are known to enable contraction of actin arrays including stress fibers [196]. Cell cortex has gel-like mesh network of actins [196]. Cell surface tension is regulated by both actin cortex and myosin-driven stresses [197]. Contractility and alignment of actin and myosin networks were pointed out to be important for mechanical interplay in tissue shaping by the cells [198]. Mechanical response of stress fibers was reported to be remarkably greater than mechanical response of cytosol according to AFM-based measurement results: stiffness of actin fibers was reported as 11.3 kPa whereas cytosolic region had a stiffness of 2 kPa, both values in average [199]. There is not sufficient quantitative information on how actin fiber thickening influences cell stiffness. Recently, recovery of actins was shown to occur near-instantaneously in the study carried by Andrew Pelling group, where cell membrane recovery happened within a few minutes after a large deformation was introduced [200].

Cell nucleoskeletal components like lamin, emerin and SUN proteins, nuclear pore complexes and chromatin organization were reported to actively modulate nuclear mechanics [201].

Chapter 2

Design of custom atomic force microscope (AFM) probes for imaging and force mapping of live cells

2.1 Study background and hypothesis

AFM probe choice is very important in biological sampling. For live cell AFM imaging, spring constant of cantilevers should be sufficiently low that the cells should not be harmed via plastic deformations when the tip contacts the cells repeatedly. 0.01 N/m to 0.1 N/m spring constants are typical values for measurements of force curves and force maps. Young's moduli of cells remain typically between 0.1 kPa and 100 kPa. Adhesion of the tip to the sample is unwanted; thus, antifouling probe design would be helpful for getting easier and more repeatable AFM measurements and images. Both nanoscale sharp tips (*i.e.* usually 5-10 nm) and colloidal probes with micron scale diameters (*e.g.* 2.5 µm and 5 µm) have been preferred very frequently in the literature. Another parameter to be considered in the probe selection would be resonant frequency of the cantilever.

For example, a high-speed AFM would need a MHz scale frequency and would usually have a very small cantilever size. In this thesis, a Teflon-like thin film was coated to a contact mode silicon nitride AFM probe. The coated probes were used for AFM imaging and force mapping of live mesenchymal stem cells (MSCs).

2.2 Materials and methods

2.2.1 Fabrication of AFM probes with Teflon-like coating

Pyramidal silicon nitride (SiNi) AFM probes (purchased from Budget Sensors, Bulgaria) were coated with a Teflon-like fluoropolymer thin film via an Inductively Coupled Plasma (ICP). The coating process was performed with C_4F_8 plasma for 10 min at a rate of 80 sccm. A power of 400 W was used.

2.2.2 SEM imaging

The coated AFM probe was placed on a double-sided sticky carbon tape sticked on an SEM stub. A FEI Quanta 200 FEG SEM with an ETD detector in high vacuum mode was used for acquiring the images. Working distance was set to 10 mm. SEM's stage was tilted 40°.

2.2.3 Contact angle measurement

Droplets of water and ethylene glycol were dropped on a C_4F_8 coated silicon wafer piece via micropipette. Measurements were conducted with a custom contact angle measurement device setup.

2.2.4 AFM imaging

Rat MSCs at passage 7 were imaged. About 75% confluent sample (good cell sample for AFM imaging) and an overconfluent sample (challenging for AFM imaging) of rMSCs were imaged in growth medium solution (contains low glucose Dulbecco's Modified Eagle Medium (DMEM), 10% Fetal bovine serum (FBS) and 1% penicillin/streptomycin antibiotics).

2.3 Results and discussion

2.3.1 Characterization of Teflon-like coated AFM probes

A sphero-conical shape was obtained at the tip apex as a result of Teflon-like thin film coating as analyzed by SEM imaging (Figure 2.1A and 2.1B). Contact angle measurements showed that the coating was highly hydrophobic with a water droplet contact angle of 110° and ethylene glycol contact angle of 62° (Figure 2.1C and 2.1D).

2.3.2 AFM imaging and force mapping of live cells via AFM probes with Teflon-like coating

Teflon-like thin film coated silicon nitride AFM probes (Budget Sensors), same as the coated probe shown in Figure 2.1, were used for live cell AFM imaging of a confluent sample of rat mesenchymal stem cells (rMSCs) at passage P7 at a resolution of 1024 x 256 (Points x Lines) (Fig 2.2). Since there are great differences at the position of cytoskeletal images between Trace and Retrace images, it can be claimed that AFM tip disturbs the cell while scanning. Even so, the cytoskeletal elements are distinguishable on the images obtained from such a challenging (confluent) live cell sample for AFM imaging.

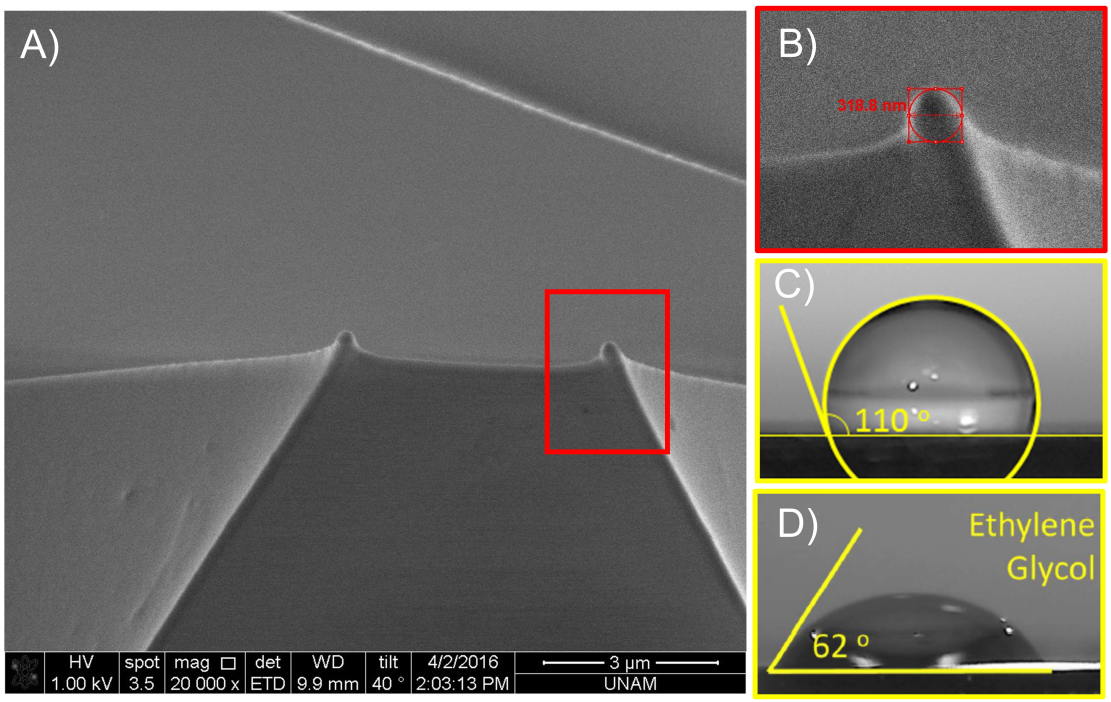


Figure 2.1: (A, B) SEM images of Teflon-like film coated silicon nitride AFM tip. Diameter of the tip apex is 318.8 nm. (C) Contact-angle measurement result of a water droplet on the silicon surface with same coating.

Force mapping was tried with the Teflon-like coated SiNi probes from the same rMSC sample (Fig. 2.3), which showed that the coated tips were reliable for force mapping measurements.

Tapping mode imaging on live rMSCs was achieved without too much disturbing the cells (Fig. 2.4). After observing that these probes can be used confirming reliable usage for both scanning and force mapping measurements, it was decided to continue using them for mechanical characterization of rMSC osteogenic differentiating on the peptide nanofibers.

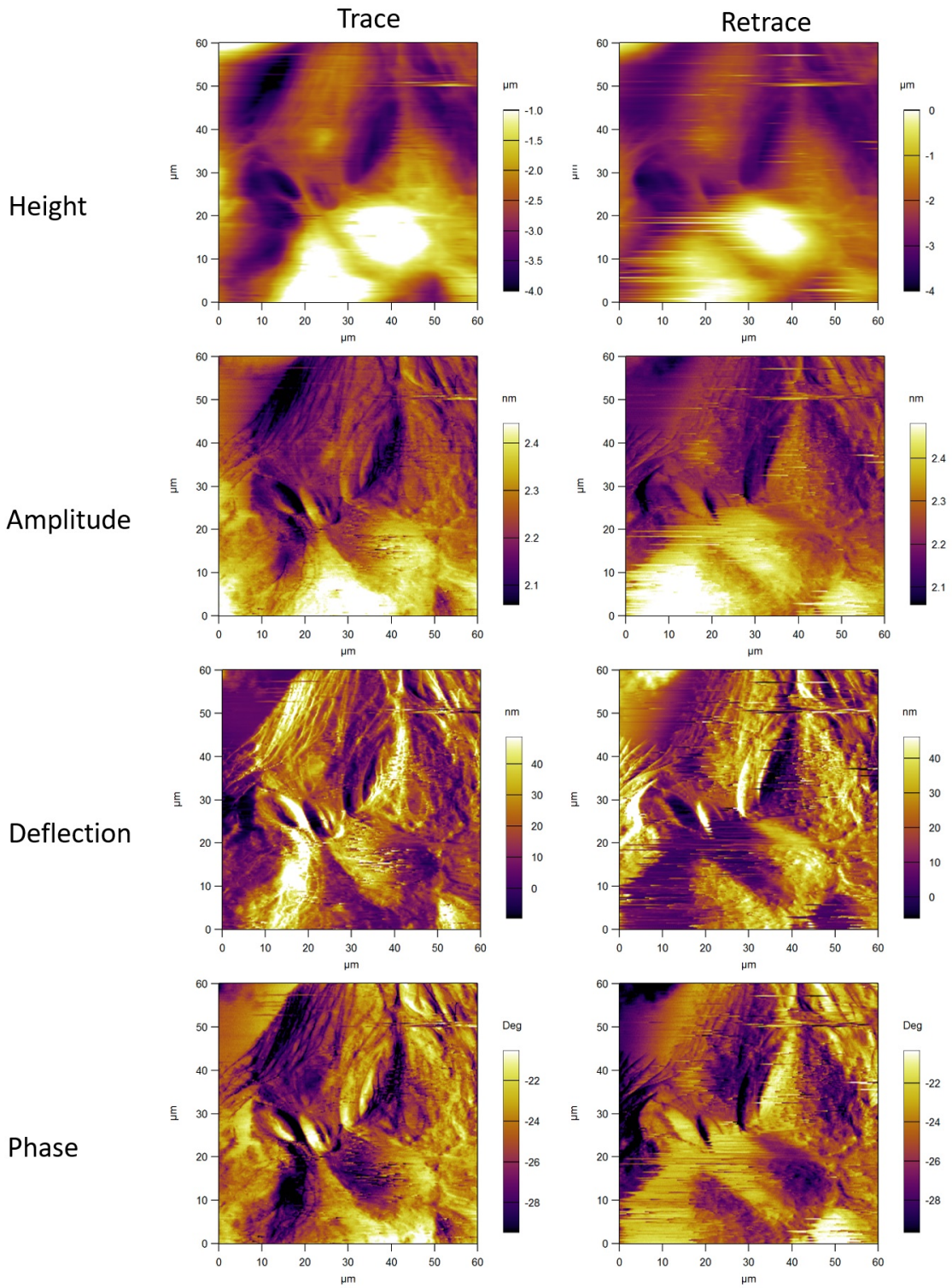


Figure 2.2: AFM images of confluent rMSCs using Teflon-like thin film coated AFM probes.

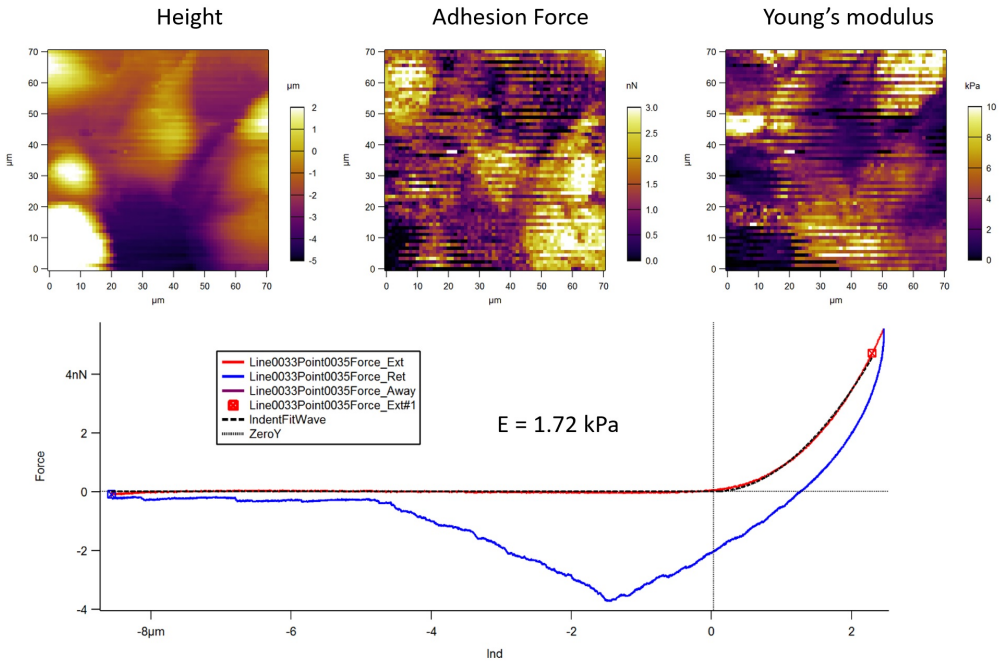


Figure 2.3: 64 x 64 force map measurement trial using Teflon-like coated AFM probes. Young's modulus map and a representative force curve with fit (black dashed line) were obtained via fitting approach curves based on Hertz Cone model.

2.3.3 Optimization of Teflon-like thin film coating recipe at ICP

There was a bending problem which caused the sum signal to decrease during measurements (Figure 2.5). Even tough there was bending at the bright region, it was possible to gather nice AFM images with these Teflon-like probes even from an overconfluent sample as shown in Figure 2.2 and also smooth force curves as shown in Figures 2.3. The laser of AFM was shined on a dark region of the back of the cantilever (dark regions allowed having high sum signals as usual), and the force mapping experiments were performed with the coated probes and the measurements were successful.

Because some of the coated probes showed the bending problem, I tried to obtain non-bending AFM probes coated with C_4F_8 material. Whether a high temperature caused the bending problem during the process at ICP due to high

power was suspected. So, the process was optimized eventually by trying at a lower power, 150 W, and for a longer coating duration, 45 min. At AFM, in aqueous environment, the probe showed no bending at all with the 150 W optimization (Figure 2.6).

150 W, 45 min coated SiNi probe was imaged with SEM (Figure 2.6A) and HUVEC imaging was done using the same probe afterwards (Figure 2.6B). SEM image was measured tilted and no bending was observed at the cantilever, and the coating was confirmed. AFM images showed that the probe coated at 150 W for 45 min was able to image HUVECs although the sample was somewhat challenging because of greater heights of the cells (they are bigger than MSCs).

2.4 Conclusion

Custom AFM probes with anti-fouling properties were designed by coating the silicon nitride probes with octafluorocyclobutane and used in the high resolution AFM imaging of live cells and for investigating the mechanical properties of cells during cellular differentiation. Antifouling properties of Teflon-like fluoropolymer octafluorocyclobutane coated probes allowed measurement of smooth force-distance curves on living cells. Imaging results showed that nicely prepared live cell samples could be measured to obtain AFM images with good resolution and quality, and with minimal tip disturbances on the cell, and that overconfluent cells could also be successfully imaged using these probes. Cell nucleus can be easily identified from phase images and cytoskeletal elements can be seen in the images as well. Optimization of deposition recipe of C_4F_8 plasma at ICP using lower power (*i.e.* 150 W) and a longer duration helped solving the bending problem observed at some of the cantilevers coated at 400 W.

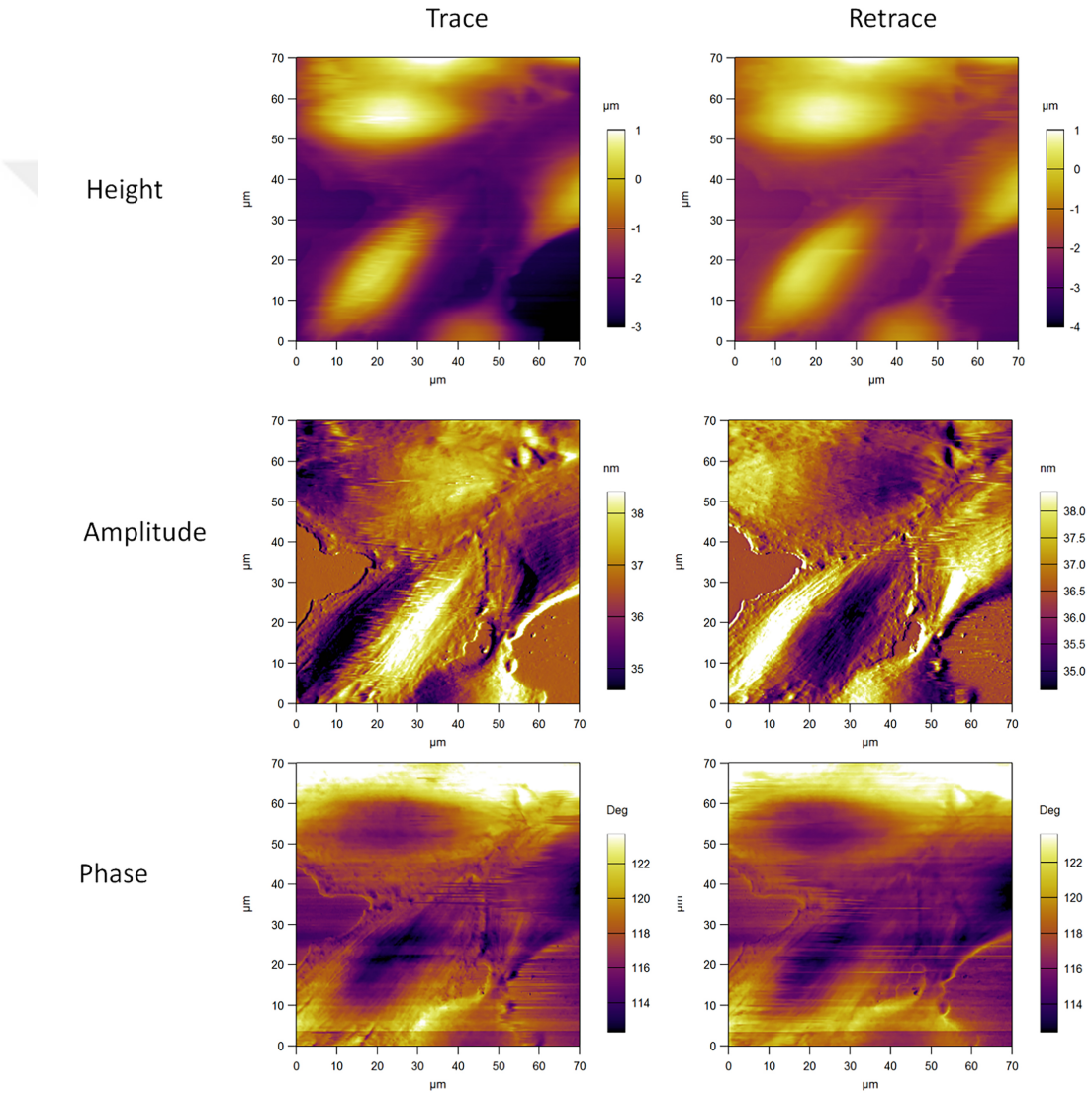


Figure 2.4: Tapping mode AFM images of less confluent rMSCs measured using Teflon-like coated SiNi AFM probes. Images were obtained without too much disturbing rMSCs. The resolution of the images is 1024 x 256 (Points x Lines).

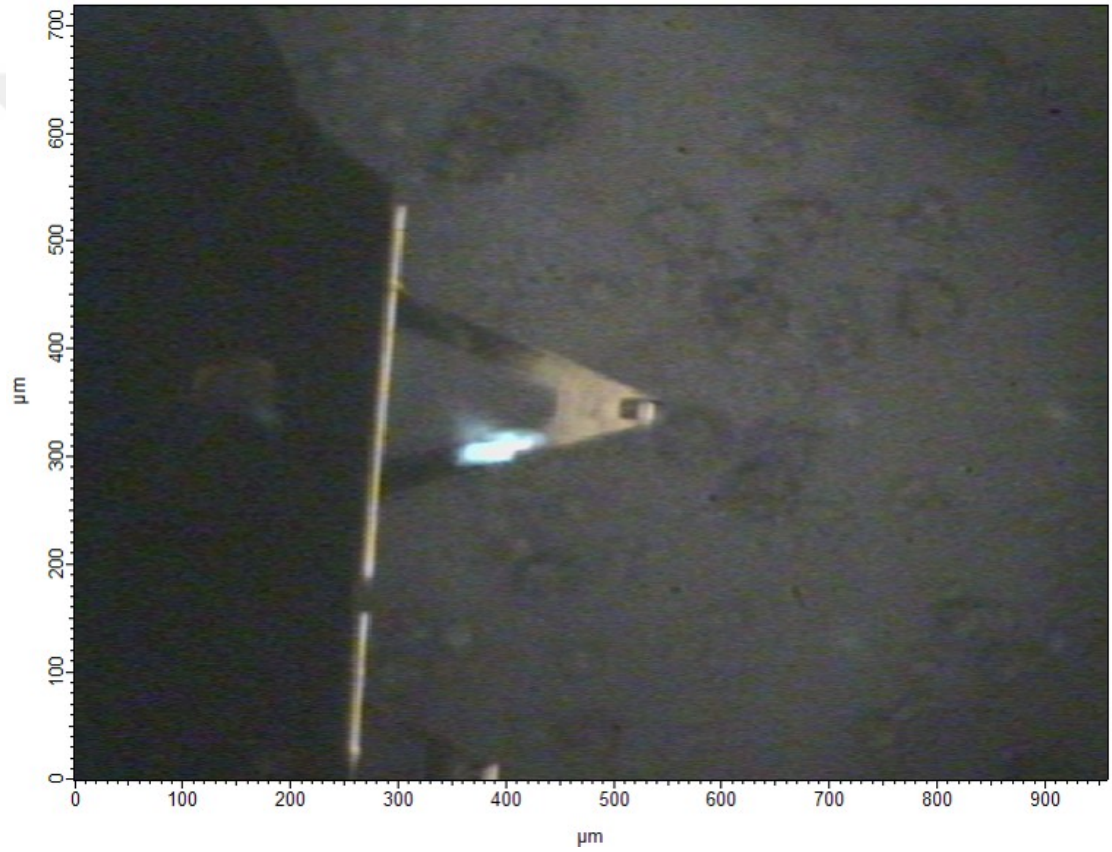


Figure 2.5: Bending problem of Teflon-like probes fabricated with a power of 400 W at ICP. The laser is shined on a dark region of the back of the cantilever and high sum signals can still be obtained like 4 V. When the bright region is shined, a very low sum signal like 1 V is obtained and AFM analysis is not possible. The probe is in liquid, in the cell culture medium and the sample is osteospheroid rMSCs on peptide nanofiber hydrogel coated on glass coverslip.

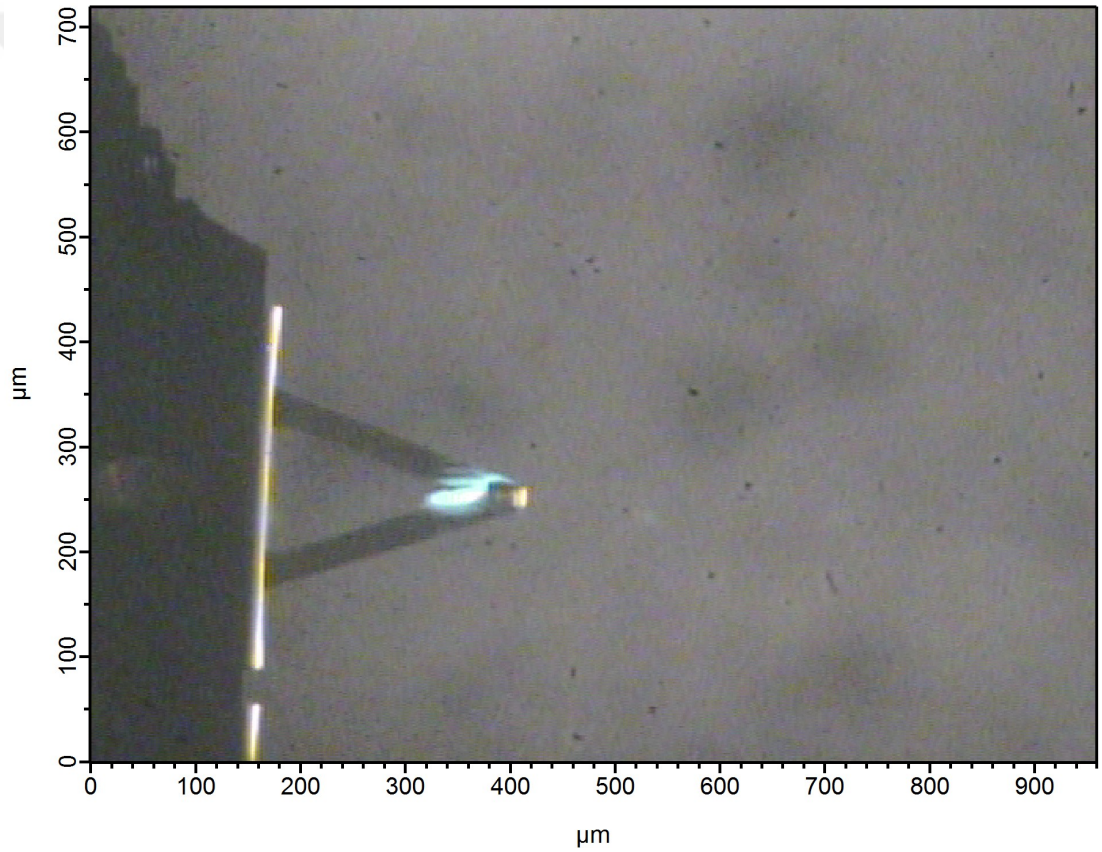


Figure 2.6: Appearance of AFM probe coated at 150 W in aqueous environment; the bending problem was solved. No bright region is observed after optimization of the deposition recipe at ICP.

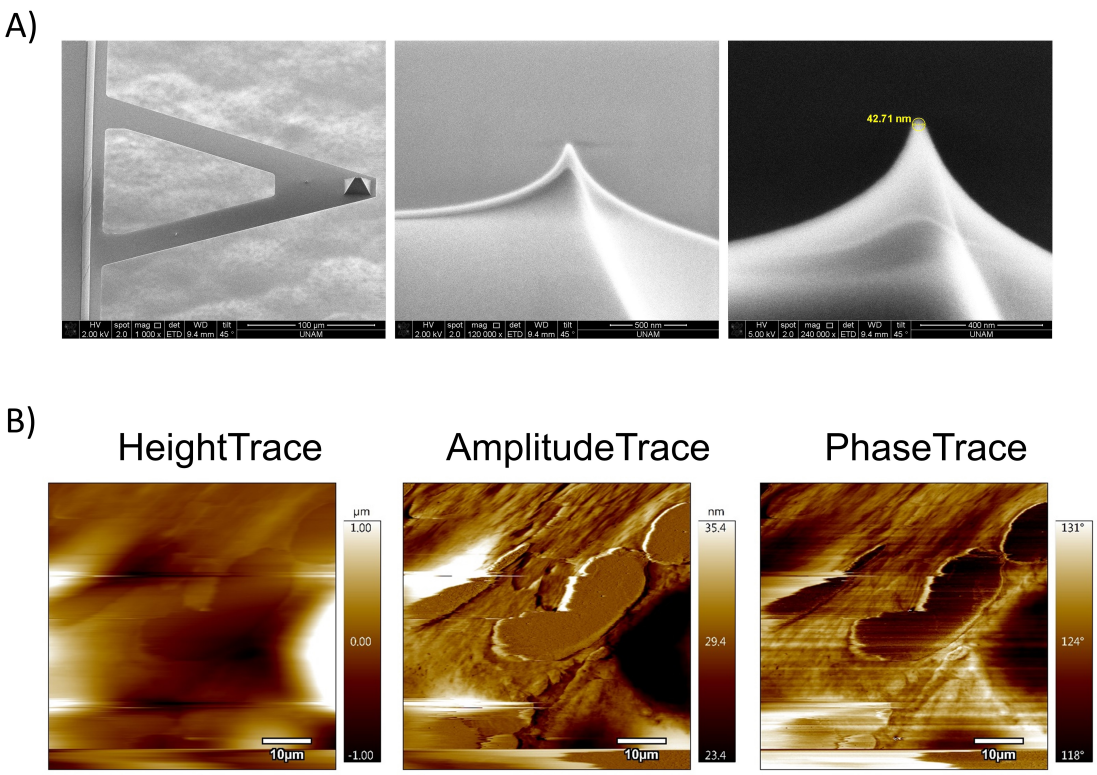


Figure 2.7: A) SEM images of 150 W coated probe and B) AFM images of live HUVECs measured using the same probe via tapping mode imaging in cell culture medium.

Chapter 3

Force mapping and Alizarin red staining reveal that Young's moduli of differentiating mesenchymal stem cells increase with biomineralization on osteoinductive peptide nanofibers

This work is partially described in the following publication:

Topal, A. E. *et al.* Nanomechanical Characterization of Osteogenic Differentiation of Mesenchymal Stem Cells on Bioactive Peptide Nanofiber Hydrogels. *Advanced Materials Interfaces* 1700090 (2017). doi:10.1002/admi.201700090

3.1 Study background and hypothesis

Mechanical properties of MSCs and osteogenic differentiating cells have been investigated before on glass substrate or on Petri dishes, however, there is still need for better investigating the mechanical properties of MSCs that are cultured in an extracellular matrix-like environment and differentiating into osteogenic lineage. Mechanical mapping of adherent cells can be done via force mapping capability of AFM. Most of such mechanical characterization studies in the literature that calculate Young's modulus of adherent cells are performed using AFM. Here, I studied Young's moduli of rat MSCs (rMSCs) differentiating on bioactive peptide nanofibers by using AFM, of which, I believe there is room for more investigation. I expect that this study might contribute to elaboration of mechanical behavior of MSCs differentiating into osteogenic lineage *in vivo*. Furthermore, a mechanical marker for osteogenic differentiation can be suggested based on the Young's modulus of cells. Although stiffness of a material changes based on its geometry, Young's moduli of materials are independent of their geometry because Young's modulus is an intensive property unlike the stiffness, which is an extensive property. Which factors do have an influence on the Young's moduli of cells? Most studies that analyze local Young's modulus of cells attribute changes to cytoskeletal elements due to their dynamic rearrangements. There rises a question for differentiating bone cells that whether calcium mineralization during osteogenic differentiation might influence Young's modulus of cells as well. Only one study has attributed an increase of Young's modulus of MSCs to mineralization so far [193]. In this thesis work, I intended to investigate mechanical properties of MSCs differentiating on osteoinductive peptide nanofibers by characterizing Young's moduli of the cells using AFM's force mapping capability.

3.2 Materials and methods

3.2.1 Design and synthesis of peptide amphiphile (PA) molecules

Two peptide amphiphile (PA) molecules, Lauryl-VVAGEEE (E_3-PA) and Lauryl-VVAGKKK-Am (K_3-PA) (Figure 3.1), were synthesized using Fmoc-solid-phase peptide synthesis. E_3-PA was constructed on Fmoc-Glu(OtBu)-Wang resin (100-200 mesh) from Novabiochem® whereas Rink Amide MBHA resin (100-200 mesh) from Novabiochem® was used as solid support for K_3-PA. Automated peptide synthesizer was used for the synthesis. Amino acid coupling reactions were performed with 2 molar equivalents of Fmoc-protected amino acid, 1.95 molar equivalents of HBTU, and 3 molar equivalents of DIEA for 3 h. The Fmoc protecting group removal was performed with a 20% piperidine in dimethylformamide (DMF) solution for 20 min. In order to block free amine groups after amino acid coupling, 10% acetic anhydride in DMF solution was used. The resin was washed by using DMF and dichloromethane (DCM) after each step. Cleavage of the peptides from the resin was carried out in 10 mL solution of trifluoroacetic acid (TFA)/triisopropylsilane (TIS)/ddH_2O prepared with ratio of 95/2.5/2.5, respectively for 2 h. Excess TFA was removed by rotary evaporation. The remaining peptide was triturated via overnight incubation at $-20\,^{\circ}C$ in diethyl ether. After a centrifugation step, the precipitate was collected by drying the pellet and dissolving in double-distilled water. The peptide was frozen and incubated at $-80\,^{\circ}C$ overnight. The frozen peptide was lyophilized for 3 days.

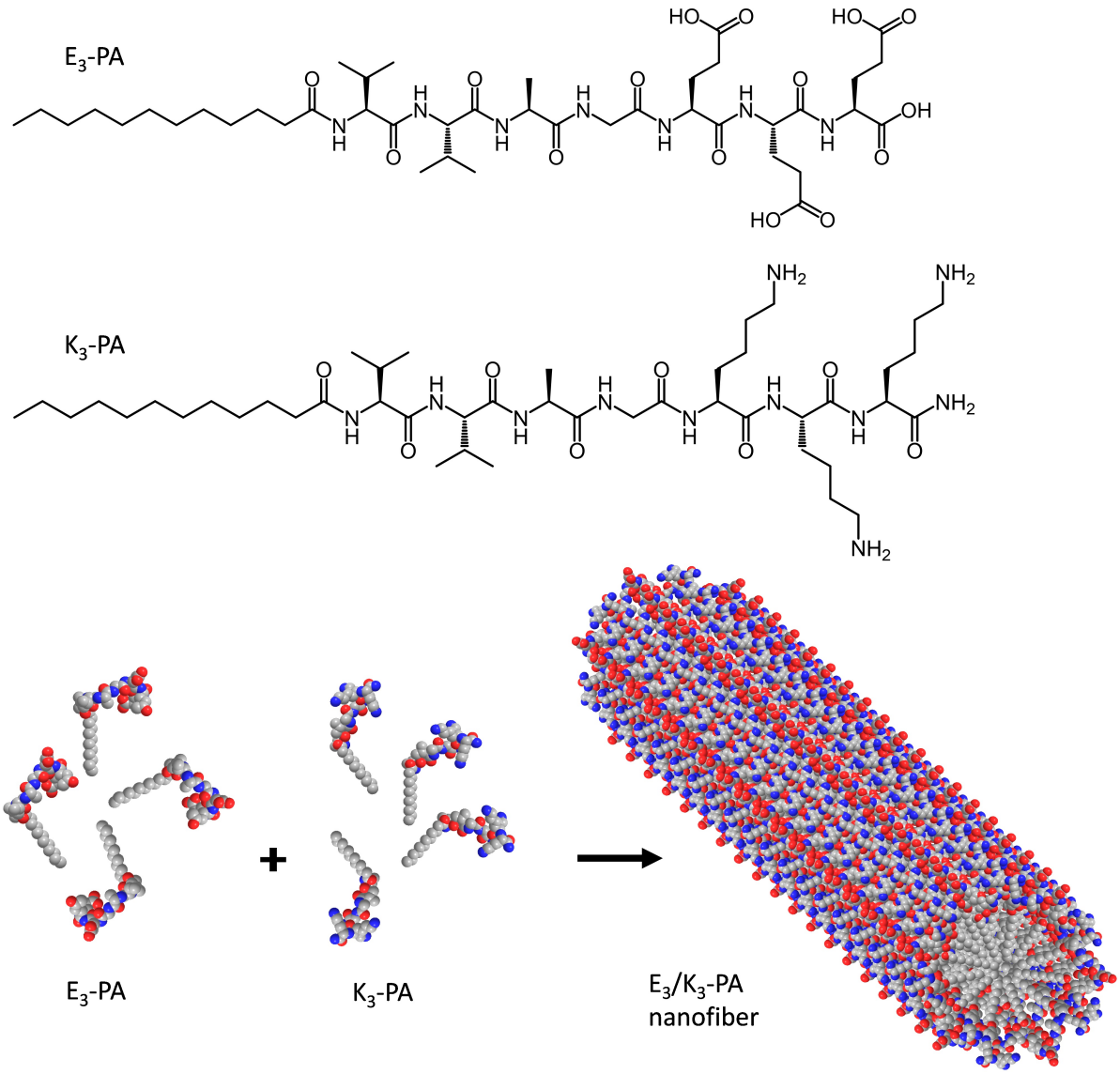


Figure 3.1: Chemical representations of PA molecules Lauryl-VVAGEEE (E_3-PA) and Lauryl-VVAGKKK-Am (K_3-PA), and their self-assembly into proposed E_3/K_3-PA nanofiber structure.

3.2.2 Characterizations of PA molecules and the peptide nanofibers

3.2.2.1 Oscillatory rheology of the peptide gel

Time sweep oscillatory rheology of 1% (w/v) PA mixture was performed using a traditional rheometer (Anton Paar). A total volume of 250 µL was used from a mixture of 108 µL E_3-PA (11 mM) and 144 µL K_3-PA (11 mM). A PP25-SN17979 measuring device having a diameter of 25 mm was used. The measuring distance was determined as 0.5 mm. Measurements were performed with three repeats. Time sweep tests were carried out for 30 min with a measurement point duration of 0.5 min. Angular frequency and strain magnitude were kept constant as ω = 10 rad/s and γ = 0.1%, respectively. Frequency sweep test was performed by sweeping logarithmically from ω = 1 rad/s^{-1} to 1000 rad/s^{-1} and by setting amplitude gamma (γ) constant as 0.1%. Amplitude sweep (strain sweep) test was performed by ramping logarithmically from 0.01% to 100% strain and by keeping the frequency constant ω=10 rad/s.

3.2.3 Force mapping and data analysis

Procedure for cantilever spring constant calibration and sample preparation can be found in Appendix A. Force measurements were performed with the Teflon-like thin-film (∼200 nm) coated probes (C_4F_8 coating at 400 W for 5 or 10 min) having a diameter of approximately 350 nm at the tip apex. An MFP-3D model Asylum Research AFM was used to perform force mapping at contact-mode. Each sample was measured within 1.5 hours at room temperature in DMEM medium. Force maps were measured at a resolution of 16 x 16 or 32 x 32 within a 50 µm x 50 µm area. A trigger point of 0.5 V was applied at force mapping.

Force distances were set at either 10 µm or 5 µm. Vertical deflection correction was performed before starting force map measurements. Cells were grown on bare glass coverslips (13 mm) or on peptide-coated coverslips at a density of 4 x

10^4 cells per coverslip. Coverslips were glued onto glass slides using nail polish before AFM measurements in order to fix the coverslip. Used AFM probes were cleaned either with double-distilled water, acetone and double-distilled water, respectively, or with only double-distilled water from a wash bottle.

3.2.3.1 AFM data analysis

12 random force curves were selected per cell. Each coverslip sample was measured within 1.5 h to lessen the effects of environmental conditions (*e.g.* temperature, CO_2, pH) on the cells. Cells were analyzed at following counts: 45, 58 and 44 at days 3, 7 and 14 for rMSCs on bare glass; 29, 35, 32 at days 3, 7 and 14; for rMSCs on E_3/K_3 peptide nanofibers; 65, 90 and 42 at days 3, 7, 14 for rMSCs on gelatin, all counts were indicated here with respect to the days of osteogenic differentiation. Force curves were randomly selected from each cell area. The conical Hertz model was applied to calculate Young's moduli from approach curves using the Igor Pro AFM analysis software [202]. Half-cone angle was assumed to be 36°, the Poisson's ratio of the cells was assumed to be 0.33, and the tip radius was assumed to be 150 nm.

3.3 Results and discussion

3.3.1 Characterization of the PAs and peptide nanofibers

Cell lineage specific differentiation of MSCs can be controlled by culturing them on two-dimensional bioactive peptide amphiphile hydrogels. Two different peptide amphiphile (PA) molecules were designed so that they would form nanofibrous peptide assemblies when mixed and the nanofibers would also expose bioactive sequences that would induce osteogenic differentiation.

3.3.1.1 Characterization of individual PA molecules

Peptides were characterized using LC-MS (Agilent Technologies 65301200 Accurate-Mass Q-TOF) analysis (Fig. 3.2-3.5). One milligram of the peptide sample was dissolved in double distilled water and sonicated for 15 min. Peptide samples that have purities lower than 95% were purified using reverse-phase preparative high performance liquid chromatography (HPLC).

3.3.1.2 Formation of self-assembled PA nanofibers

Stock solutions of PAs were prepared in double distilled water. For nanofiber formation, 0.75 mM solution of E_3-PA was mixed with 1 mM solution of K_3-PA at 1:1 (v/v) ratios, respectively, in order to stabilize all net charges. Tissue culture plate surfaces were coated with first E_3-PA; then, K_3-PA was added by pipetting or by gently mixing using tip of micropipette and then plates were placed in a laminar air flow hood and dried overnight. After drying, they were sterilized under exposure to UV light for an hour before cell seeding for cell culture studies. In order to characterize the formation of nanofibrous assemblies, SEM imaging was performed (Fig. 3.4).

AFM imaging of peptide nanofibers was studied both in air (dried) (Fig. 3.5) and in aqueous environment (*in solution*) (Fig. 3.6).

For both dried and in liquid AFM imaging measurements, same PA concentration was used. To prepare the self-assembled PA nanofiber samples, E_3-PA (0.75 mM) was mixed with K_3-PA (1 mM) at 1:1 (v/v) ratios. For dried conditions, cleaned glass coverslips were used as substrates. For in liquid imaging, cleaved mica surface was used as the substratum and a silicon nitride probe was used for the contact mode imaging. At first, nothing was observed on the mica surface, $\sim$1 h later, nanofibrils started to appear with small lengths. Afterwards, AFM images were measured continuously from a selected area without stopping the scanning for an hour and images shown in Figure 3.6 were recorded.

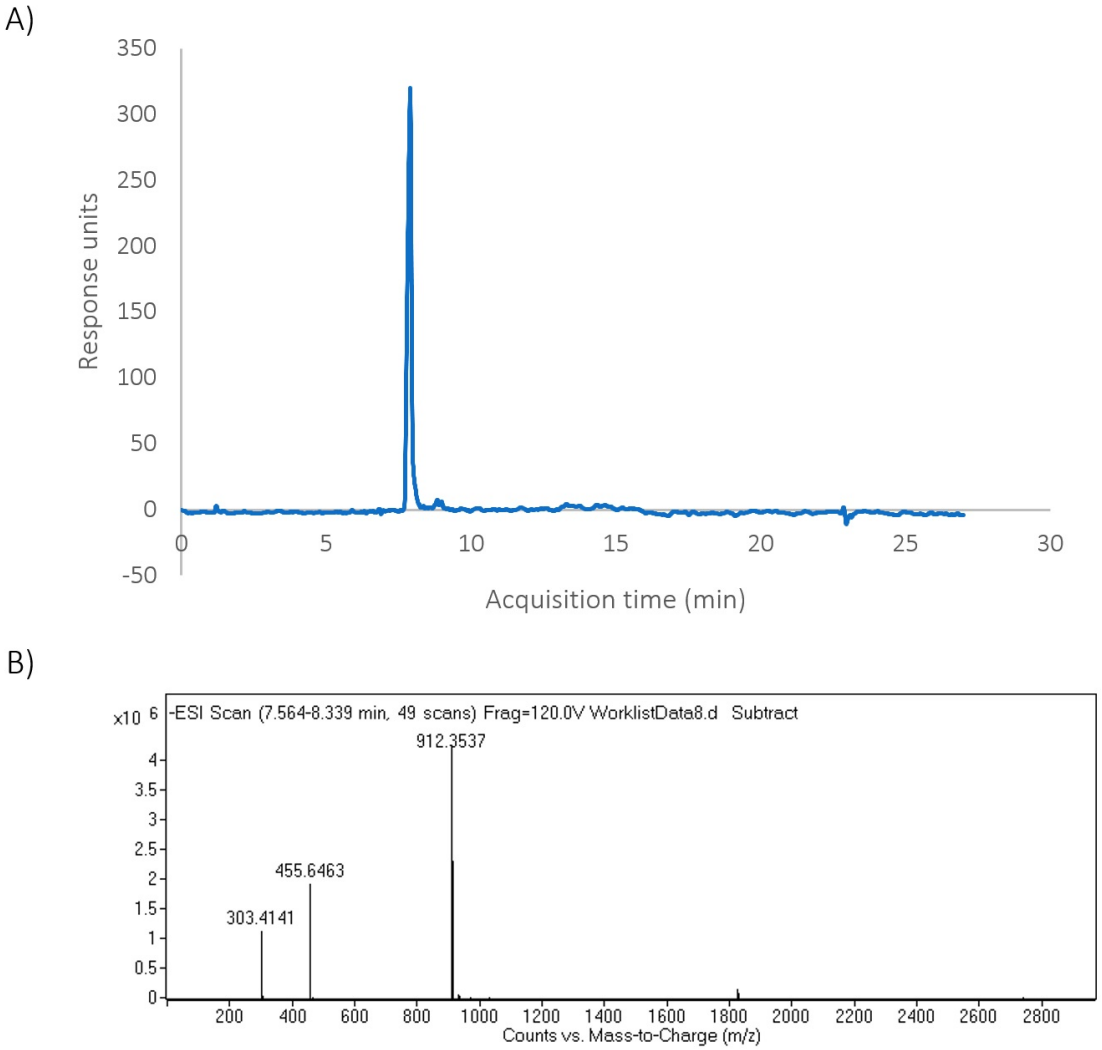


Figure 3.2: A) RP-HPLC chromatogram of E_3-PA, the change of response units with respect to time at 220 nm. B) [M] (calculated): 913.5008; $[M-H]^-$ (observed): 912.3537; $[M-2H]^{-2}/2$ (observed): 455.6463; $[M-3H]^{-3}/3$ (observed): 303.4141.

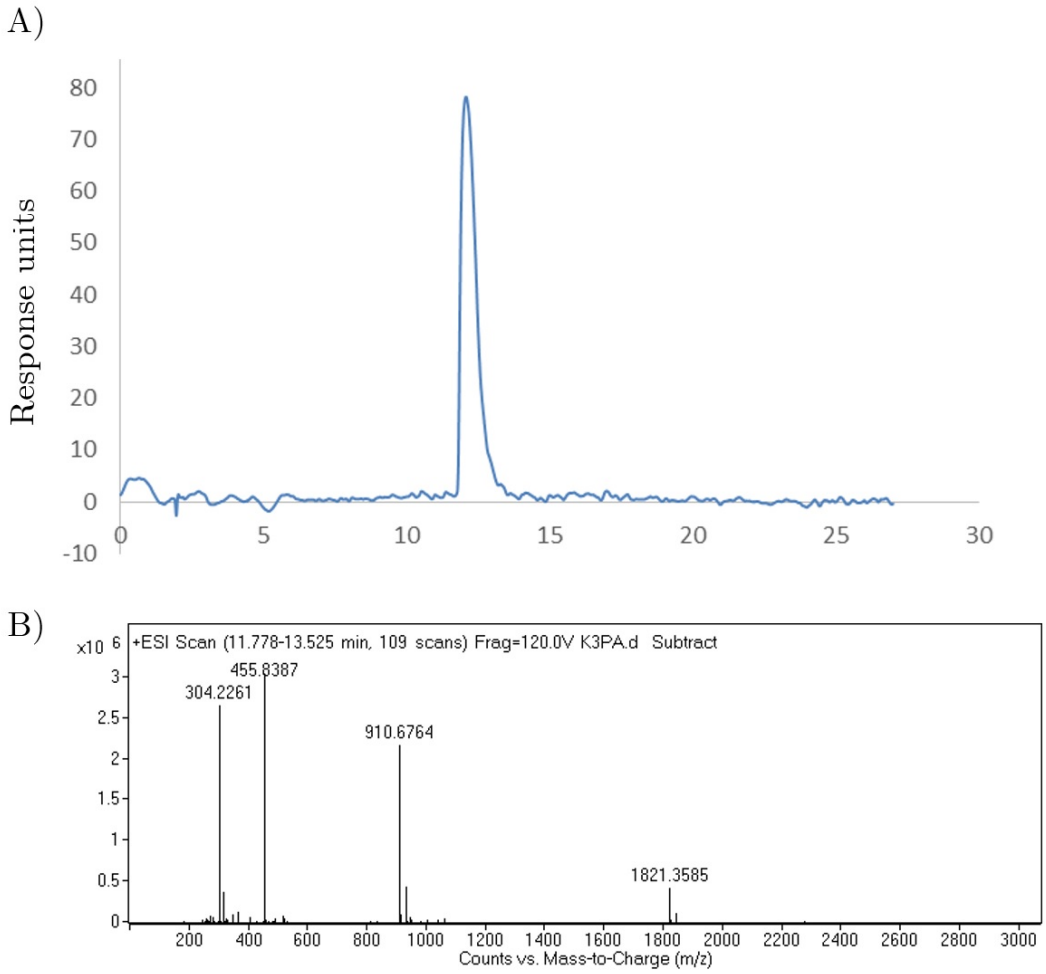


Figure 3.3: A) RP-HPLC chromatogram of K_3-PA, the change of response units with respect to time at 220 nm. B) [M] (calculated): 909.6739; $[M+H]^+$ (observed): 910.6764; $[M+2H]^{+2}/2$ (observed): 455.8387; $[M+3H]^{+3}/3$ (observed): 304.2261; $[2M+H]^+$ (observed): 1821.3585 for the dimer.

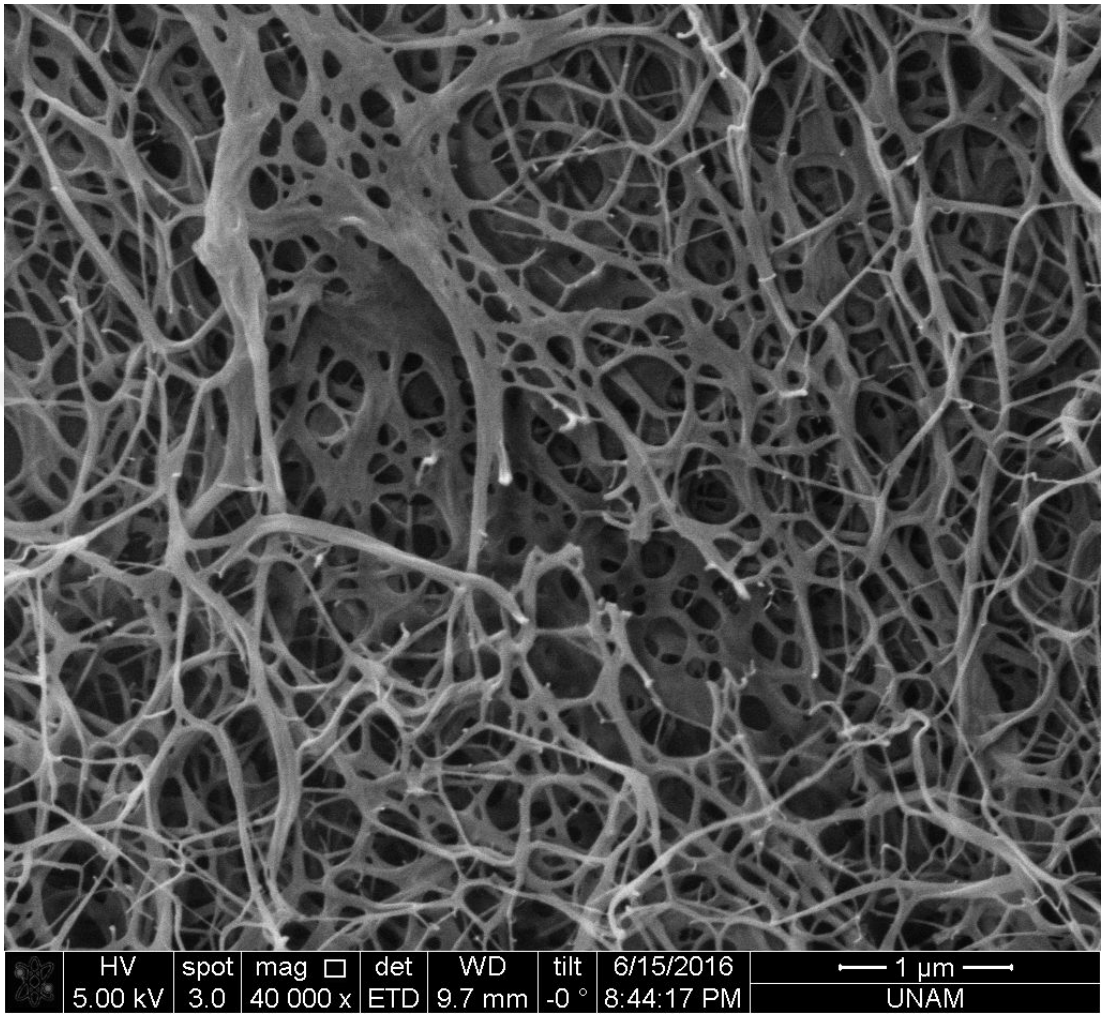


Figure 3.4: SEM image of critical point dried 1% E_3/K_3-PA nanofibers formed on a cleaned silicon wafer.

Rheology analysis of 1% w/v concentration of E_3/K_3-PA showed that the resulting material had hydrogel character because its storage modulus (G') was higher than its loss modulus (G'') (Fig. 3.7, Fig. B.1A). Frequency sweep and amplitude (strain) sweep test results were also performed following time sweep test, for each sample of three replicates (Fig. B.1, see Appendix B). Storage modulus of E_3/K_3-PA gel is independent of oscillation frequency (Fig. B.1B). In the first two measurements of amplitude sweep test, E_3/K_3-PA gel remained in the linear viscoelastic range (*i.e.* constant plateau of the storage modulus) up to 1% strain (Fig. B.1C). It was not the case with the third measurement, but because the first two almost perfectly overlap, it might be reasonable to consider

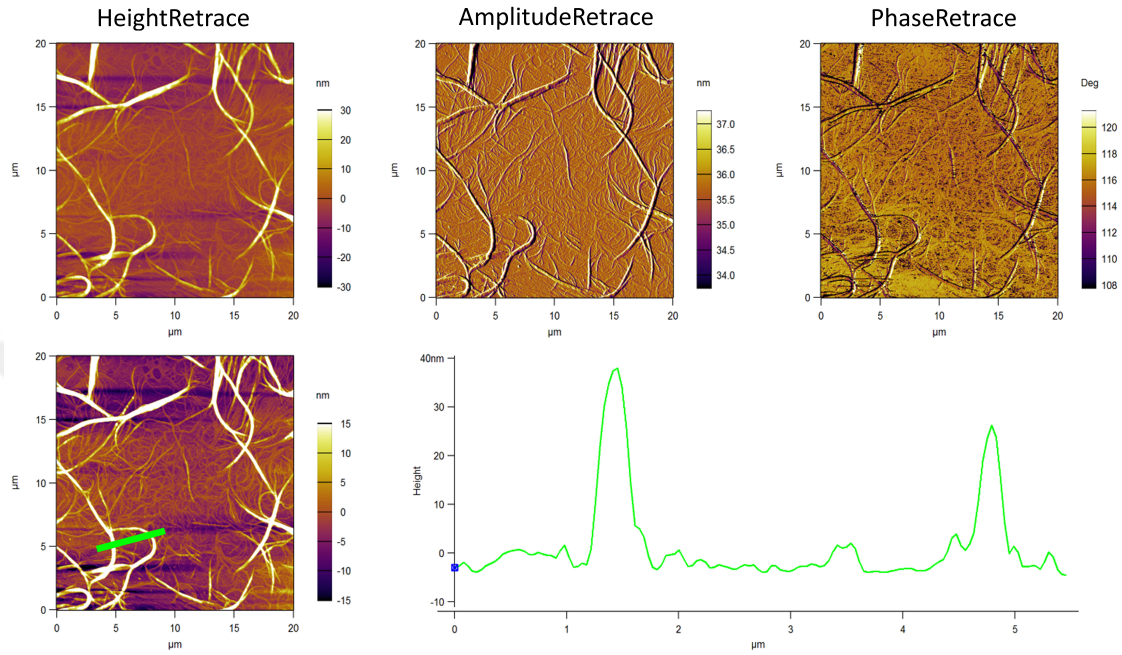


Figure 3.5: Tapping mode AFM images of E_3/K_3-PA dried on a cleaned glass coverslip.

the first two measurements as more reliable.

3.3.2 Commitment of rat mesenchymal stem cells (rMSCs) to osteogenic differentiation on the peptide nanofibers

3.3.2.1 Viability rMSCs on the osteoinductive peptide nanofibers

Viability of rMSCs was checked using live/dead assay after 24 h of incubation (Fig. 3.8). These results showed that peptide nanofibers provide a biocompatible environment and were not toxic to cells.

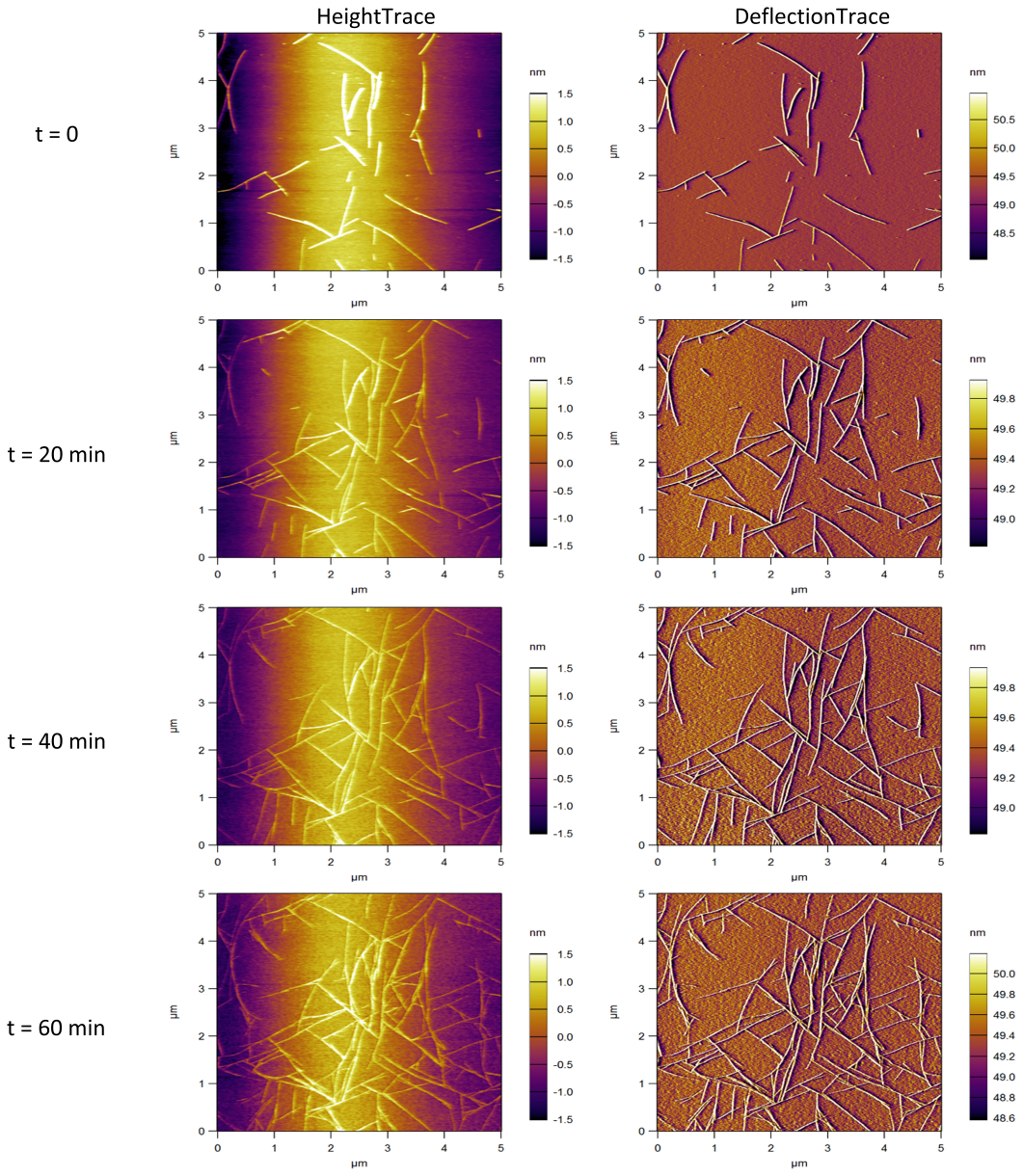


Figure 3.6: Contact-mode AFM images of self-assembly process of E_3/K_3-PA nanofibers formed on mica surface in solution. Each image was measured at approximately 10 min.

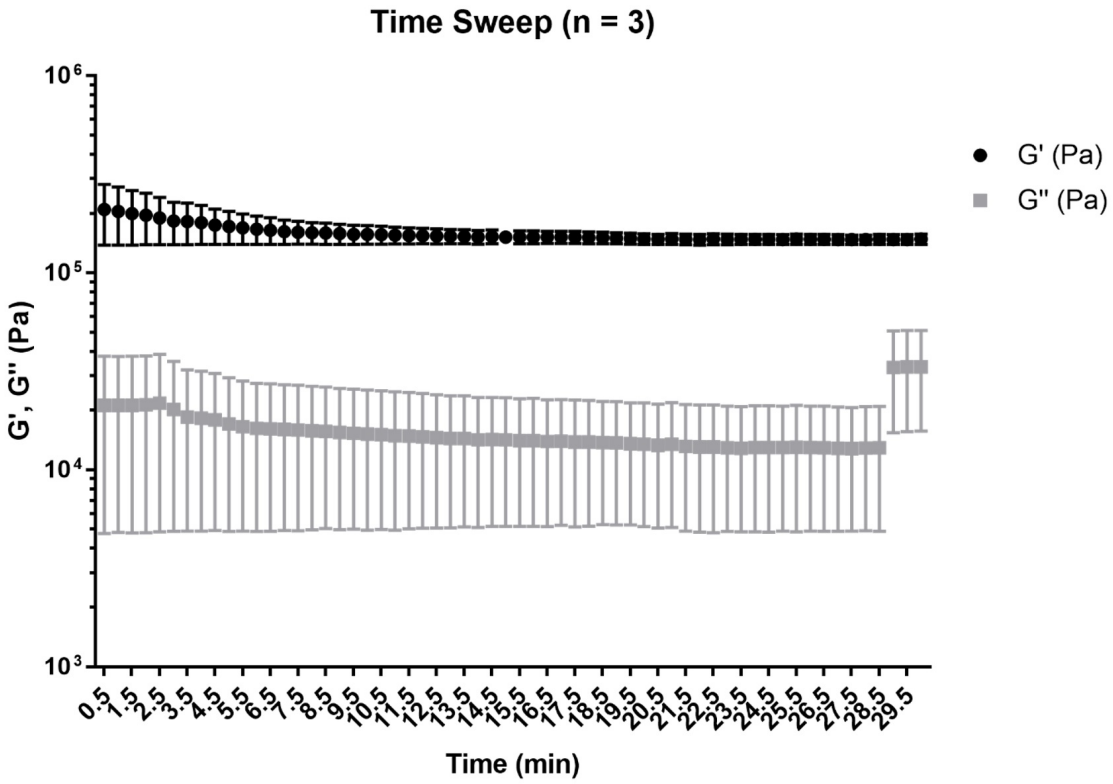


Figure 3.7: Time sweep rheology analysis of E_3/K_3-PA. 1% w/v concentration of individual PAs were mixed on the sample holder of rheometer and the measurement was performed immediately after the mixing. Results are given with three repeats. Error bars are mean ± SEM.

3.3.3 Force mapping reveals stiffening of rMSCs differentiating on the osteoinductive self-assembled peptide nanofibers

Mechanical properties of rMSCs that formed cell clusters on E_3/K_3-PA nanofibers were investigated using force-distance curve-based AFM (Fig. 3.9). Force mapping measurements were performed on rMSC cell clusters on peptide nanofibers and rMSCs on bare glass. The Teflon-like C_4F_8 thin film-coated antifouling AFM probes were used for the force mapping measurements (Fig. 2.1).

Young's modulus values were calculated by fitting approach curves with conical Hertz model. 12 force curves per cell were used in data analysis and presented

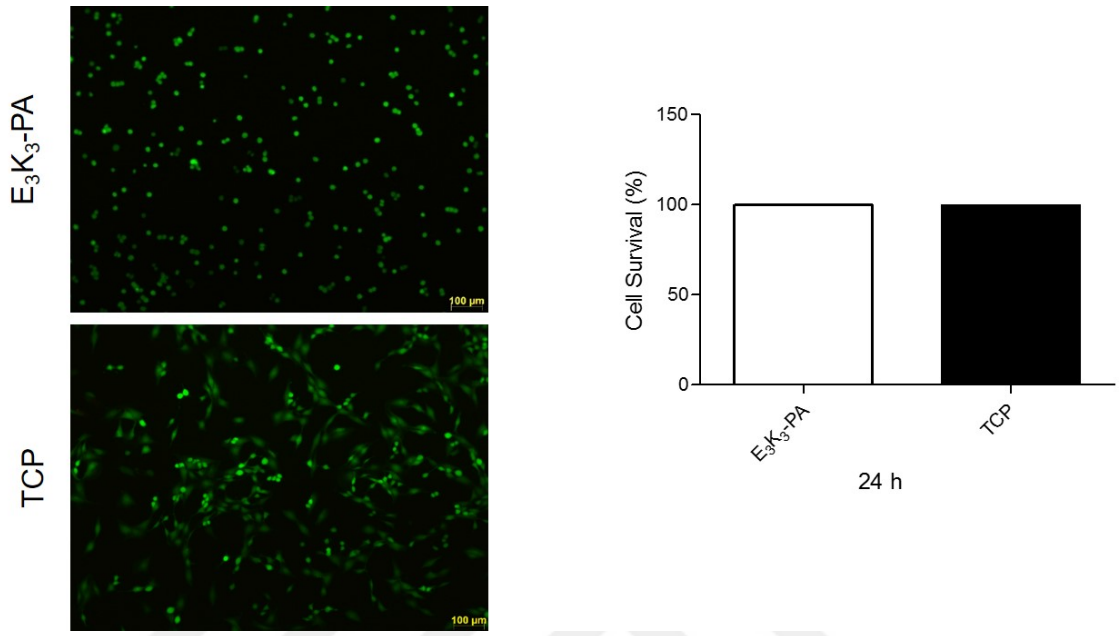


Figure 3.8: Live/dead assay of rMSCs on E_3/K_3-PA nanofiber gel. Green is calcein-AM that shows live cells. Red color is ethidium homodimer (which is not seen here because there are not any dead cells) that indicates dead cells. Quantitative result of cell survival obtained from cell counts was shown on the graph on the right. Samples were analyzed with three repeats.

in histograms (Fig. 3.10 and 3.11). Results indicated that rMSCs significantly increased their average Young's moduli on peptide nanofibers in osteogenic medium between day 3 and day 7, from an average value of 1.43 ± 0.16 kPa at day 3 to 2.19 ± 0.19 kPa at day 7. In addition, Young's moduli of rMSCs remained high on peptide nanofibers on day 14 (2.30 ± 0.25 kPa). In contrast, the elasticity of rMSCs on glass decreased significantly from day 3 to day 7 (Fig. 3.10 and 3.11). On day 3, rMSCs on glass had an average Young's modulus value of 2.60 ± 0.17 kPa, while this value dropped sharply on day 7 (to 0.74 ± 0.09 kPa) and further on day 14 (to 0.67 ± 0.04 kPa).

Peptide-coated coverslips were also measured by AFM to obtain Young's modulus changes that happen to the peptide nanofiber hydrogel due to incubation in the osteogenic medium (Fig. 3.12). As a result, the elastic modulus of peptide nanofiber hydrogel was found in a range suitable for osteogenic differentiation,

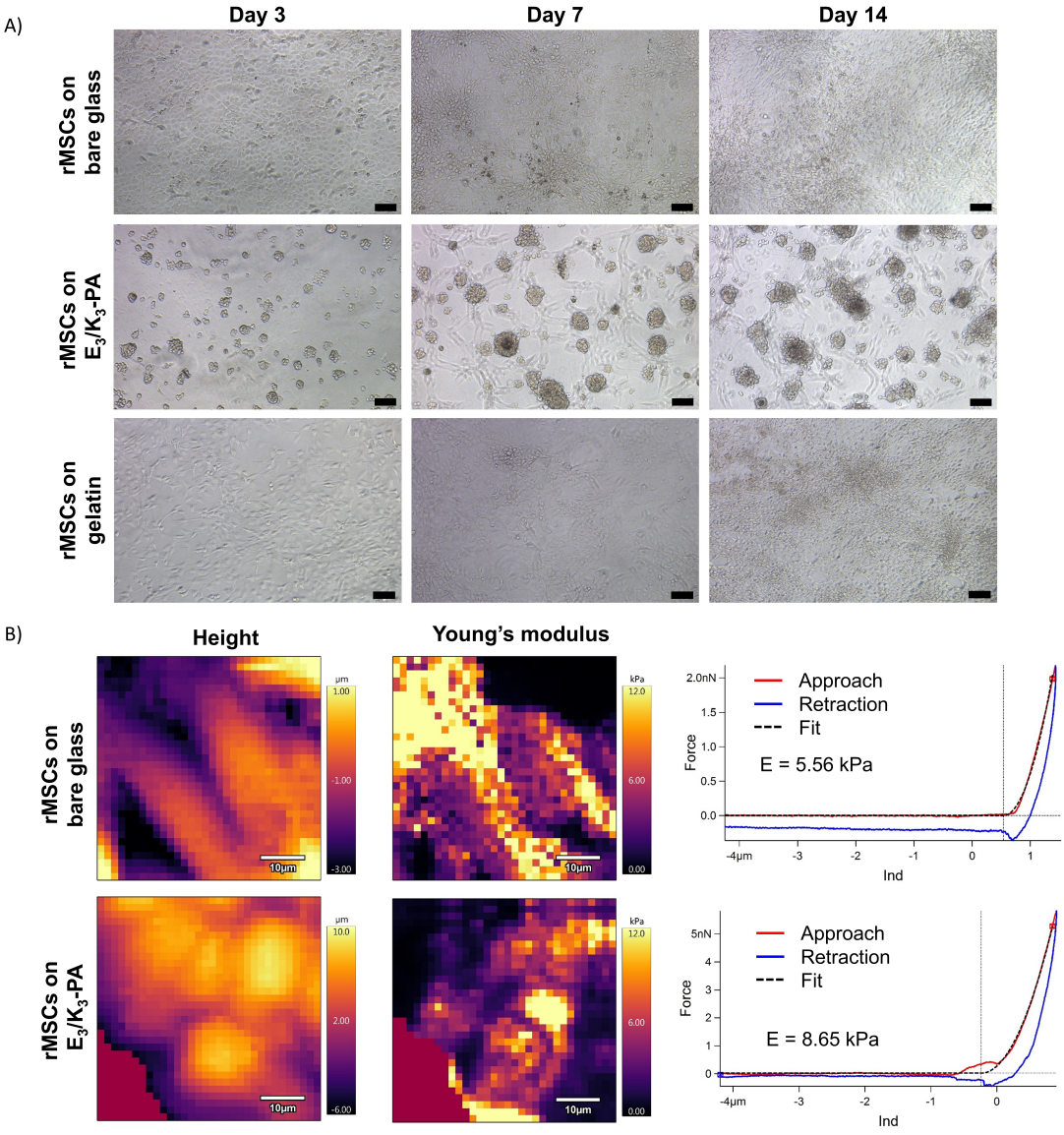


Figure 3.9: A) Optical microscope images of rMSCs on glass, E_3/K_3-PA and gelatin, all in osteogenic differentiation medium. Scale bars are 100 µm. B) Representative force maps of rMSCs on glass surface and aggregates of rMSCs on the peptide nanofibers. Force curves shown on the right of the maps belong to a random point on a map on its lane. The force maps were measured from cells on day 3 (for bare glass) or day 7 (for E_3/K_3-PA) of osteogenic differentiation.

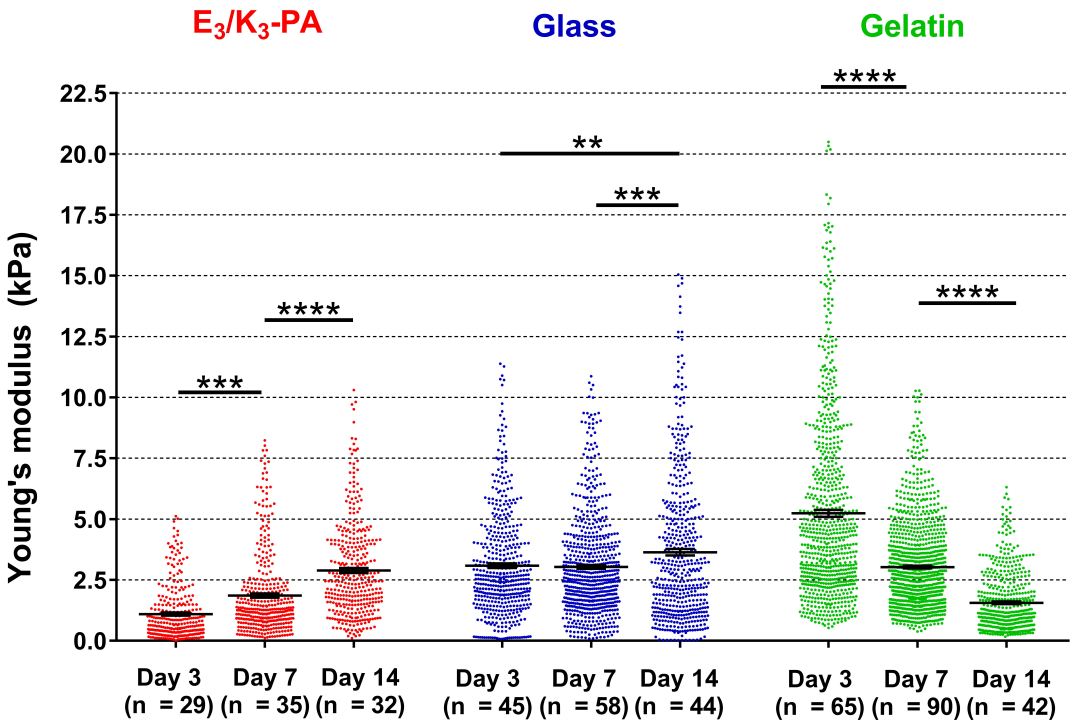


Figure 3.10: Young's modulus histograms of rMSCs on days 3, 7 and 14 of osteogenic differentiation on E_3/K_3-coated glass, bare glass and gelatin-coated glass. ****p<0.0001, ***p<0.001, **p<0.01, *p<0.05. n indicates the number of cells analyzed. Error bars are standard errors of mean. Each dot corresponds to a force-distance measurement. 12 force curves per cell were selected from force maps and stacked for each substrate/matrix groups.

that is, between 20 and 100 kPa, as Discher group suggested [29]. Elastic modulus values of the osteoinductive peptide nanofiber hydrogel on day 7 and 14 are at the optimum, which might be a reason for the remarkable increase in biomineralization after day 3. This result also rules out the possibility that the increase observed in cellular elastic moduli between day 3 and day 7 might be due matrix/substrate effects, which is not the case because the matrix Young's modulus values of the peptide nanofiber hydrogel are higher on day 3 than day 7.

Close and intensive cell-cell contacts were observed at the osteogenic differentiating cells on the peptide nanofibers. This observation agrees with a report in the

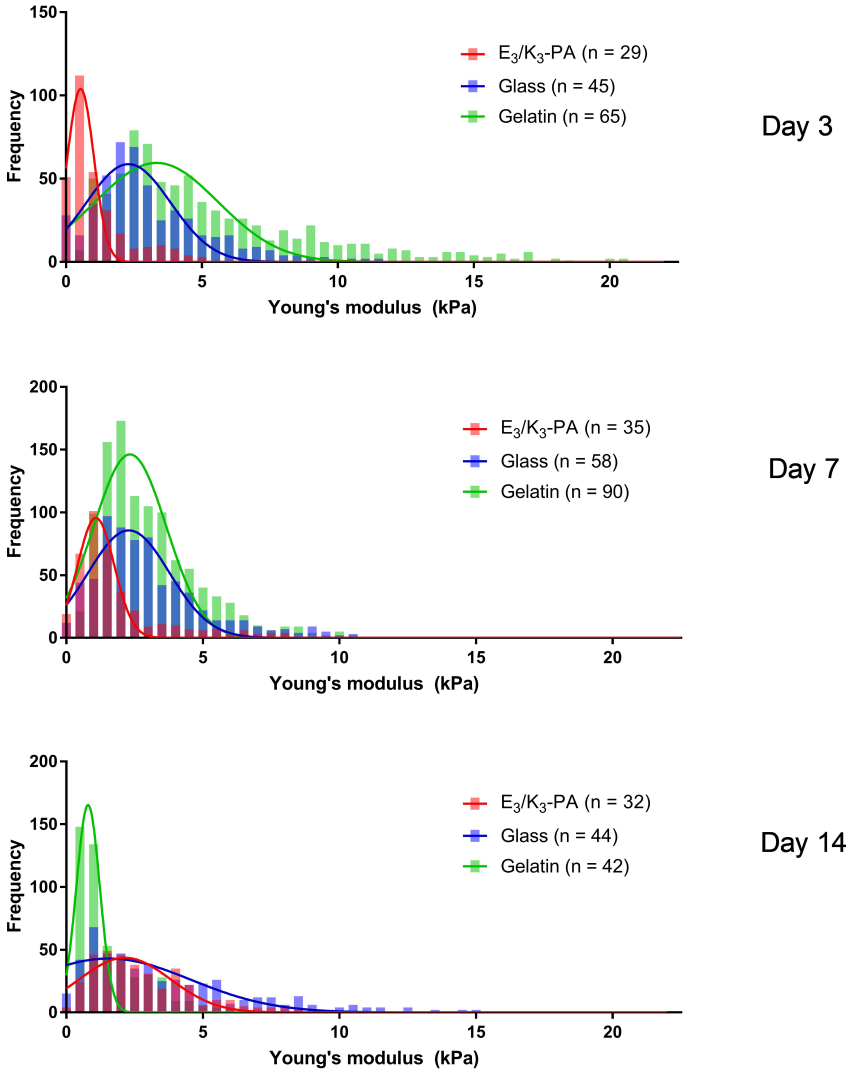


Figure 3.11: Nanomechanical characterization results graphed as frequency distribution histograms with Gaussian curves.

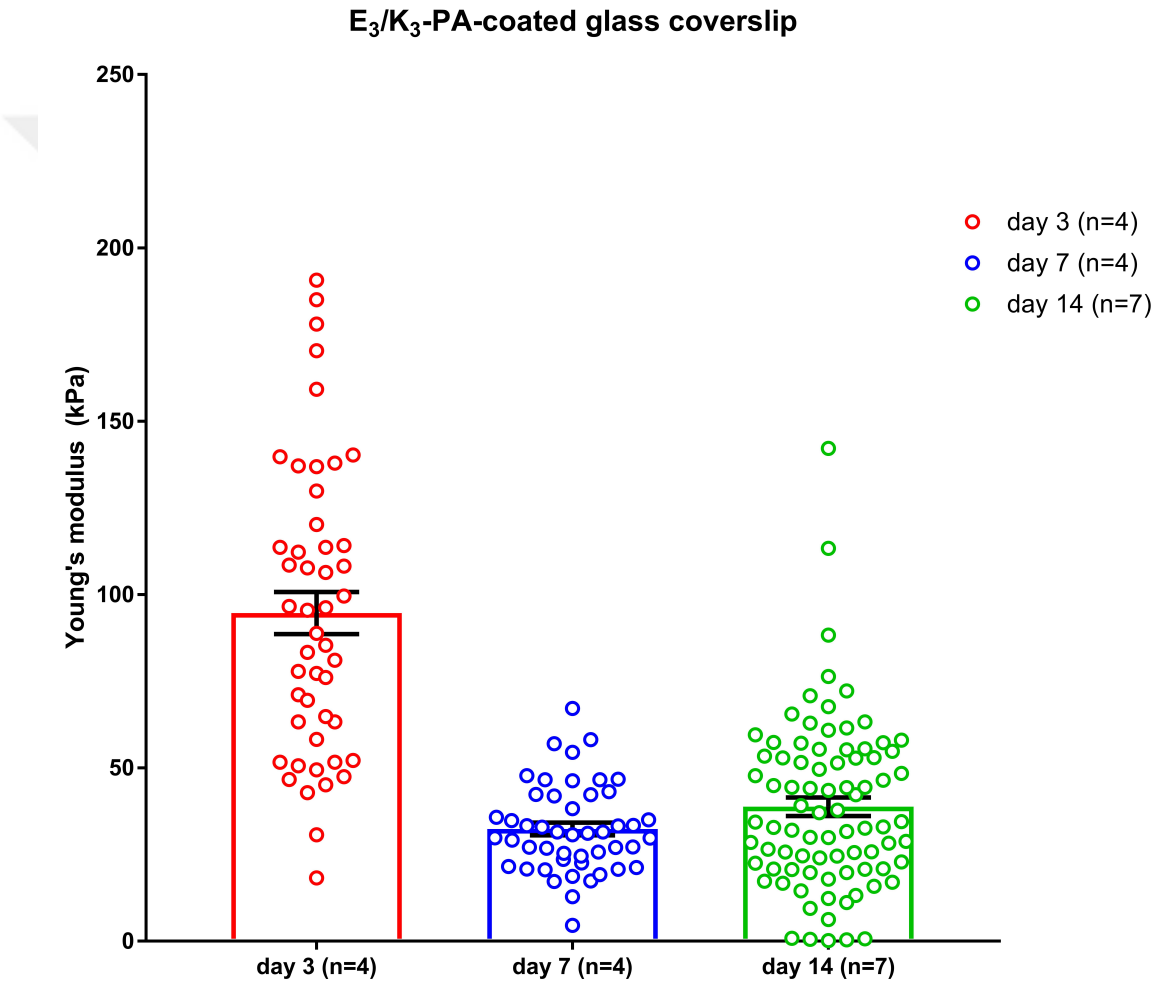


Figure 3.12: Young's moduli derived from AFM force mapping of E_3/K_3 only control samples (peptide-coated glass coverslips without cells) incubated in osteogenic medium. n is the number of force maps measured and analyzed from the samples.

literature that osteoblasts have close contacts with each other [26]. Mature osteoblasts operate as bone lining cells which were shown in close contact with each other in related studies in the literature [169, 203]. In contrast to osteoblasts, osteocytes were shown to be regulated with intercellular separation [26]. Moreover, condensation of mesenchymal stromal cells was previously reported to be correlated with osteogenic differentiation in the literature [204], suggesting an indication of osteogenic differentiation of rMSCs on E_3-PA/E_3-PA nanofibers.

3.3.4 Mineralization profile of the differentiating cells on the peptide nanofibers

Alizarin red staining was performed to analyze calcium deposition by the cells on the peptide nanofibers (Fig. 3.13). Mineralization correlates well with cell stiffness increase on the peptide nanofibers (Fig. 3.10 and 3.11). Hence it can be argued that osteoblast maturation on the bioactive peptide nanofibers causes cell stiffening due to extensive mineral deposition during osteogenic differentiation of rMSCs. For the mineral deposition, it can be speculated that a mineral nucleation occurs on the peptide nanofibers because of the cell-material interaction (*i.e.* cell-peptide interaction) since calcium deposition occurs extensively at the differentiated cells (*i.e.* osteogenic cells, osteoblasts) and calcium crystals are extracellularly deposited and also that negatively charged triple glutamic acid sequence that is found on E_3-PA might attract positively charged calcium. Another speculation, this regarding to cell stiffening, can be done for the osteogenic differentiating cells *in vivo* that there must be such a cell stiffening due to mineralization of mature osteoblasts after differentiating from MSCs because peptide nanofibers might mimic the natural ECM better than other Young's modulus characterization studies of adherent MSCs differentiating on flat substrates and the measurements performed with AFM.

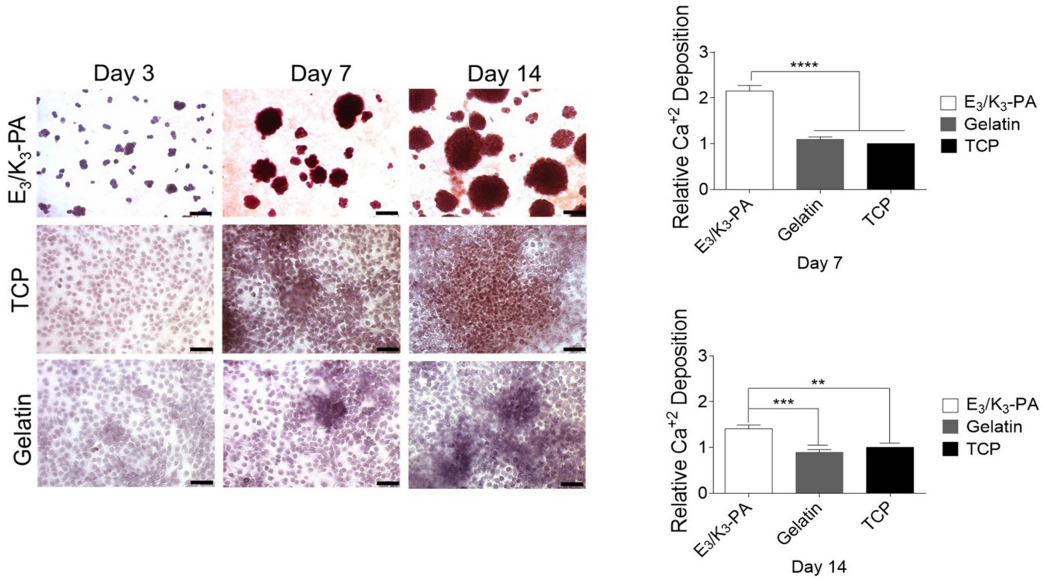


Figure 3.13: Calcium deposition profiles of cells on the bioactive peptide nanofibers and on the TCP. A) Optical microscope images with Alizarin red staining. Scale bars are 100 µm. B) Quantification of Ca^{2+} deposition on peptide nanofibers and TCP on days 7 and day 14.

3.4 Conclusion and future perspectives

rMSCs efficiently differentiated into osteogenic lineage on the osteoinductive peptide nanofibers. They formed osteogenic cell clusters, also called bone nodules, which deposited remarkable amounts of calcium. Their Young's moduli had an increasing pattern which might have resulted from the calcium mineralization on the osteoinductive peptide nanofibers. In contrast, rMSCs on the gelatin-coated glass showed a decreasing pattern of Young's modulus which could be explained by lack of sufficient mineralization profile of the cells.

Young's modulus of osteogenic differentiating cells at the adherent state might increase with mineral deposition by the cells. Also importantly, the osteoinductive peptide nanofibers that I utilized are smart biomaterials that can be used for tuning the rate of biomineralization and hence the osteoblast differentiation, thus they are promising to be utilized for bone tissue engineering applications.

Chapter 4

Force Mapping the Osteospheroids with Colloidal Microbead AFM Probes

4.1 Study background and hypothesis

To investigate if the tip choice has any effect on the results of mechanical measurements performed on the cells, I also performed force mapping experiments by using commercial colloidal microspherical bead attached AFM cantilevers. I expected a similar increasing trend of Young's moduli of osteospheroids on the osteoinductive peptide nanofibers in the results.

4.2 Materials and methods

Cell culture experimental method is the same as in Chapter 3 except in the followings that days of differentiation were different, that I did not include gelatin group, and that cell density was chosen as 5,000 cells/well of 24-well plate during

cell seeding step, differently. Same peptide amphiphiles E_3/K_3-PA were used. Gold microsphere sQube® probes having a diameter of 5.2 µm were used for AFM force mapping measurements (Figure 4.1) and Young's modulus of rMSCs differentiated on nanofibers in osteogenic medium was obtained by applying JKR model at Igor Pro, software of AFM. Young's modulus of rMSCs grown on bare glass in the normal growth medium was calculated by applying Hertz model to approach curve of the force distance curves. rMSCs on glass were grown only in normal growth medium. However, rMSCs on peptide nanofibers were transferred to osteogenic medium 4 days after inital seeding and after reaching to some degree of confluency.

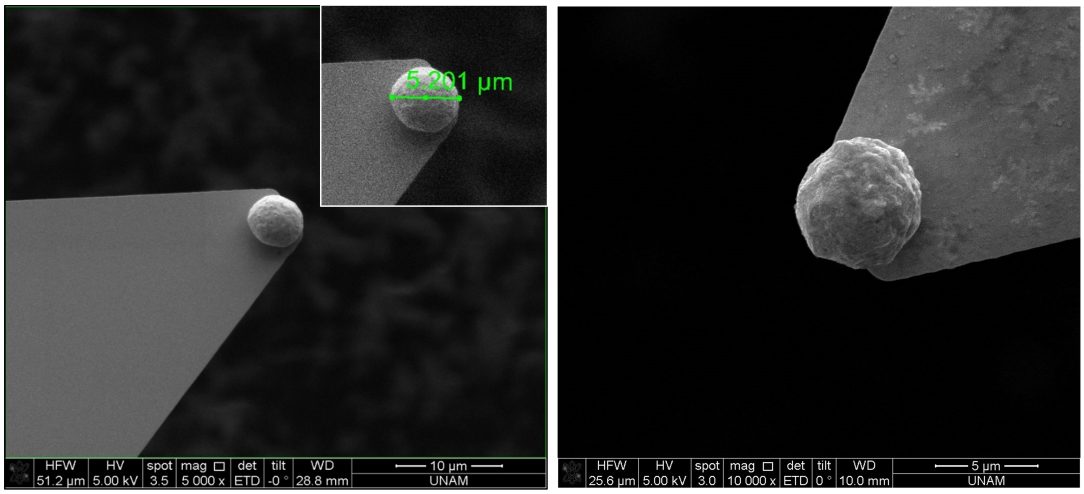


Figure 4.1: Scanning electron microscope (SEM) images of gold colloidal microsphere AFM probes (sQube®) before (left) and after (right) use in AFM force mapping measurements.

4.3 Results and discussion

Viability of the cells cultured on peptide nanofibers was tested. Experiment result is shown with 24 h, 48 h and 72 h results, which showed that the cells were viable (Figure 4.2). Cells on the osteoinductive peptide nanofibers were allowed to differentiate until day 24 of osteogenic differentiation as shown via inverted optical microscope images (Figure 4.3) and AFM measurements were performed on the

cells at the indicated days of osteogenic differentiation. Day of transfer from cell maintenance medium to osteogenic differentiation induction medium was marked as Day 0 because it was the start of osteogenic differentiation. Representative 16 x 16 force maps are shown in Figure 4.4. Histograms with scatter plots were graphed for both rMSCs on E_3/K_3-PA (Figure 4.5) and rMSCs on bare glass (Figure 4.6). Cells on bare glass are on a stable Young's moduli trend while there is a somewhat increasing pattern of Young's moduli of cells on E_3/K_3-PA, correlating with the nanomechanical measurement results (Figure 3.10 and A.1). Although the sample numbers are low in the microindentation experiments, these results still show that Young's modulus values of cells are not very far from the nanomechanical characterization results presented in the previous chapter of this thesis work. In the literature, studies comparing elastic modulus values of cells measured with sharp and microsphere probe, like that of Sokolov group's, found great variances between elastic modulus values of cell between nano and microindentation AFM experiments as the sharp probe yielded much greater numbers (mostly around 10, 15 and 20 kPa) of elastic moduli whereas microsphere probe (having a diameter of $\sim$5 µm) yielded around 1, 2 and 3 kPa on human cervical epithelial cells [130]. Nanomechanical characterization results performed by Teflon-like AFM probes do not correlate with that study for example. Sharp probes usually result with higher error margins when compared to microindentation based results [205]. One reason that I get similar elastic modulus values from my experiments of both nano- and micromechanical characterizations might be that the Teflon-like probes are promising for obtaining more precise force curve measurements than that conventional sharp probes can provide and since the curve fittings were quite not bad based on the Hertz Cone model as shown with representative curve fittings in Figure 3.9, AFM's software must have given realistic elastic modulus values.

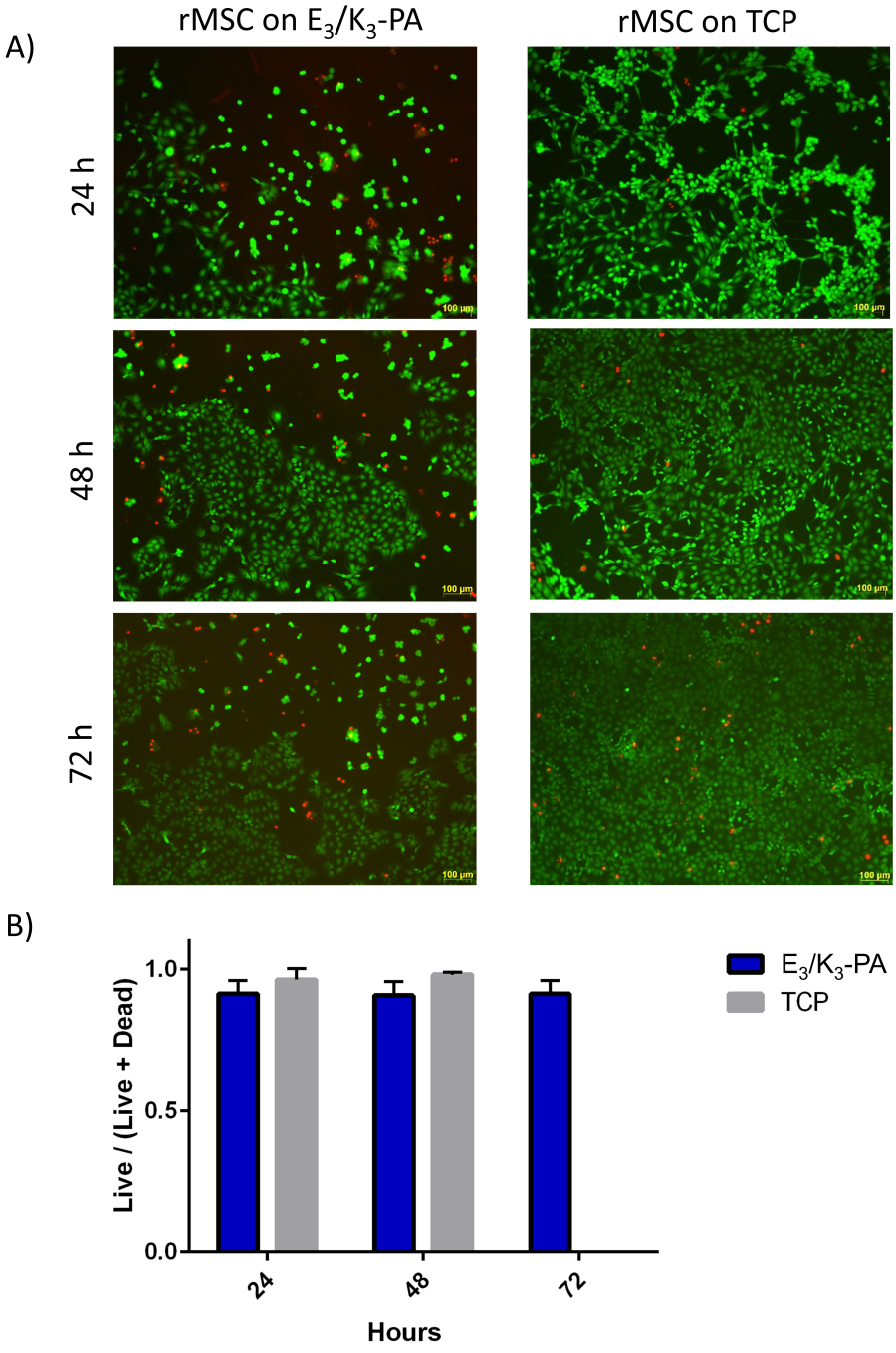


Figure 4.2: Live/dead assay repeat experiment result of rMSCs cultured on E_3/K_3-PA nanofibers. Representative fluorescence microscope images are shown. Quantitative result was calculated from three repeats samples. 72 h result of TCP was excluded due to overconfluency.

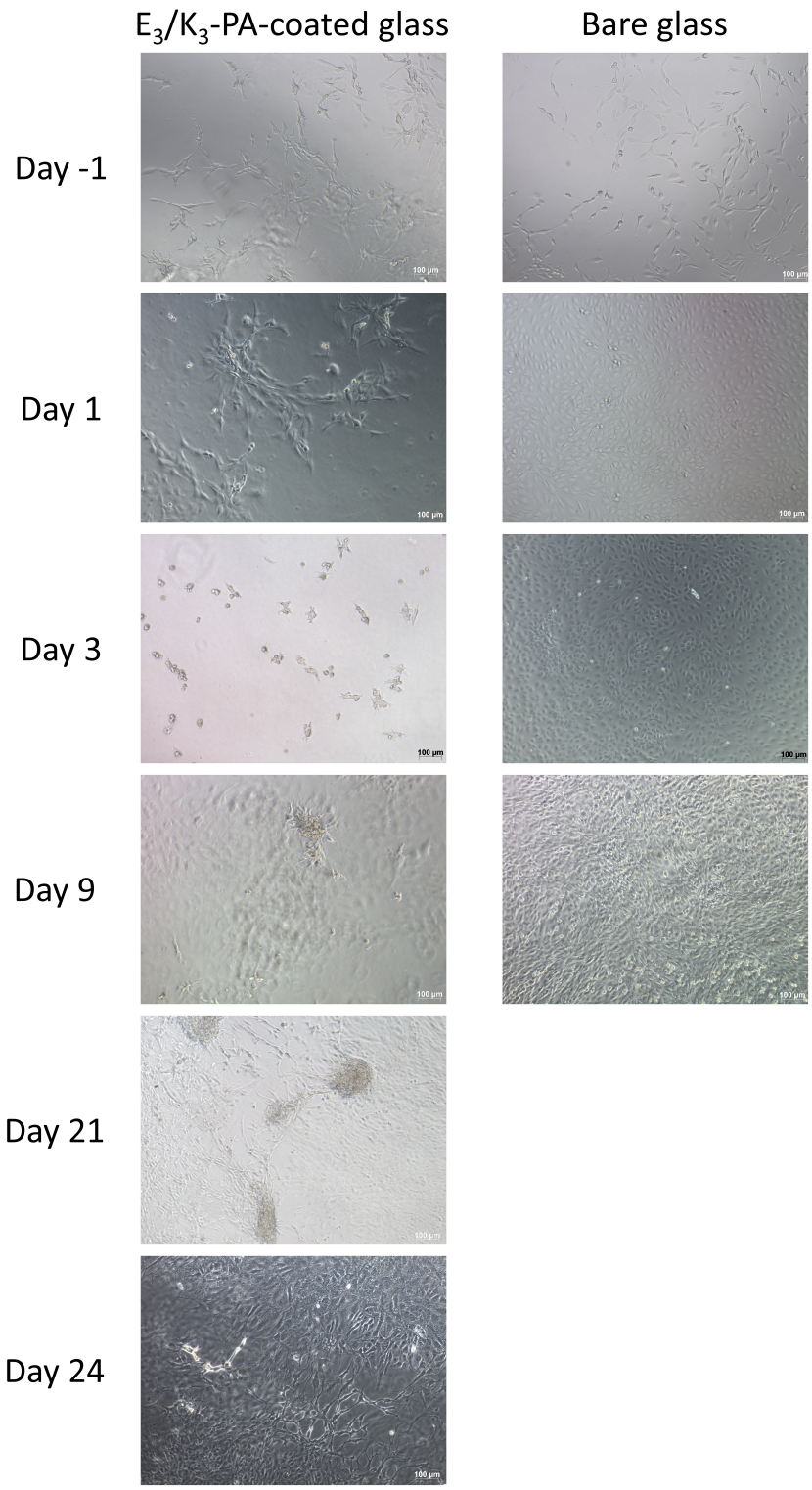


Figure 4.3: Optical microscope images of rMSCs on osteoinductive peptide nanofiber-coated glass coverslip in osteogenic medium (on the left) versus rMSCs on bare glass coverslip (on the right) in maintenance medium are shown.

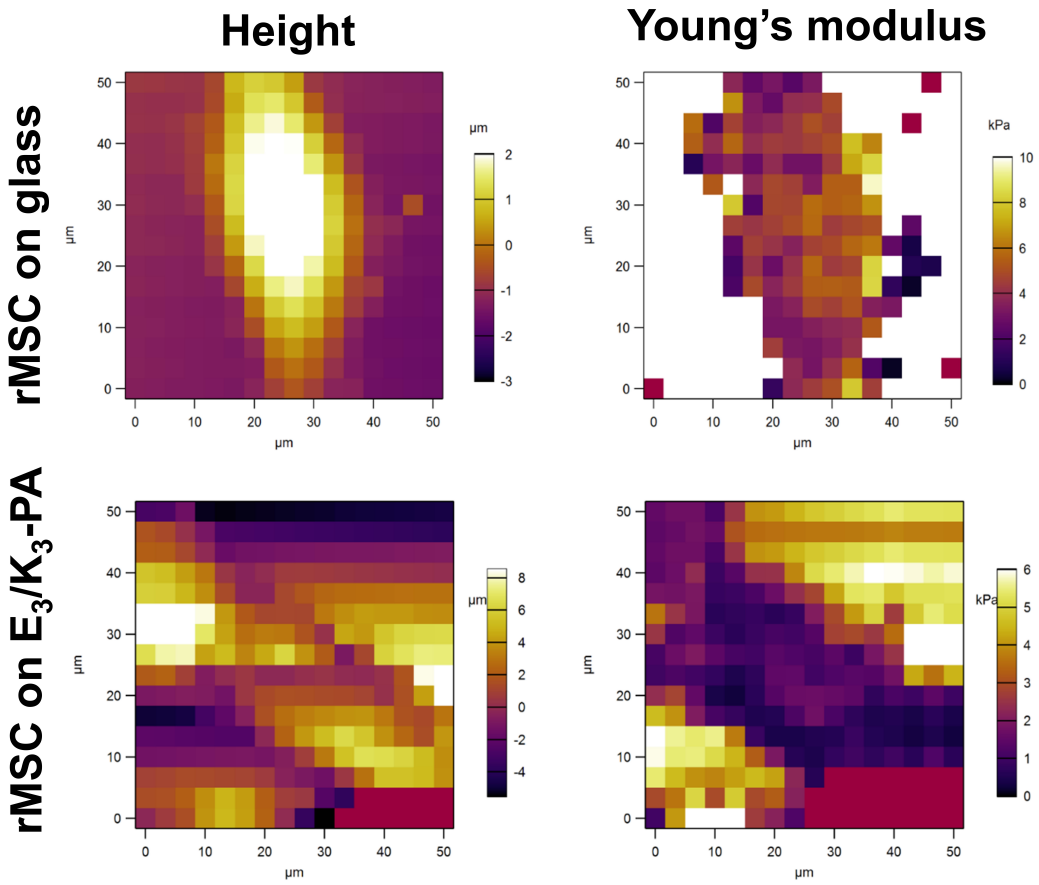


Figure 4.4: Representative force map results of rMSCs cultured on bare glass and rMSC on E_3/K_3-PA-coated glass. Height maps and converted Young's modulus maps are shown.

4.4 Conclusion and future perspectives

rMSCs efficiently differentiated into osteogenic lineage on the osteoinductive peptide nanofibers. They formed osteogenic cell clusters. Micromechanical measurements on the cells using the colloidal probe showed that Young's modulus of differentiating rMSCs had an increasing pattern on the osteoinductive peptide nanofibers while rMSCs on the bare glass coverslips did not show such pattern but showed a stationary trend of average Young's modulus changes in normal growth medium because the cells were expected not to differentiate.

Teflon-like spheroconical probes are promising for elastic modulus characterization of living cells as they gave results similar to microindentation experiment results at range, and if a suitable contact mechanics model can be derived, which can surpass the Sneddon model, that better describes the probe geometry and the indentation, and is better at estimating the elastic modulus values of cells, more reliable and repeatable results can be obtained from cell mechanics experiments when Teflon-like spheroconical probes are utilized.

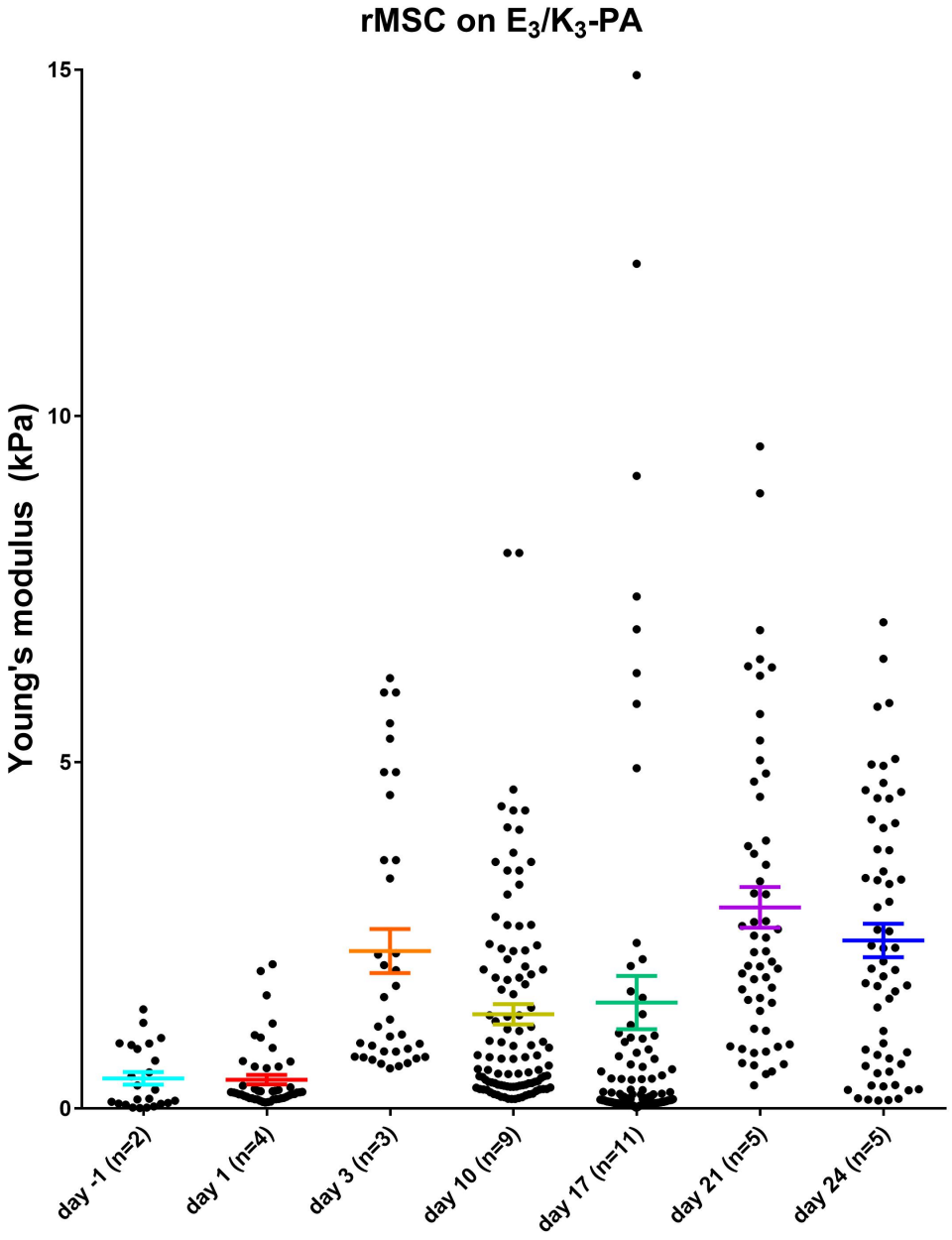


Figure 4.5: AFM Young's modulus results of differentiating rMSCs cultured on E_3/K_3-PA peptide nanofibers shown via columns with scatter plot. Each dot represents an analysis of a single force-distance curve measurement. n is the number of cells analyzed at indicated day of differentiation. Young's modulus of rMSCs differentiated on nanofibers in osteogenic medium was obtained by applying JKR model at Igor Pro, software of AFM. Normal growth medium of rMSCs on peptide nanofibers were replaced with osteogenic medium at 4th day after initial seeding in order to reach sufficient confluency.

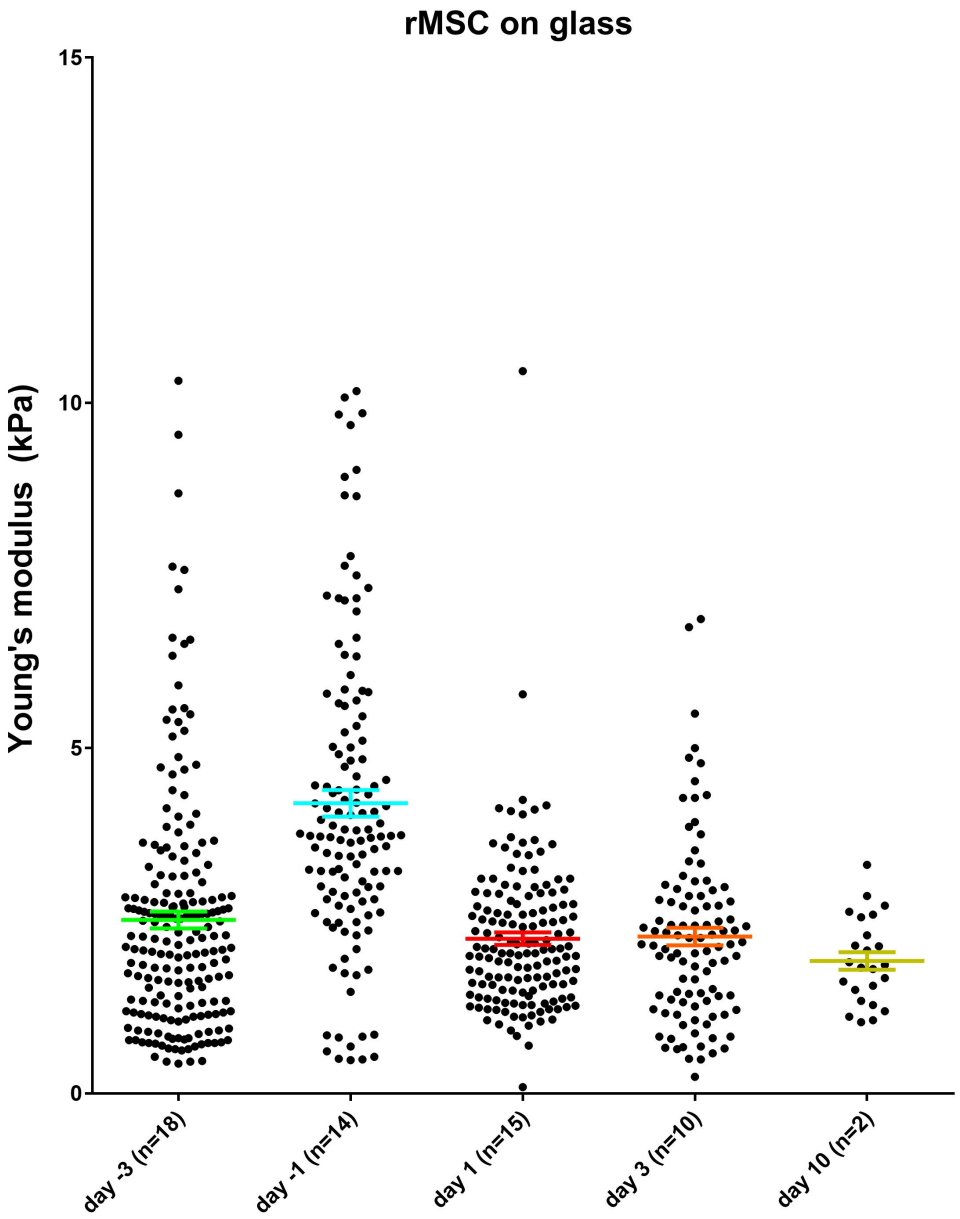


Figure 4.6: AFM Young's modulus results of differentiating rMSCs cultured on bare glass coverslip. Each dot represents an analysis of a single force-distance curve measurement. n is the number of cells analyzed at indicated day of differentiation. Young's moduli of rMSCs in the normal growth medium on glass coverslip were calculated by applying Hertz model to approach curve of the force distance curves. rMSCs on glass were grown only in normal growth medium.

Chapter 5

Conclusions and Future Perspectives

5.1 General conclusions

Bioactive peptide nanofiber hydrogels can be used as osteoinductive scaffolds to induce osteogenic differentiation of rMSCs in which the cells form cell clusters on the nanofibers during differentiation in osteogenic medium. The average Young's modulus value of cells increases on the osteoinductive peptide nanofibers while the values are lower when compared to the bare glass and gelatin groups. The same trend is not present for the rMSCs on the bare glass group because there is no significant increase of average Young's modulus value of the cells between days 3 and 7 on the glass. It can be speculated that cell stiffening that happens on the osteoinductive peptide nanofibers might imply that MSCs must be undergoing a stiffening process throughout their differentiation into mature osteoblasts *in vivo* and that mineralization *in vivo* might cause the osteogenic differentiating MSCs to stiffen effectively. Furthermore, the peptide nanofiber hydrogel utilized here had Young's modulus values between 20-100 kPa range when incubated at the same conditions as the cells cultured on scaffolds. This might suggest that MSCs increase their Young's moduli in an ECM-like environment. Since there

was not significant mineralization by rMSCs on the gelatin, it is reasonable to conclude that the osteoinductive peptide nanofibers might have increased the rate of osteogenic differentiation of rMSCs because the mineralization happened quickly on the peptide nanofibers.

5.2 Future perspectives

As a future perspective, the osteospheroids can be used for therapeutic purposes, as they are readily formed on the osteoinductive peptide nanofibers during osteogenic differentiation. The osteospheroids can be collected and administered to local areas of injury for enhancing bone regeneration and biomineralization.

For future studies, longer periods of differentiation (*e.g.* until day 28) can be studied with mechanical measurements with increased number of repeats so that n can be increased and results of later stages of differentiation can be achieved. Hence, not only osteoblast differentiation from MSCs but also osteocyte differentiation might be possible for evaluation of cellular elasticity and identification of related biophysical markers. I tried to do it with microsphere probe already but my cell number which can be analyzed is relatively low at most of the days.

In this thesis work, nuclear and cytoskeletal mechanics were not analyzed separately. AFM analyses might be feasable to decouple nuclear and cytoskeletal contributions to cellular mechanical responses because state-of-the-art AFMs can be capable of measuring images at higher speeds and resolutions for mechanical analysis.

Modifying AFM tips with Teflon-like coating allowed obtaining elastic modulus values of cells reliably and similar to the values of elastic modulus of cells derived upon force mapping with microsphere probe, which suggests that Teflon-like probes are better than conventional sharp AFM tips whose force curve measurements on cells might typically result elastic modulus values 10 times larger than that of microsphere probe used measurements.

5.3 Challenges encountered during AFM measurements for mechanical characterization of spheroids on the peptide nanofiber hydrogels

One of the challenges associated with AFM experiments of spherical cell aggregates on the peptide nanofibers is the limited Z range of AFM, which is typically 10 µm or 20 µm at most commercial AFMs. If aggregates constisting of few cells are measured on the peptide nanofiber hydrogel, then there is the issue of topography of the hydrogel. In my experiments, the Z range of Asylum Research MFP-3D AFM is ∼10 µm, sometimes even the hydrogel topography was too variant and rough that not only I had difficulties of completing force mapping measurements, but also distinguishing cells from the hydrogel became by itself difficult when I wanted to measure force maps of aggregates having small heights. Measurement of the spheroids with very large heights, say spheroids having more than 100 cells, became possible only when AFM probe was manually positioned on top of the spheroid when engaging. Also, keeping the force distance at 10 µm allowed acquiring more force curves which can result with good fitting and contain the horizontal part, which were another issue for doing a reliable data analysis.

Especially with the gold microsphere probes, the adhesion between cells and the tip was very high and sometimes a spheroid attached to the tip and stayed attached, preventing the continuation of the measurements with the same probe. Teflon-like probes did not cause such problems.

Bibliography

[1] F. Barry and M. Murphy, "Mesenchymal stem cells in joint disease and repair," *Nature Reviews Rheumatology*, vol. 9, no. 10, pp. 584–594, 2013.

[2] E. A. Jones, P. V. Giannoudis, and D. Kouroupis, "Bone repair with skeletal stem cells: rationale, progress to date and clinical application," *Therapeutic Advances in Musculoskeletal Disease*, p. 1759720X16642372, 2016.

[3] A. I. Caplan, "Mesenchymal stem cells," *Journal of Orthopaedic Research*, vol. 9, no. 5, pp. 641–650, 1991.

[4] G. Yourek, M. A. Hussain, and J. J. Mao, "Cytoskeletal changes of mesenchymal stem cells during differentiation," *ASAIO journal (American Society for Artificial Internal Organs: 1992)*, vol. 53, no. 2, p. 219, 2007.

[5] T. Tondreau, L. Lagneaux, M. Dejeneffe, M. Massy, C. Mortier, A. Delforge, and D. Bron, "Bone marrow–derived mesenchymal stem cells already express specific neural proteins before any differentiation," *Differentiation*, vol. 72, no. 7, pp. 319–326, 2004.

[6] G. Chamberlain, J. Fox, B. Ashton, and J. Middleton, "Concise review: mesenchymal stem cells: their phenotype, differentiation capacity, immunological features, and potential for homing," *Stem Cells*, vol. 25, no. 11, pp. 2739–2749, 2007.

[7] G. Muñoz-Elías, D. Woodbury, and I. B. Black, "Marrow stromal cells, mitosis, and neuronal differentiation: stem cell and precursor functions," *Stem Cells*, vol. 21, no. 4, pp. 437–448, 2003.

[8] A. I. Caplan and S. P. Bruder, "Mesenchymal stem cells: building blocks for molecular medicine in the 21st century," *Trends in Molecular Medicine*, vol. 7, no. 6, pp. 259–264, 2001.

[9] P. Charbord, "Bone marrow mesenchymal stem cells: historical overview and concepts," *Human Gene Therapy*, vol. 21, no. 9, pp. 1045–1056, 2010.

[10] G. Ren, L. Zhang, X. Zhao, G. Xu, Y. Zhang, A. I. Roberts, R. C. Zhao, and Y. Shi, "Mesenchymal Stem Cell-Mediated Immunosuppression Occurs via Concerted Action of Chemokines and Nitric Oxide," *Cell Stem Cell*, vol. 2, no. 2, pp. 141–150, 2008.

[11] T. Albrektsson and C. Johansson, "Osteoinduction, osteoconduction and osseointegration," *European Spine Journal*, vol. 10, no. 2, pp. S96–S101, 2001.

[12] P. Rosset, F. Deschaseaux, and P. Layrolle, "Cell therapy for bone repair," *Orthopaedics & Traumatology: Surgery & Research*, vol. 100, no. 1, pp. S107–S112, 2014.

[13] B. von Lospichl, S. Hemmati-Sadeghi, P. Dey, T. Dehne, R. Haag, M. Sittinger, J. Ringe, and M. Gradzielski, "Injectable hydrogels for treatment of osteoarthritis a rheological study," *Colloids and Surfaces B: Biointerfaces*, 2017.

[14] E. Jones and R. Schäfer, "Where is the common ground between bone marrow mesenchymal stem/stromal cells from different donors and species?," *Stem Cell Research & Therapy*, vol. 6, no. 1, p. 143, 2015.

[15] T. K.-P. Goh, Z.-Y. Zhang, A. K.-L. Chen, S. Reuveny, M. Choolani, J. K. Y. Chan, and S. K.-W. Oh, "Microcarrier culture for efficient expansion and osteogenic differentiation of human fetal mesenchymal stem cells," *BioResearch Open Access*, vol. 2, no. 2, pp. 84–97, 2013.

[16] J. J. Bara, R. G. Richards, M. Alini, and M. J. Stoddart, "Concise review: Bone marrow-derived mesenchymal stem cells change phenotype following in vitro culture: implications for basic research and the clinic," *Stem cells*, vol. 32, no. 7, pp. 1713–1723, 2014.

[17] F.-J. Lv, R. S. Tuan, K. Cheung, and V. Y. L. Leung, "Concise review: the surface markers and identity of human mesenchymal stem cells," *Stem Cells*, vol. 32, no. 6, pp. 1408–1419, 2014.

[18] M. B. Murphy, K. Moncivais, and A. I. Caplan, "Mesenchymal stem cells: environmentally responsive therapeutics for regenerative medicine," *Experimental & Molecular Medicine*, vol. 45, no. 11, p. e54, 2013.

[19] S. R. Ghaemi, F. J. Harding, B. Delalat, S. Gronthos, and N. H. Voelcker, "Exploring the mesenchymal stem cell niche using high throughput screening," *Biomaterials*, vol. 34, no. 31, pp. 7601–7615, 2013.

[20] T. Ma, A.-C. Tsai, and Y. Liu, "Biomanufacturing of human mesenchymal stem cells in cell therapy: Influence of microenvironment on scalable expansion in bioreactors," *Biochemical Engineering Journal*, vol. 108, pp. 44–50, 2016.

[21] R. Rakian, T. J. Block, S. M. Johnson, M. Marinkovic, J. Wu, Q. Dai, D. D. Dean, and X.-D. Chen, "Native extracellular matrix preserves mesenchymal stem cell "stemness" and differentiation potential under serum-free culture conditions," *Stem cell Research & Therapy*, vol. 6, no. 1, p. 235, 2015.

[22] J. M. Maloney, *Chemomechanics of Attached and Suspended cells*. PhD thesis, 2011.

[23] O. Frank, M. Heim, M. Jakob, A. Barbero, D. Schäfer, I. Bendik, W. Dick, M. Heberer, and I. Martin, "Real-time quantitative rt-pcr analysis of human bone marrow stromal cells during osteogenic differentiation in vitro," *Journal of Cellular Biochemistry*, vol. 85, no. 4, pp. 737–746, 2002.

[24] J. C. Crockett, M. J. Rogers, F. P. Coxon, L. J. Hocking, and M. H. Helfrich, "Bone remodelling at a glance," *Journal of Cell Science*, vol. 124, no. 7, pp. 991–998, 2011.

[25] A. S. Mao, J.-W. Shin, and D. J. Mooney, "Effects of substrate stiffness and cell-cell contact on mesenchymal stem cell differentiation," *Biomaterials*, 2016.

[26] C. A. Mullen, M. G. Haugh, M. B. Schaffler, R. J. Majeska, and L. M. McNamara, "Osteocyte differentiation is regulated by extracellular matrix stiffness and intercellular separation," *Journal of the Mechanical Behavior of Biomedical materials*, vol. 28, pp. 183–194, 2013.

[27] M. S. Rahman, N. Akhtar, H. M. Jamil, R. S. Banik, and S. M. Asaduzzaman, "TGF-β/BMP signaling and other molecular events: regulation of osteoblastogenesis and bone formation," *Bone Research*, vol. 3, p. 15005, 2015.

[28] T. R. Nayak, H. Andersen, V. S. Makam, C. Khaw, S. Bae, X. Xu, P.-L. R. Ee, J.-H. Ahn, B. H. Hong, G. Pastorin, and B. Özyilmaz, "Graphene for controlled and accelerated osteogenic differentiation of human mesenchymal stem cells.," *ACS Nano*, vol. 5, pp. 4670–8, jun 2011.

[29] J. Irianto, C. R. Pfeifer, Y. Xia, and D. E. Discher, "SnapShot: Mechanosensing Matrix," *Cell*, vol. 165, no. 7, pp. 1820–1820. e1, 2016.

[30] N. Huebsch, E. Lippens, K. Lee, M. Mehta, S. T. Koshy, M. C. Darnell, R. M. Desai, C. M. Madl, M. Xu, X. Zhao, *et al.*, "Matrix elasticity of void-forming hydrogels controls transplanted-stem-cell-mediated bone formation," *Nature Materials*, vol. 14, no. 12, pp. 1269–1277, 2015.

[31] M. Zaidi, "Skeletal remodeling in health and disease," *Nature Medicine*, vol. 13, no. 7, pp. 791–801, 2007.

[32] W. Tang, Y. Li, L. Osimiri, and C. Zhang, "Osteoblast-specific transcription factor Osterix (Osx) is an upstream regulator of Satb2 during bone formation," *Journal of Biological Chemistry*, vol. 286, no. 38, pp. 32995–33002, 2011.

[33] C. Zhang, K. Cho, Y. Huang, J. P. Lyons, X. Zhou, K. Sinha, P. D. McCrea, and B. de Crombrugghe, "Inhibition of Wnt signaling by the osteoblast-specific transcription factor Osterix," *Proceedings of the National Academy of Sciences*, vol. 105, no. 19, pp. 6936–6941, 2008.

[34] H. Madry and M. Cucchiarini, "Signalling pathways in osteochondral defect regeneration," in *A Tissue Regeneration Approach to Bone and Cartilage Repair*, pp. 219–228, Springer, 2015.

[35] N. Reznikov, J. A. M. Steele, P. Fratzl, and M. M. Stevens, "A materials science vision of extracellular matrix mineralization," *Nature Reviews Materials*, vol. 1, p. 16041, 2016.

[36] S. Ravindran and A. George, "Multifunctional ECM proteins in bone and teeth," *Experimental Cell Research*, vol. 325, no. 2, pp. 148–154, 2014.

[37] P. V. Hauschka, "Osteocalcin: the vitamin K-dependent Ca2+-binding protein of bone matrix," *Pathophysiology of Haemostasis and Thrombosis*, vol. 16, no. 3-4, pp. 258–272, 1986.

[38] A. I. Alford and K. D. Hankenson, "Matricellular proteins: extracellular modulators of bone development, remodeling, and regeneration," *Bone*, vol. 38, no. 6, pp. 749–757, 2006.

[39] E. J. Mackie and S. Ramsey, "Modulation of osteoblast behaviour by tenascin," *Journal of Cell Science*, vol. 109, no. 6, pp. 1597–1604, 1996.

[40] F. S. Jones and P. L. Jones, "The tenascin family of ECM glycoproteins: structure, function, and regulation during embryonic development and tissue remodeling," *Developmental Dynamics*, vol. 218, no. 2, pp. 235–259, 2000.

[41] Z. Amso, J. Cornish, and M. A. Brimble, "Short Anabolic Peptides for Bone Growth," *Medicinal Research Reviews*, vol. 36, pp. 579–640, jul 2016.

[42] B. C. Silva and J. P. Bilezikian, "Parathyroid hormone: anabolic and catabolic actions on the skeleton," *Current Opinion in Pharmacology*, vol. 22, pp. 41 – 50, 2015. Respiratory • Musculoskeletal.

[43] E. A. A. Neel, A. Aljabo, A. Strange, S. Ibrahim, M. Coathup, A. M. Young, L. Bozec, and V. Mudera, "Demineralization–remineralization dynamics in teeth and bone," *International Journal of Nanomedicine*, vol. 11, p. 4743, 2016.

[44] A. L. Boskey and E. Villarreal-Ramirez, "Intrinsically disordered proteins and biomineralization," *Matrix Biology*, vol. 52-54, pp. 43–59, may 2016.

[45] U. G. Wegst, H. Bai, E. Saiz, A. P. Tomsia, and R. O. Ritchie, "Bioinspired structural materials," *Nature Materials*, vol. 14, no. 1, pp. 23–36, 2015.

[46] B. Ecarot-Charrier, F. H. Glorieux, M. Van Der Rest, and G. Pereira, "Osteoblasts isolated from mouse calvaria initiate matrix mineralization in culture.," *The Journal of Cell Biology*, vol. 96, no. 3, pp. 639–643, 1983.

[47] J. Silvent, N. Nassif, C. Helary, T. Azaïs, J.-Y. Sire, and M. M. G. Guille, "Collagen osteoid-like model allows kinetic gene expression studies of non-collagenous proteins in relation with mineral development to understand bone biomineralization," *PloS one*, vol. 8, no. 2, p. e57344, 2013.

[48] A. I. Alford, K. M. Kozloff, and K. D. Hankenson, "Extracellular matrix networks in bone remodeling," *The International Journal of Biochemistry Cell Biology*, vol. 65, pp. 20 – 31, 2015.

[49] E. A. Zimmermann and R. O. Ritchie, "Bone as a structural material," *Advanced Healthcare Materials*, vol. 4, no. 9, pp. 1287–1304, 2015.

[50] J. Mahamid, A. Sharir, D. Gur, E. Zelzer, L. Addadi, and S. Weiner, "Bone mineralization proceeds through intracellular calcium phosphate loaded vesicles: A cryo-electron microscopy study," *Journal of Structural Biology*, vol. 174, no. 3, pp. 527 – 535, 2011.

[51] S. Boonrungsiman, E. Gentleman, R. Carzaniga, N. D. Evans, D. W. McComb, A. E. Porter, and M. M. Stevens, "The role of intracellular calcium phosphate in osteoblast-mediated bone apatite formation," *Proceedings of the National Academy of Sciences*, vol. 109, no. 35, pp. 14170–14175, 2012.

[52] M. Capulli, R. Paone, and N. Rucci, "Osteoblast and osteocyte: Games without frontiers," *Archives of Biochemistry and Biophysics*, vol. 561, pp. 3 – 12, 2014. Bone: A dynamic and integrating tissue.

[53] W. Bouleftour, L. Juignet, G. Bouet, R. N. Granito, A. Vanden-Bossche, N. Laroche, J. E. Aubin, M.-H. Lafage-Proust, L. Vico, and L. Malaval,

"The role of the SIBLING, Bone Sialoprotein in skeletal biology — Contribution of mouse experimental genetics," *Matrix Biology*, vol. 52-54, pp. 60–77, may 2016.

[54] O. Frank, M. Heim, M. Jakob, A. Barbero, D. Schäfer, I. Bendik, W. Dick, M. Heberer, and I. Martin, "Real-time quantitative RT-PCR analysis of human bone marrow stromal cells during osteogenic differentiation in vitro," *Journal of Cellular Biochemistry*, vol. 85, no. 4, pp. 737–746, 2002.

[55] M. Tavafoghi and M. Cerruti, "The role of amino acids in hydroxyapatite mineralization," *Journal of The Royal Society Interface*, vol. 13, no. 123, p. 20160462, 2016.

[56] E. S. Place, N. D. Evans, and M. M. Stevens, "Complexity in biomaterials for tissue engineering," *Nature Materials*, vol. 8, no. 6, p. 457, 2009.

[57] G. K. Hunter and H. A. Goldberg, "Modulation of crystal formation by bone phosphoproteins: role of glutamic acid-rich sequences in the nucleation of hydroxyapatite by bone sialoprotein," *Biochemical Journal*, vol. 302, no. 1, pp. 175–179, 1994.

[58] J. L. Bain, B. K. Culpepper, M. S. Reddy, and S. L. Bellis, "Comparing variable-length polyglutamate domains to anchor an osteoinductive collagen-mimetic peptide to diverse bone grafting materials," *The International Journal of Oral & Maxillofacial Implants*, vol. 29, no. 6, p. 1437, 2014.

[59] W. Bouleftour, O. Sabido, C. Lescale, M. Thomas, J. E. Aubin, M. Goodhardt, L. Vico, L. Malaval, *et al.*, "Absence of bone sialoprotein (bsp) alters profoundly hematopoiesis and upregulates osteopontin," *Journal of Cellular Physiology*, vol. 230, no. 6, pp. 1342–1351, 2015.

[60] G. Bouet, W. Bouleftour, L. Juignet, M.-T. Linossier, M. Thomas, A. Vanden-Bossche, J. E. Aubin, L. Vico, D. Marchat, and L. Malaval, "The impairment of osteogenesis in bone sialoprotein (bsp) knockout calvaria cell cultures is cell density dependent," *PloS one*, vol. 10, no. 2, p. e0117402, 2015.

[61] P. Manduca, A. Castagnino, D. Lombardini, S. Marchisio, S. Soldano, V. Ulivi, S. Zanotti, C. Garbi, N. Ferrari, and D. Palmieri, "Role of MT1-MMP in the osteogenic differentiation," *Bone*, vol. 44, no. 2, pp. 251–265, 2009.

[62] S. G. Almalki and D. K. Agrawal, "Effects of matrix metalloproteinases on the fate of mesenchymal stem cells," *Stem Cell Research & Therapy*, vol. 7, no. 1, p. 129, 2016.

[63] L. Kalmar, D. Homola, G. Varga, and P. Tompa, "Structural disorder in proteins brings order to crystal growth in biomineralization," *Bone*, vol. 51, no. 3, pp. 528–534, 2012.

[64] A. Arora and D. S. Katti, "Understanding the influence of phosphorylation and polysialylation of gelatin on mineralization and osteogenic differentiation," *Materials Science and Engineering: C*, vol. 65, pp. 9–18, 2016.

[65] X. Wang, C. Sun, P. Li, T. Wu, H. Zhou, D. Yang, Y. Liu, X. Ma, Z. Song, and Q. Nian, "Vaccine Engineering with Dual-Functional Mineral Shell: A Promising Strategy to Overcome Preexisting Immunity," *Advanced Materials*, vol. 28, no. 4, pp. 694–700, 2016.

[66] J. D. Currey and K. Brear, "Hardness, Young's modulus and yield stress in mammalian mineralized tissues," *Journal of Materials Science: Materials in Medicine*, vol. 1, no. 1, pp. 14–20, 1990.

[67] J. H. Kinney, M. Balooch, G. W. Marshall, and S. J. Marshall, "A micromechanics model of the elastic properties of human dentine," *Archives of Oral Biology*, vol. 44, no. 10, pp. 813–822, 1999.

[68] J. Y. Rho, R. B. Ashman, and C. H. Turner, "Young's modulus of trabecular and cortical bone material: ultrasonic and microtensile measurements," *Journal of Biomechanics*, vol. 26, no. 2, pp. 111–119, 1993.

[69] D.-G. Kim, Y.-H. Jeong, E. Kosel, A. M. Agnew, D. W. McComb, K. Bodnyk, R. T. Hart, M. K. Kim, S. Y. Han, and W. M. Johnston, "Regional variation of bone tissue properties at the human mandibular condyle," *Bone*, vol. 77, pp. 98 – 106, 2015.

[70] Y. Wang, T. Azaïs, M. Robin, A. Vallée, C. Catania, P. Legriel, G. Pehau-Arnaudet, F. Babonneau, M.-M. Giraud-Guille, and N. Nassif, "The predominant role of collagen in the nucleation, growth, structure and orientation of bone apatite," *Nature Materials*, vol. 11, no. 8, pp. 724–733, 2012.

[71] D. W. Weisgerber, S. R. Caliari, and B. A. C. Harley, "Mineralized collagen scaffolds induce hMSC osteogenesis and matrix remodeling," *Biomaterials Science*, vol. 3, no. 3, pp. 533–542, 2015.

[72] K. Guevorkian and J.-L. Maître, "Micropipette aspiration: a unique tool for exploring cell and tissue mechanics in vivo," *Methods in Cell Biology*, 2016.

[73] D. Gonzalez-Rodriguez, L. Bonnemay, J. Elgeti, S. Dufour, D. Cuvelier, and F. Brochard-Wyart, "Detachment and fracture of cellular aggregates," *Soft Matter*, vol. 9, no. 7, pp. 2282–2290, 2013.

[74] S. Sart, A.-C. Tsai, Y. Li, and T. Ma, "Three-dimensional aggregates of mesenchymal stem cells: cellular mechanisms, biological properties, and applications," *Tissue Engineering Part B: Reviews*, vol. 20, no. 5, pp. 365–380, 2013.

[75] S. V. Hadjiantoniou, D. Sean, M. Ignacio, M. Godin, G. W. Slater, and A. E. Pelling, "Physical confinement signals regulate the organization of stem cells in three dimensions," *Journal of The Royal Society Interface*, vol. 13, no. 123, p. 20160613, 2016.

[76] H. Turlier and J.-L. Maître, "Mechanics of tissue compaction," in *Seminars in Cell & Developmental Biology*, vol. 47, pp. 110–117, Elsevier, 2015.

[77] A. Shekaran and A. J. Garcia, "Nanoscale engineering of extracellular matrix-mimetic bioadhesive surfaces and implants for tissue engineering," *Biochimica et Biophysica Acta (BBA)-General Subjects*, vol. 1810, no. 3, pp. 350–360, 2011.

[78] K. C. Murphy, A. I. Hoch, J. N. Harvestine, D. Zhou, and J. K. Leach, "Mesenchymal Stem Cell Spheroids Retain Osteogenic Phenotype Through

$\alpha 2\beta 1$ Signaling," *Stem Cells Translational Medicine*, vol. 5, no. 9, pp. 1229–1237, 2016.

[79] J. R. Lange and B. Fabry, "Cell and tissue mechanics in cell migration," *Experimental Cell Research*, vol. 319, no. 16, pp. 2418 – 2423, 2013. Special Issue: Cell Motility and Mechanics.

[80] S. Douezan, K. Guevorkian, R. Naouar, S. Dufour, D. Cuvelier, and F. Brochard-Wyart, "Spreading dynamics and wetting transition of cellular aggregates," *Proceedings of the National Academy of Sciences*, vol. 108, no. 18, pp. 7315–7320, 2011.

[81] M. W. Laschke and M. D. Menger, "Life is 3D: Boosting Spheroid Function for Tissue Engineering," *Trends in Biotechnology*, 2016.

[82] C. R. Jacobs, H. Huang, and R. Y. Kwon, *Introduction to Cell Mechanics and Mechanobiology*. Garland Science, 2012.

[83] M.-J. Oh, F. Kuhr, F. Byfield, and I. Levitan, "Micropipette aspiration of substrate-attached cells to estimate cell stiffness," *JoVE (Journal of Visualized Experiments)*, no. 67, pp. e3886–e3886, 2012.

[84] C. Lim, E. Zhou, and S. Quek, "Mechanical models for living cells—a review," *Journal of Biomechanics*, vol. 39, no. 2, pp. 195–216, 2006.

[85] K. Sliogeryte, S. D. Thorpe, D. A. Lee, L. Botto, and M. M. Knight, "Stem cell differentiation increases membrane-actin adhesion regulating cell blebability, migration and mechanics," *Scientific Reports*, vol. 4, p. 7307, 2014.

[86] H. Yu, C. Y. Tay, W. S. Leong, S. C. W. Tan, K. Liao, and L. P. Tan, "Mechanical behavior of human mesenchymal stem cells during adipogenic and osteogenic differentiation," *Biochemical and Biophysical Research Communications*, vol. 393, no. 1, pp. 150–155, 2010.

[87] J. D. Pajerowski, K. N. Dahl, F. L. Zhong, P. J. Sammak, and D. E. Discher, "Physical plasticity of the nucleus in stem cell differentiation," *Proceedings of the National Academy of Sciences*, vol. 104, no. 40, pp. 15619–15624, 2007.

[88] K. Guevorkian, M.-J. Colbert, M. Durth, S. Dufour, and F. Brochard-Wyart, "Aspiration of biological viscoelastic drops," *Physical Review Letters*, vol. 104, no. 21, p. 218101, 2010.

[89] Z. Zhang, J. Stenson, and C. Thomas, "Micromanipulation in mechanical characterisation of single particles," *Advances in Chemical Engineering*, vol. 37, pp. 29–85, 2009.

[90] K. E. Kasza, D. Vader, S. Köster, N. Wang, and D. A. Weitz, "Imaging Techniques for Measuring the Materials Properties of Cells," *Cold Spring Harbor Protocols*, vol. 2011, no. 4, p. pdb. top107, 2011.

[91] F. H. C. Crick and A. F. W. Hughes, "The physical properties of cytoplasm: A study by means of the magnetic particle method Part I. Experimental," *Experimental Cell Research*, vol. 1, no. 1, pp. 37–80, 1950.

[92] S. Yamada, D. Wirtz, and S. C. Kuo, "Mechanics of living cells measured by laser tracking microrheology," *Biophysical Journal*, vol. 78, no. 4, pp. 1736–1747, 2000.

[93] R. Conroy, "Force spectroscopy with optical and magnetic tweezers," in *Handbook of Molecular Force Spectroscopy*, pp. 23–96, Springer, 2008.

[94] A. Ashkin, J. M. Dziedzic, J. E. Bjorkholm, and S. Chu, "Observation of a single-beam gradient force optical trap for dielectric particles," *Optics Letters*, vol. 11, no. 5, pp. 288–290, 1986.

[95] J. Guck, R. Ananthakrishnan, H. Mahmood, T. J. Moon, C. C. Cunningham, and J. Käs, "The optical stretcher: a novel laser tool to micromanipulate cells," *Biophysical Journal*, vol. 81, no. 2, pp. 767–784, 2001.

[96] T. Kolb, J. Kraxner, K. Skodzek, M. Haug, D. Crawford, K. K. Maaß, K. E. Aifantis, and G. Whyte, "Optomechanical measurement of the role of lamins in whole cell deformability," *Journal of Biophotonics*, 2017.

[97] B. Sabass, M. L. Gardel, C. M. Waterman, and U. S. Schwarz, "High resolution traction force microscopy based on experimental and computational advances," *Biophysical journal*, vol. 94, no. 1, pp. 207–220, 2008.

[98] C. Franck, S. A. Maskarinec, D. A. Tirrell, and G. Ravichandran, "Three-dimensional traction force microscopy: a new tool for quantifying cell-matrix interactions," *PloS one*, vol. 6, no. 3, p. e17833, 2011.

[99] W. R. Legant, J. S. Miller, B. L. Blakely, D. M. Cohen, G. M. Genin, and C. S. Chen, "Measurement of mechanical tractions exerted by cells in three-dimensional matrices," *Nature Methods*, vol. 7, no. 12, pp. 969–971, 2010.

[100] S. Banerjee, *Cell Mechanics: From Cytoskeletal Dynamics to Tissue-Scale Mechanical Phenomena*. PhD thesis, 2013.

[101] W. J. Polacheck and C. S. Chen, "Measuring cell-generated forces: a guide to the available tools," *Nature Methods*, vol. 13, no. 5, pp. 415–423, 2016.

[102] T. Iskratsch, H. Wolfenson, and M. P. Sheetz, "Appreciating force and shape [mdash] the rise of mechanotransduction in cell biology," *Nature Reviews Molecular Cell Biology*, vol. 15, no. 12, pp. 825–833, 2014.

[103] M. Murrell, P. W. Oakes, M. Lenz, and M. L. Gardel, "Forcing cells into shape: the mechanics of actomyosin contractility," *Nature Reviews Molecular Cell Biology*, vol. 16, no. 8, pp. 486–498, 2015.

[104] G. Scarcelli and S. H. Yun, "Confocal brillouin microscopy for three-dimensional mechanical imaging," *Nature Photonics*, vol. 2, no. 1, pp. 39–43, 2008.

[105] G. Scarcelli, W. J. Polacheck, H. T. Nia, K. Patel, A. J. Grodzinsky, R. D. Kamm, and S. H. Yun, "Noncontact three-dimensional mapping of intracellular hydro-mechanical properties by brillouin microscopy," *Nature Methods*, vol. 12, no. 12, p. 1132, 2015.

[106] B. F. Kennedy, P. Wijesinghe, and D. D. Sampson, "The emergence of optical elastography in biomedicine," *Nature Photonics*, vol. 11, no. 4, pp. 215–221, 2017.

[107] J. Zhang, C. Wu, R. Raghunathan, K. V. Larin, and G. Scarcelli, "Non-invasive structural and biomechanical imaging of the developing embryos

(conference presentation)," in *SPIE BiOS*, pp. 100670W–100670W, International Society for Optics and Photonics, 2017.

[108] A. Vaziri and A. Gopinath, "Cell and biomolecular mechanics in silico," *Nature Materials*, vol. 7, no. 1, pp. 15–23, 2008.

[109] V. Vadillo-Rodriguez and J. R. Dutcher, "Dynamic viscoelastic behavior of individual gram-negative bacterial cells," *Soft Matter*, vol. 5, no. 24, pp. 5012–5019, 2009.

[110] A. Cartagena and A. Raman, "Local viscoelastic properties of live cells investigated using dynamic and quasi-static atomic force microscopy methods," *Biophysical Journal*, vol. 106, no. 5, pp. 1033–1043, 2014.

[111] E. Moeendarbary, L. Valon, M. Fritzsche, A. R. Harris, D. A. Moulding, A. J. Thrasher, E. Stride, L. Mahadevan, and G. T. Charras, "The cytoplasm of living cells behaves as a poroelastic material," *Nature Materials*, vol. 12, no. 3, pp. 253–261, 2013.

[112] B. H. Blehm, A. Devine, J. R. Staunton, and K. Tanner, "In vivo tissue has non-linear rheological behavior distinct from 3d biomimetic hydrogels, as determined by {AMOTIV} microscopy," *Biomaterials*, vol. 83, pp. 66 – 78, 2016.

[113] E. T. Herruzo, A. P. Perrino, and R. Garcia, "Fast nanomechanical spectroscopy of soft matter," *Nature Communications*, vol. 5, 2014.

[114] F. M. Hecht, J. Rheinlaender, N. Schierbaum, W. H. Goldmann, B. Fabry, and T. E. Schäffer, "Imaging viscoelastic properties of live cells by afm: power-law rheology on the nanoscale," *Soft Matter*, vol. 11, no. 23, pp. 4584–4591, 2015.

[115] D. C. Lin and F. Horkay, "Nanomechanics of polymer gels and biological tissues: a critical review of analytical approaches in the hertzian regime and beyond," *Soft Matter*, vol. 4, no. 4, pp. 669–682, 2008.

[116] M. Glaubitz, N. Medvedev, D. Pussak, L. Hartmann, S. Schmidt, C. A. Helm, and M. Delcea, "A novel contact model for afm indentation experiments on soft spherical cell-like particles," *Soft Matter*, vol. 10, no. 35, pp. 6732–6741, 2014.

[117] E. K. Dimitriadis, F. Horkay, J. Maresca, B. Kachar, and R. S. Chadwick, "Determination of elastic moduli of thin layers of soft material using the atomic force microscope," *Biophysical Journal*, vol. 82, no. 5, pp. 2798–2810, 2002.

[118] A. J. Engler, L. Richert, J. Y. Wong, C. Picart, and D. E. Discher, "Surface probe measurements of the elasticity of sectioned tissue, thin gels and polyelectrolyte multilayer films: correlations between substrate stiffness and cell adhesion," *Surface Science*, vol. 570, no. 1, pp. 142–154, 2004.

[119] S. Vichare, M. M. Inamdar, and S. Sen, "Influence of cell spreading and contractility on stiffness measurements using afm," *Soft Matter*, vol. 8, no. 40, pp. 10464–10471, 2012.

[120] A. Love, "Boussinesq's problem for a rigid cone," *The Quarterly Journal of Mathematics*, vol. 10, pp. 161–175, 1939.

[121] I. N. Sneddon, "Boussinesq's problem for a rigid cone," in *Mathematical Proceedings of the Cambridge Philosophical Society*, vol. 44, pp. 492–507, Cambridge Univ Press, 1948.

[122] A. Selvadurai, "On boussinesq's problem," *International Journal of Engineering Science*, vol. 39, no. 3, pp. 317–322, 2001.

[123] J. R. Staunton, B. L. Doss, S. Lindsay, and R. Ros, "Correlating confocal microscopy and atomic force indentation reveals metastatic cancer cells stiffen during invasion into collagen i matrices," *Scientific Reports*, vol. 6, 2016.

[124] Y. M. Efremov, D. Bagrov, M. Kirpichnikov, and K. Shaitan, "Application of the johnson–kendall–roberts model in afm-based mechanical measurements on cells and gel.," *Colloids and Surfaces B: Biointerfaces*, vol. 134, pp. 131–139, 2015.

[125] P. C. Nalam, N. N. Gosvami, M. A. Caporizzo, R. J. Composto, and R. W. Carpick, "Nano-rheology of hydrogels using direct drive force modulation atomic force microscopy," *Soft Matter*, vol. 11, no. 41, pp. 8165–8178, 2015.

[126] M. K. Shah, I. H. Garcia-Pak, and E. M. Darling, "Influence of inherent mechanophenotype on competitive cellular adherence," *Annals of Biomedical Engineering*, pp. 1–12, 2017.

[127] N. Nguyen, Y. Shao, A. Wineman, J. Fu, and A. Waas, "Atomic force microscopy indentation and inverse analysis for non-linear viscoelastic identification of breast cancer cells," *Mathematical Biosciences*, vol. 277, pp. 77–88, 2016.

[128] I. Sokolov, S. Iyer, V. Subba-Rao, R. M. Gaikwad, and C. D. Woodworth, "Detection of surface brush on biological cells in vitro with atomic force microscopy," *Applied Physics Letters*, vol. 91, no. 2, p. 023902, 2007.

[129] M. E. Dokukin, N. V. Guz, and I. Sokolov, "Quantitative study of the elastic modulus of loosely attached cells in afm indentation experiments," *Biophysical Journal*, vol. 104, no. 10, pp. 2123–2131, 2013.

[130] N. Guz, M. Dokukin, V. Kalaparthi, and I. Sokolov, "If cell mechanics can be described by elastic modulus: study of different models and probes used in indentation experiments," *Biophysical Journal*, vol. 107, no. 3, pp. 564–575, 2014.

[131] M. Dokukin, Y. Ablaeva, V. Kalaparthi, A. Seluanov, V. Gorbunova, and I. Sokolov, "Pericellular brush and mechanics of guinea pig fibroblast cells studied with afm," *Biophysical Journal*, vol. 111, no. 1, pp. 236–246, 2016.

[132] A. Calzado-Martin, M. Encinar, J. Tamayo, M. Calleja, and A. San Paulo, "Effect of actin organization on the stiffness of living breast cancer cells revealed by peak-force modulation atomic force microscopy," *ACS Nano*, vol. 10, no. 3, pp. 3365–3374, 2016.

[133] S. Sen, S. Subramanian, and D. E. Discher, "Indentation and adhesive probing of a cell membrane with afm: theoretical model and experiments," *Biophysical Journal*, vol. 89, no. 5, pp. 3203–3213, 2005.

[134] D. Schneider, T. Baronsky, A. Pietuch, J. Rother, M. Oelkers, D. Fichtner, D. Wedlich, and A. Janshoff, "Tension monitoring during epithelial-to-mesenchymal transition links the switch of phenotype to expression of moesin and cadherins in nmumg cells," *PLoS One*, vol. 8, no. 12, p. e80068, 2013.

[135] D. Needham and R. Hochmuth, "Rapid flow of passive neutrophils into a 4 m pipet and measurement of cytoplasmic viscosity," *Journal of Biomechanical Engineering*, vol. 112, pp. 269–276, 1990.

[136] G. Esteban-Manzanares, B. González-Bermúdez, J. Cruces, M. De la Fuente, Q. Li, G. V. Guinea, J. Pérez-Rigueiro, M. Elices, and G. R. Plaza, "Improved measurement of elastic properties of cells by micropipette aspiration and its application to lymphocytes," *Annals of Biomedical Engineering*, vol. 45, no. 5, pp. 1375–1385, 2017.

[137] G. R. Plaza, T. Q. Uyeda, Z. Mirzaei, and C. A. Simmons, "Study of the influence of actin-binding proteins using linear analyses of cell deformability," *Soft Matter*, vol. 11, no. 27, pp. 5435–5446, 2015.

[138] S. Khakshour, T. V. Beischlag, C. Sparrey, and E. J. Park, "Mechanical characterization of art-treated jurkat cells using optical tweezers," in *Engineering in Medicine and Biology Society (EMBC), 2014 36th Annual International Conference of the IEEE*, pp. 6806–6809, IEEE, 2014.

[139] A. Mietke, O. Otto, S. Girardo, P. Rosendahl, A. Taubenberger, S. Golfier, E. Ulbricht, S. Aland, J. Guck, and E. Fischer-Friedrich, "Extracting cell stiffness from real-time deformability cytometry: Theory and experiment," *Biophysical Journal*, vol. 109, no. 10, pp. 2023 – 2036, 2015.

[140] S. C. Tan, W. X. Pan, G. Ma, N. Cai, K. W. Leong, and K. Liao, "Viscoelastic behaviour of human mesenchymal stem cells," *BMC Cell Biology*, vol. 9, no. 1, p. 40, 2008.

[141] J. M. Maloney, D. Nikova, F. Lautenschläger, E. Clarke, R. Langer, J. Guck, and K. J. Van Vliet, "Mesenchymal stem cell mechanics from the attached

to the suspended state," *Biophysical Journal*, vol. 99, no. 8, pp. 2479–2487, 2010.

[142] D. E. Ingber, "Tensegrity i. cell structure and hierarchical systems biology," *Journal of Cell Science*, vol. 116, no. 7, pp. 1157–1173, 2003.

[143] D. E. Ingber, "Tensegrity-based mechanosensing from macro to micro," *Progress in Biophysics and Molecular Biology*, vol. 97, no. 2, pp. 163–179, 2008.

[144] S. Kumar, I. Z. Maxwell, A. Heisterkamp, T. R. Polte, T. P. Lele, M. Salanga, E. Mazur, and D. E. Ingber, "Viscoelastic retraction of single living stress fibers and its impact on cell shape, cytoskeletal organization, and extracellular matrix mechanics," *Biophysical Journal*, vol. 90, no. 10, pp. 3762–3773, 2006.

[145] N. Wang, J. D. Tytell, and D. E. Ingber, "Mechanotransduction at a distance: mechanically coupling the extracellular matrix with the nucleus," *Nature Reviews Molecular Cell Biology*, vol. 10, no. 1, pp. 75–82, 2009.

[146] K. E. Kasza, A. C. Rowat, J. Liu, T. E. Angelini, C. P. Brangwynne, G. H. Koenderink, and D. A. Weitz, "The cell as a material," *Current Opinion in Cell Biology*, vol. 19, no. 1, pp. 101 – 107, 2007. Cell structure and dynamics.

[147] M. M. Nava, M. T. Raimondi, and R. Pietrabissa, "Bio-chemo-mechanical models for nuclear deformation in adherent eukaryotic cells," *Biomechanics and Modeling in Mechanobiology*, vol. 13, no. 5, pp. 929–943, 2014.

[148] B. Cheng, M. Lin, G. Huang, Y. Li, B. Ji, G. M. Genin, V. S. Deshpande, T. J. Lu, and F. Xu, "Cellular mechanosensing of the biophysical microenvironment: A review of mathematical models of biophysical regulation of cell responses," *Physics of Life Reviews*, 2017.

[149] D. Stamenović and M. F. Coughlin, "The role of prestress and architecture of the cytoskeleton and deformability of cytoskeletal filaments in mechanics of adherent cells: a quantitative analysis," *Journal of Theoretical Biology*, vol. 201, no. 1, pp. 63 – 74, 1999.

[150] J. P. Marquez, E. L. Elson, and G. M. Genin, "Whole cell mechanics of contractile fibroblasts: relations between effective cellular and extracellular matrix moduli," *Philosophical Transactions of the Royal Society of London A: Mathematical, Physical and Engineering Sciences*, vol. 368, no. 1912, pp. 635–654, 2010.

[151] G. Binnig, C. F. Quate, and C. Gerber, "Atomic force microscope," *Physical Review Letters*, vol. 56, no. 9, p. 930, 1986.

[152] D. Alsteens, H. E. Gaub, R. Newton, M. Pfreundschuh, C. Gerber, and D. J. Müller, "Atomic force microscopy-based characterization and design of biointerfaces," *Nature Reviews Materials*, vol. 2, p. 17008, 2017.

[153] Y. S. Dagdas, M. N. Aslan, A. B. Tekinay, M. O. Guler, and A. Dâna, "Nanomechanical characterization by double-pass force–distance mapping," *Nanotechnology*, vol. 22, no. 29, p. 295704, 2011.

[154] M. Dong, S. Husale, and O. Sahin, "Determination of protein structural flexibility by microsecond force spectroscopy," *Nature Nanotechnology*, vol. 4, no. 8, pp. 514–517, 2009.

[155] J. S. Lee, J. Song, S. O. Kim, S. Kim, W. Lee, J. A. Jackman, D. Kim, N.-J. Cho, and J. Lee, "Multifunctional hydrogel nano-probes for atomic force microscopy," *Nature communications*, vol. 7, 2016.

[156] "2016 kavli prize in nanoscience." http://www.kavliprize.org/prizes-and-laureates/prizes/2016-kavli-prize-nanoscience. Accessed: April 13, 2017.

[157] K. C. Morton and L. a. Baker, "Atomic force microscopy-based bioanalysis for the study of disease," *Analytical Methods*, vol. 6, no. 14, p. 4932, 2014.

[158] M. Pfreundschuh, D. Martinez-Martin, E. Mulvihill, S. Wegmann, and D. J. Muller, "Multiparametric high-resolution imaging of native proteins by force-distance curve-based AFM.," *Nature Protocols*, vol. 9, pp. 1113–30, may 2014.

[159] "How to Choose the Right AFM Probe," 2016.

[160] C. M. Hammer and T. E. Schäffer, "Atomic force microscopy crosslinks interdisciplinary eye research," *Medical Hypothesis, Discovery and Innovation in Ophthalmology*, vol. 4, no. 1, p. 1, 2015.

[161] E. Darling, "Force scanning: a rapid, high-resolution approach for spatial mechanical property mapping," *Nanotechnology*, vol. 22, no. 17, p. 175707, 2011.

[162] A. D. Ozkan, A. E. Topal, A. Dana, M. O. Guler, and A. B. Tekinay, "Atomic force microscopy for the investigation of molecular and cellular behavior," *Micron*, vol. 89, pp. 60–76, 2016.

[163] E. M. Darling, M. Topel, S. Zauscher, T. P. Vail, and F. Guilak, "Viscoelastic properties of human mesenchymally-derived stem cells and primary osteoblasts, chondrocytes, and adipocytes.," *Journal of Biomechanics*, vol. 41, pp. 454–64, jan 2008.

[164] T. Bongiorno, J. Kazlow, R. Mezencev, S. Griffiths, R. Olivares-Navarrete, J. F. McDonald, Z. Schwartz, B. D. Boyan, T. C. McDevitt, and T. Sulchek, "Mechanical stiffness as an improved single-cell indicator of osteoblastic human mesenchymal stem cell differentiation," *Journal of Biomechanics*, vol. 47, no. 9, pp. 2197–2204, 2014.

[165] I. Titushkin and M. Cho, "Modulation of cellular mechanics during osteogenic differentiation of human mesenchymal stem cells.," *Biophysical Journal*, vol. 93, pp. 3693–702, nov 2007.

[166] E. Takai, K. D. Costa, A. Shaheen, C. T. Hung, and X. E. Guo, "Osteoblast elastic modulus measured by atomic force microscopy is substrate dependent," *Annals of Biomedical Engineering*, vol. 33, no. 7, pp. 963–971, 2005.

[167] H. Ceylan, S. Kocabey, H. U. Gulsuner, O. S. Balcik, M. O. Guler, and A. B. Tekinay, "Bone-Like Mineral Nucleating Peptide Nanofibers Induce Differentiation of Human Mesenchymal Stem Cells into Mature Osteoblasts," 2014.

[168] M. Göktaş, "Bioactive porous peg-peptide composite hydrogels with tunable mechanical properties," Master's thesis, 2014.

[169] S. Kocabey, H. Ceylan, A. B. Tekinay, and M. O. Guler, "Glycosaminoglycan mimetic peptide nanofibers promote mineralization by osteogenic cells," *Acta Biomaterialia*, vol. 9, no. 11, pp. 9075–9085, 2013.

[170] M. Sever, B. Mammadov, M. O. Guler, and A. B. Tekinay, "Tenascin-C mimetic peptide nanofibers direct stem cell differentiation to osteogenic lineage," *Biomacromolecules*, vol. 15, no. 12, pp. 4480–4487, 2014.

[171] G. Tansik, E. Kilic, M. Beter, B. Demiralp, G. K. Sendur, N. Can, H. Ozkan, E. Ergul, M. O. Guler, and A. B. Tekinay, "A glycosaminoglycan mimetic peptide nanofiber gel as an osteoinductive scaffold," *Biomaterials Science*, vol. 4, no. 9, pp. 1328–1339, 2016.

[172] Y. Wang, X. Yu, C. Baker, W. L. Murphy, and T. C. McDevitt, "Mineral particles modulate osteo-chondrogenic differentiation of embryonic stem cell aggregates," *Acta Biomaterialia*, vol. 29, pp. 42–51, 2016.

[173] F. M. Hecht, J. Rheinlaender, N. Schierbaum, W. H. Goldmann, B. Fabry, and T. E. Schäffer, "Imaging viscoelastic properties of live cells by AFM: power-law rheology on the nanoscale," *Soft Matter*, pp. 0–7, 2015.

[174] P. Cai, Y. Mizutani, M. Tsuchiya, J. M. Maloney, B. Fabry, K. J. Van Vliet, and T. Okajima, "Quantifying cell-to-cell variation in power-law rheology," *Biophysical Journal*, vol. 105, no. 5, pp. 1093–1102, 2013.

[175] C. M. Scott, C. L. Forster, and E. Kokkoli, "Three-Dimensional Cell Entrapment as a Function of the Weight Percent of Peptide-Amphiphile Hydrogels," *Langmuir*, vol. 31, no. 22, pp. 6122–6129, 2015.

[176] N. L. Angeloni, C. W. Bond, Y. Tang, D. A. Harrington, S. Zhang, S. I. Stupp, K. E. McKenna, and C. A. Podlasek, "Regeneration of the cavernous nerve by Sonic hedgehog using aligned peptide amphiphile nanofibers," *Biomaterials*, vol. 32, no. 4, pp. 1091–1101, 2011.

[177] K. Saha, J. F. Pollock, D. V. Schaffer, and K. E. Healy, "Designing synthetic materials to control stem cell phenotype," *Current Opinion in Chemical Biology*, vol. 11, no. 4, pp. 381–387, 2007.

[178] M. J. Dalby, N. Gadegaard, R. Tare, A. Andar, M. O. Riehle, P. Herzyk, C. D. W. Wilkinson, and R. O. C. Oreffo, "The control of human mesenchymal cell differentiation using nanoscale symmetry and disorder," *Nature Materials*, vol. 6, no. 12, pp. 997–1003, 2007.

[179] A. J. Engler, S. Sen, H. L. Sweeney, and D. E. Discher, "Matrix elasticity directs stem cell lineage specification.," *Cell*, vol. 126, pp. 677–89, aug 2006.

[180] R. Mammadov, G. Cinar, N. Gunduz, M. Goktas, H. Kayhan, S. Tohumeken, A. E. Topal, I. Orujalipoor, T. Delibasi, and A. Dana, "Virus-like nanostructures for tuning immune response," *Scientific Reports*, vol. 5, 2015.

[181] G. Gulseren, I. C. Yasa, O. Ustahuseyin, E. D. Tekin, A. B. Tekinay, and M. O. Guler, "Alkaline phosphatase-mimicking peptide nanofibers for osteogenic differentiation," *Biomacromolecules*, vol. 16, no. 7, pp. 2198–2208, 2015.

[182] S. U. Yaylaci, M. Sen, O. Bulut, E. Arslan, M. O. Guler, and A. B. Tekinay, "Chondrogenic differentiation of mesenchymal stem cells on glycosaminoglycan-mimetic peptide nanofibers," *ACS Biomaterials Science & Engineering*, vol. 2, no. 5, pp. 871–878, 2016.

[183] E. Arslan, M. O. Guler, and A. B. Tekinay, "Glycosaminoglycan-mimetic signals direct the osteo/chondrogenic differentiation of mesenchymal stem cells in a three-dimensional peptide nanofiber extracellular matrix mimetic environment," *Biomacromolecules*, vol. 17, no. 4, pp. 1280–1291, 2016.

[184] S. I. Stupp, J. J. Donners, G. A. Silva, H. A. Behanna, and S. G. Anthony, "Self-assembling peptide amphiphiles and related methods for growth factor delivery," Nov. 12 2013. US Patent 8,580,923.

[185] S. Ustun Yaylaci, M. Sardan Ekiz, E. Arslan, N. Can, E. Kilic, H. Ozkan, I. Orujalipoor, S. Ide, A. B. Tekinay, and M. O. Guler, "Supramolecular GAG-like Self-Assembled Glycopeptide Nanofibers Induce Chondrogenesis and Cartilage Regeneration," *Biomacromolecules*, vol. 17, no. 2, pp. 679–689, 2016.

[186] M. Mizuno, R. Fujisawa, and Y. Kuboki, "Type I collagen-induced osteoblastic differentiation of bone-marrow cells mediated by collagen-$\alpha 2\beta 1$ integrin interaction," *Journal of Cellular Physiology*, vol. 184, no. 2, pp. 207–213, 2000.

[187] S. Kocabey, H. Ceylan, A. B. Tekinay, and M. O. Guler, "Glycosaminoglycan mimetic peptide nanofibers promote mineralization by osteogenic cells," *Acta Biomaterialia*, vol. 9, no. 11, pp. 9075–9085, 2013.

[188] A. Zengin, G. Cinar, and M. O. Guler, "Controlled enzymatic stability and release characteristics of supramolecular chiral peptide amphiphile nanofiber gels," *Current Applied Physics*, mar 2017.

[189] G. Cinar, A. Ozdemir, S. Hamsici, G. Gunay, A. Dana, A. B. Tekinay, and M. O. Guler, "Local delivery of doxorubicin through supramolecular peptide amphiphile nanofiber gels," *Biomaterials Science*, vol. 5, no. 1, pp. 67–76, 2017.

[190] S. Dupont, L. Morsut, M. Aragona, E. Enzo, S. Giulitti, M. Cordenonsi, F. Zanconato, J. Le Digabel, M. Forcato, and S. Bicciato, "Role of YAP/TAZ in mechanotransduction," *Nature*, vol. 474, no. 7350, pp. 179–183, 2011.

[191] G. Halder, S. Dupont, and S. Piccolo, "Transduction of mechanical and cytoskeletal cues by YAP and TAZ," *Nature Reviews Molecular Cell Biology*, vol. 13, no. 9, pp. 591–600, 2012.

[192] I. Titushkin and M. Cho, "Modulation of Cellular Mechanics during Osteogenic Differentiation of Human Mesenchymal Stem Cells," *Biophysical Journal*, vol. 93, pp. 3693–3702, nov 2007.

[193] R. Subbiah, M. Suhaeri, M. P. Hwang, W. Kim, and K. Park, "Investigation of the changes of biophysical/mechanical characteristics of differentiating preosteoblasts in vitro," *Biomaterials Research*, vol. 19, no. 1, p. 1, 2015.

[194] D. A. Fletcher and R. D. Mullins, "Cell mechanics and the cytoskeleton," *Nature*, vol. 463, no. 7280, pp. 485–492, 2010.

[195] N. Gavara and R. S. Chadwick, "Relationship between cell stiffness and stress fiber amount, assessed by simultaneous atomic force microscopy and live-cell fluorescence imaging," *Biomechanics and Modeling in Mechanobiology*, vol. 15, no. 3, pp. 511–523, 2016.

[196] B. Alberts, A. Johnson, J. Lewis, D. Morgan, M. Raff, K. Roberts, and P. Walter, *Molecular Biology of the Cell*. Garland Science, 6 ed., 2015.

[197] P. Chugh, A. G. Clark, M. B. Smith, D. A. Cassani, K. Dierkes, A. Ragab, P. P. Roux, G. Charras, G. Salbreux, and E. K. Paluch, "Actin cortex architecture regulates cell surface tension," *Nature Cell Biology*, 2017.

[198] L. Pasakarnis, D. Dreher, and D. Brunner, "SnapShot: Mechanical Forces in Development I," *Cell*, vol. 165, no. 3, pp. 754–754. e1, 2016.

[199] L. Lu, S. J. Oswald, H. Ngu, and F. C.-P. Yin, "Mechanical properties of actin stress fibers in living cells," *Biophysical Journal*, vol. 95, no. 12, pp. 6060–6071, 2008.

[200] K. Haase, T. N. Shendruk, and A. E. Pelling, "Rapid dynamics of cell-shape recovery in response to local deformations," *Soft Matter*, 2017.

[201] S. D. Thorpe and D. A. Lee, "Dynamic regulation of nuclear architecture and mechanics—a rheostatic role for the nucleus in tailoring cellular mechanosensitivity," *Nucleus*, no. just-accepted, pp. 00–00, 2017.

[202] J. Domke and M. Radmacher, "Measuring the elastic properties of thin polymer films with the atomic force microscope," *Langmuir*, vol. 14, no. 12, pp. 3320–3325, 1998.

[203] Y. Imai, M.-Y. Youn, K. Inoue, I. Takada, A. Kouzmenko, and S. Kato, "Nuclear receptors in bone physiology and diseases," *Physiological Reviews*, vol. 93, no. 2, pp. 481–523, 2013.

[204] H. Suenaga, K. S. Furukawa, T. Takato, T. Ushida, and T. Tateishi, "Cell condensation and 3-dimensional dynamic environment in a rotation culture upregulates osteogenic differentiation of mesenchymal stromal cells," *Asian Journal of Oral and Maxillofacial Surgery*, vol. 20, no. 4, pp. 177–183, 2008.

[205] P. Carl and H. Schillers, "Elasticity measurement of living cells with an atomic force microscope: data acquisition and processing," *Pflügers Archiv-European Journal of Physiology*, vol. 457, no. 2, p. 551, 2008.

Appendix A

Protocol for cantilever spring constant calibration for mechanical analysis of living cells by an Asylum Research MFP-3D model AFM

A.1 Materials

1. Low glucose Dulbecco's Modified Eagle Medium (DMEM) with 10% FBS, 1% L-glutamate and 1% penicillin-streptomycin. After they have been mixed together under laminal flow inside the biological safety cabinet, they have been passed through 0.2 µm filter.
2. AFM probes
3. Fingernail polish
4. Micropipettes and micropipette tips
5. Microscope slides and glass coverslips
6. Tissue culture plates (TCP) (e.g. preferably 4-well plate or 12-well plate)

7. A tweezer
8. Forceps or needles to remove the coverslip from the well plate. Tweezer might also work here.
9. Petri dishes
10. Glass slides and glass coverslips (preferably 13 mm)

A.2 Methods

A.2.1 Calibration of the AFM probe

AFM probe is mounted to cantilever holder using an appropriate tweezer. AFM's computer, illumination light and laser light of AFM are switched on. Calibration of spring constant of AFM includes two steps: calibrating the deflection inverse optical lever sensitivity (InvOLS) and fitting a Lorentzian resonant frequency peak (usually the first Brownian mode) of the cantilever from the thermal noise data to determine the spring constant of the AFM cantilever experimentally. Both steps should be performed in liquid environment.

A.2.1.1 Calibration of deflection InvOLS

Put water on glass, preferably put ∼300 µl double distilled water via micropipette on a clean 13-mm glass coverslip previously glued on a glass slide. Lower the AFM head and be careful to not crash onto the surface, it may damage the tip. When the Z-Voltage drops down dramatically, it means that the AFM tip has touched the surface of the sample. There may be sound alarm incorporated into the AFM system which is activated as the Z voltage decreases below 150 V. After the tip is in contact with the surface, you may keep the Z-Voltage at about 90-120 V. After engaging the tip on the surface at contact mode, perform a single force curve measurement at contact mode. If needed, a vertical deflection correction can be done in order to make the horizontal part of the force curve parallel to

the x-axis. Then measure again another single force curve and you will see that new measurement will come with horizontal part of the force curves parallel to the x-axis. Fit the slope of the force curve with deflection or deflection volts by placing the cursors, this time to the sloppy part of the force curve. Fit the slope by selecting DeflVolts or Deflection. Then the deflection inverse optical lever sensitivity calibration will have been accomplished. Then, click withdraw and upper the head to make sure you are not in contact with the surface anymore. Proceed with the thermal noise data capture.

A.2.1.2 Thermal noise data capture followed by peak fitting

Measure thermal noise data when above enough the surface, which allows recording the Brownian motion of the cantilever. Thermal noise spectra for Teflon-like coated SiNi probes measured in air and water are shown in Figure A.1. The thermal noise spectrum in water is shifted to the left because of the difference of the refractive index between air and water. In cell culture medium, the thermal noise spectrum is not too different from that of measured in water. First peak is the highest peak, which is ideal for selection to fit because it is the resonant frequency of first Brownian mode which it describes the motion of the cantilever that deflection having a spring constant value nearest with nominal value. When one of lower peaks are selected, the cantilever is driven at the higher order modes, ending up with greater spring constant values. For selecting a peak, put cursors that are right below the graph, and position them at the starting and ending point of the peak and do the fitting of the peak, and the spring constant will have been determined by doing so. After that, then remove the head from its position on the AFM stage. Dry the cantilever holder and remove the slide from the platform.

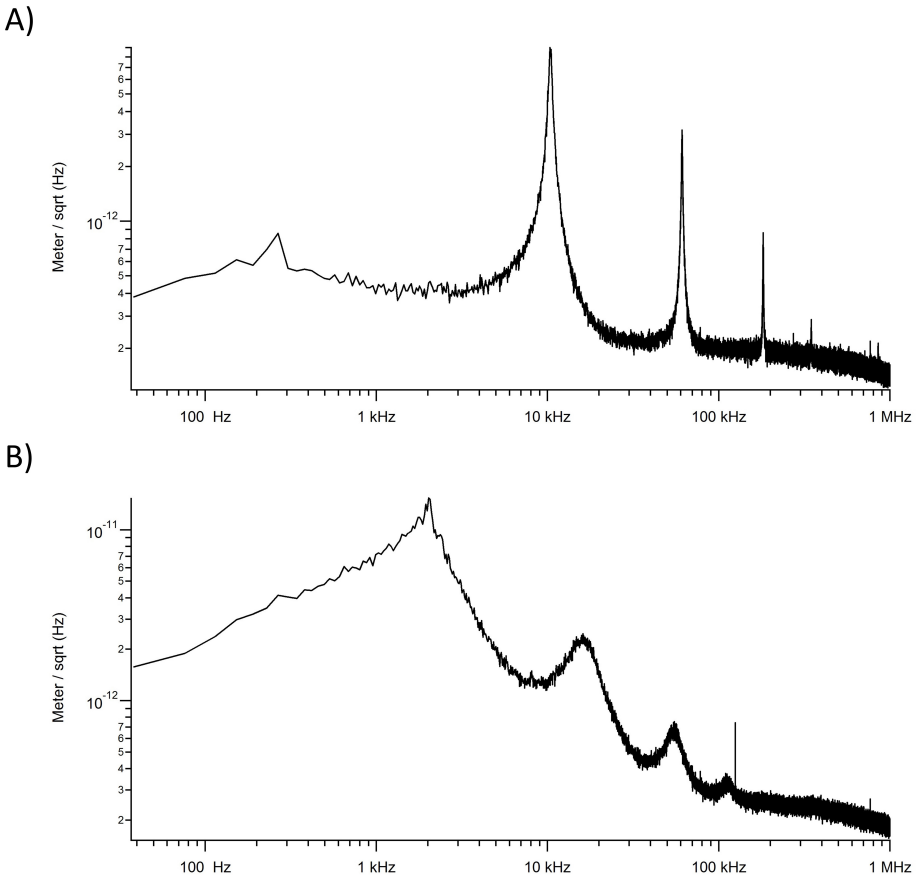


Figure A.1: Thermal noise versus frequency spectrum of Teflon-like coated silicon nitride AFM probes in air A) and in cell culture medium B).

A.2.2 Sample preparation

Cells are cultivated on 13 mm glass coverslips or peptide nanofiber hydrogel-coated glass coverslips inside well plates in the cell culture. At AFM experimentation time, first an AFM probe is mounted to the cantilever holder and calibrated in the water on a glass coverslip glued on a glass slide previously. About 300 µl of water is sufficient for covering Asylum Research MFP 3D model AFM's cantilever holder and letting a water column to form. After calibration, the cells are brought nearby to the AFM. One coverslip with cells at a time was nail polished on a glass slide to make it immobile during the measurements. For doing that, an arbitrarily sufficient nail polish is dropped on the center of a glass slide, that should not be allowed to leak above the glass coverslips with the cells, that are supposed to be removed using tweezers or with the help of a needle from dish/well-plate, and then carefully placed onto the droplet of nail polish. The sample can be pressed a little by contacting to near-edge areas of the coverslip using tweezers for the nail polish to spread more. About 50 µl of cell culture medium is gently added onto the cells using a micropipette. Wait 5-10 min for nail polish to dry so that it holds the glass coverslip immobile the AFM measurements can then safely be performed. Before putting the slide onto the AFM platform, ensure to protect the AFM's optics and electronics against liquid falling. For doing this, we put stretch film first and then place the substrate and the sample on it. Add more medium onto the cells at the AFM stage as the glass slide having sample nail polished on it is placed on the stage, as shown in Figure A.2. Magnets, in case for the presence of magnetic AFM stage, are placed upside down to both corners of the glass slide for moving it easily during measurements.

A.2.3 Measuring force curves on live cells

Apply a force distance of 5 µm or more for force mapping measurements. A trigger point of 0.5 V and a scan rate of 0.5 Hz (piezo speed would be 0.5 µm/s for 0.5 Hz scan rate and 5 µm force distance) would be enough. When the AFM tip is in interaction with the sample surface, move the slide in the x and y directions to

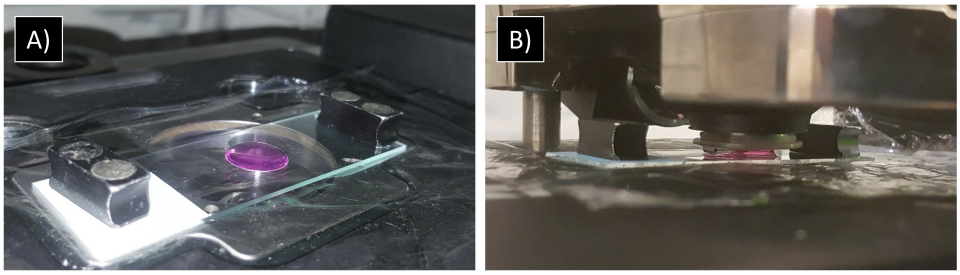


Figure A.2: Appearances of the sample on the AFM stage to make it ready for the measurements. A) Droplet of cell culture medium dropped on the sample, cells grown on coverslip, nail polished on a glass slide. Magnets are placed upside down for moving the sample easily in the x-y directions. B) Water column forms between the cantilever holder of AFM and the sample.

bring the AFM probe right above the cells on slide. Measure free force curves on the cells and correct the vertical deflection if needed (i.e. horizontal parts of the force curve are not parallel to the x-axis . Then you may proceed with the measurements. During the measurement process, check force curves being measured by AFM. In an encounter of unexpected dissonances, you may need to stop and re-adjust the z-axis, for instance, I had to do this frequently when I measured the samples that contained spherical cell aggregates (i.e. large spheroids) formed on the peptide nanofiber gel. Single session must be kept under one and a half hour because in room conditions cells start dying after this amount of time unless a carbon dioxide supply and a heater stage is used.

Depending on the type of AFM tip used, different types of models may be used for analysis. Hertz or Sneddon model from the software of AFM can be used with the parameters of a half-cone angle of 36° and a Poisson ratio of 0.5. However, different type of tips and sample-tip interactions may require the implementation of other types of models. From the force maps, it is often straightforward to visualize a microscale object like cells, and the derivation of the elastic modulus of the sample along with magnitude of adhesive forces observed at the retraction curves. To count strong adhesion at force curves in the calculation of elastic modulus, JKR model may be preferred.

Appendix B

Supplementary information

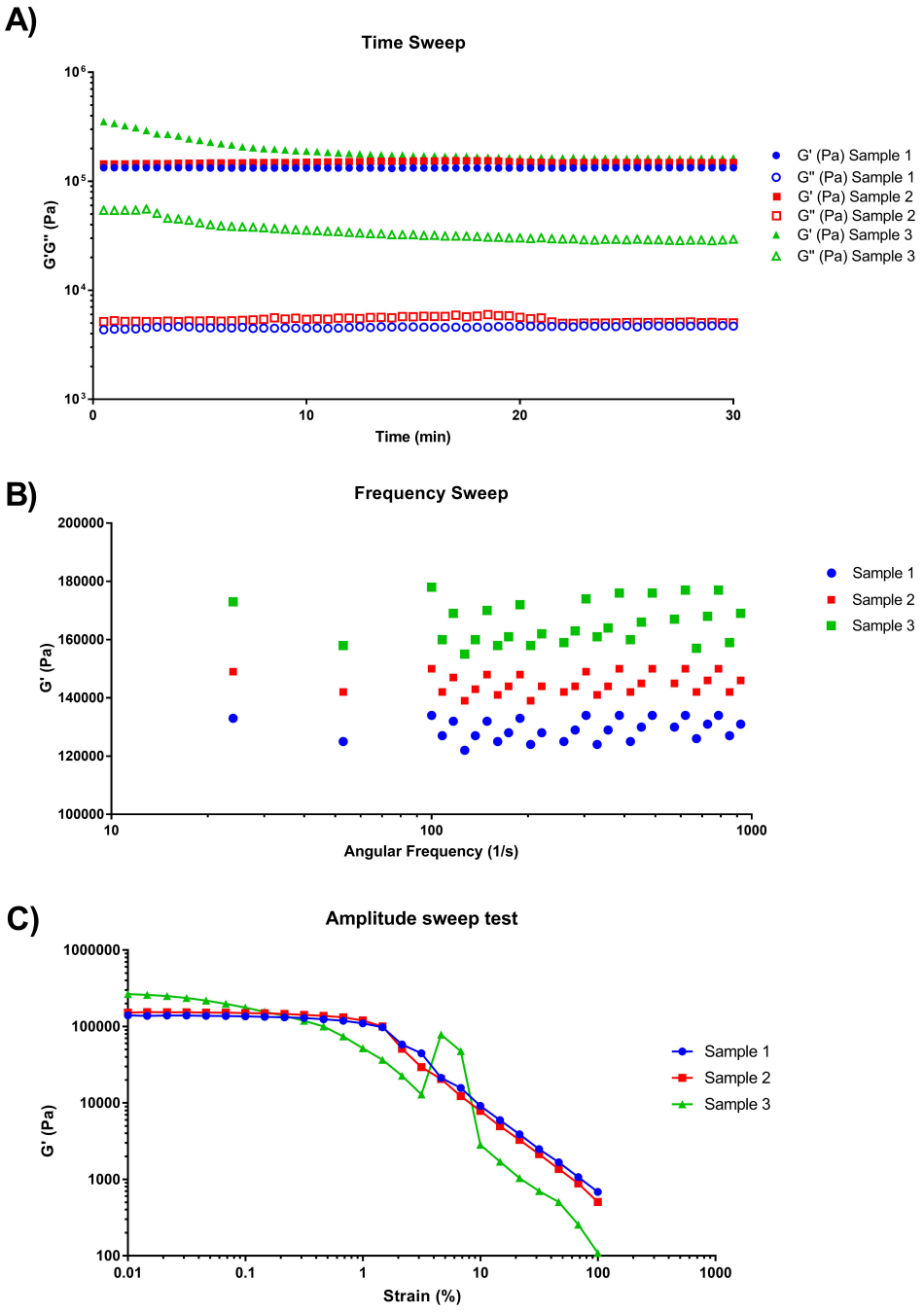


Figure B.1: A) Time sweep, B) frequency sweep and C) amplitude sweep tests of 1 wt % E_3/K_3-PA gel, three replicates are explicitly shown.